DYNAMICS, A DISPLACEMENT AND THE SUPERFLUIDITY DENSITY OF A BOSE GAS IN AN OPTICAL LATTICE

A Dissertation

Presented to the Faculty of the Graduate School

of Cornell University

in Partial Fulfillment of the Requirements for the Degree of

Doctor of Philosophy

by

Yariv David Yanay

August 2015

DYNAMICS, A DISPLACEMENT AND THE SUPERFLUIDITY DENSITY OF A BOSE GAS IN AN OPTICAL LATTICE

Yariv David Yanay, Ph.D.

Cornell University 2015

Advances in experimental atomic systems have given us access to highly tunable quantum systems, and to an unprecedented range of observables of these systems. One fundamental system that has been made accessible in this way is a gas of bosons trapped in a periodic potential.

We present here a several studies of the many-body physics of bosons in optical lattices. We discuss the ferromagnetic effects of a single vacancy in a two-species gas on a lattice. We present a derivation of the superfluid density, the order parameter for the superfluid state, and discuss the mathematical subtleties of calculating it. Finally, we calculate the dynamics of bosonic lattice systems, in the presence of inelastic light scattering used as a density measurement, and during a ramp of the interaction strength from the Mott to the superfluid phase.

BIOGRAPHICAL SKETCH

Yariv Yanay was born a long, long time ago in a country far, far away. He got his Bachelor's degree in Physics and Computer Science, as well as a Master's in Physics, at Tel Aviv University. He has done work on the magnetic form factor of the neutron, the topology of black holes in more than four dimensions, tensile strength reduction through percolation and the beam dynamics of proton and deuteron beams. In 2009, he came across the sea in a great machine made of metal and plastic, accompanied by a cat who sees the future.

אף אחד לא מבין את הקוואנטים. בעיקר לא הפיסיקאים.

אתגר קרת

ACKNOWLEDGEMENTS

I owe the greatest thanks to my parents; for their unwavering belief in my abilities, and for being more supportive and encouraging than I could ever imagine. I have equal gratitude to my brother, for keeping me sane despite their best efforts.

Erich has been a wonderful advisor. Beyond his help in guiding me along, keeping me to attainable projects and challenging what I took for granted, his enthusiasm for the work we do has been inspiring. I am a much better physicist for having worked with him.

I also owe much to the other faculty at the physics department. Mukund Vengalattore did a great job of keeping me in touch with the experimental side of the field, both through our work together and his excellent courses on ultracold atomic physics. I learned a great deal from working on smaller projects with Paul Ginsparg and Veit Elser. Yuval Grossman's intuitive approach to field theory made his class the best I took at Cornell; Itai Cohen gave me the opportunity to finally understand statistical physics by teaching it with him. And I'm indebted to Csaba Csaki for not taking me on as a student, saving me from a fate worse than death[1].

I had a set of amazing colleagues in Erich's group. Thanks to Bhuvanesh, Matt, Sayan, Shovan, Ran Wei and Junjun for doing all the physics I didn't get around to and telling me about it at group meetings.

There is a whole host of people back in Israel that launched me into Cornell. I'm thankful to Adi, Yaniv, Ori, Tamar and Omri for keeping my seat warm and available whenever I got back; to Aya for reading my long emails; to Shira for sticking with me long after the rest have gone home to their children; to Lior and Uri for keeping up with boardgames so that I didn't have to; and to Tamar – for going to Cornell first. And to Lola, for teaching me to cook, taking me to the

[1] a career in particle physics

beach and suffering through the application process with me.

My love affair with Ithaca has had its ups and downs through the years, but I always had great friends here, for which I'm grateful. Alkisti introduced me to architecture, brought a black cat into my life, and showed me the bluest, clearest sea that I have ever seen; Alessandro was my first friend in town, took me on road trips and more adventures than I can count, and fed me every other Sunday night; Matt and I survived the vagaries of second year together in Rock 237[2]; Veronica helped end that year, and forgave all my offenses for no apparent reason; Sisca and I spent hours on my porch talking on warm summer nights; Mike was an older version of me; Bob danced shirtless with me; Jen made a stencil of me; Alex and Caaaitlin lent me books that I never returned; the other Alex was never happy with my answers; Alisar showed me Ithaca's best swimming spot; Lauren is the blondest woman I've ever dated; Shivam took me to Indian dance parties; Erin took care of my cats; Natu and Kaden showed me life was good after the Mueller years; Katie's porch had the best view of the Ithaca parade; Kayla always had my back when dancing was an option; Cody has two kitties; John kept asking me what does it really mean; Tara's chemical support made this work possible; Sam and I talked Jewish erotica; Kacey put up with it; Laurie was drunk when drunkenness was called for; and Corky was Corky.

To the staff of the Bandwagon: you're welcome. I didn't really need those hundreds of dollars anyway.

Galactica and Dynamite did nothing to help me get through my this. I still love them.

I have all the love in the world for the people who have been my family these last couple of years - YJ, an excellent partner in gossip, Brian, who was always there to show me life could be worse, Lauren, who kept me up to date on what the

[2]allegedly, Richard Feynman's office when he was at Cornell

kids are watching these days, Jesse, our resident non-scientist and tree connoisseur, Ben, my identical twin, alternate universe son and all around instigator, Sam, the perfect house mate, who always let me make the bad jokes first, and most of all Caitlin, who was always there when I needed her and sometimes when I did not.

I am also thankful to the good people of the United States of America, who, as part of the miracle that is modern civilization, were kind enough to pay me to do what I love. Much of the work presented here was funded by them, through the National Science Foundation, under grant number PHY-1068165, and the Army Research Office's DARPA Optical Lattice Emulator program and MURI Non-equilibrium Many-body Dynamics grant, number 63834-PH-MUR.

And finally, I am grateful to Emma, for showing up just in time to make writing this dissertation so much more enjoyable, and to complicate life beyond Chapter 7 in the best way possible.

Yariv Yanay, May 2015

TABLE OF CONTENTS

LIST OF FIGURES

CHAPTER 1

INTRODUCTION

Some fields of physics have a patron saint, as Newton is to mechanics and Einstein to relativity. Others have a mathematical object to represent them, like elecromagnetism's Maxwell's Equations and theoretical particle physics' Feynman diagrams. Ultracold atomic physics has a false-color image. Three gaussian peaks, each successively sharper than the last, in rainbow colors, representing the momentum distribution of a gas of Sodium atoms as it was cooled down into a Bose Einstein Condensate [35].

With Ketterle's experiment, as well as Eric Cornell and Carl Wieman's parallel experiment [3] and Hulet's closely following work [18], atomic physics became an incredibly productive playground for fundamental quantum mechanics research. Multiple quantum phenomena could suddenly be observed and controlled directly in tabletop sized lab setups.

The advantages of ultracold atomic physics come down, in the end, to its scales. The gases used in atomic experiments have masses $10^3 - 10^4$ greater than the electrons of condensed matter. They are diluted until the interatomic distance is on the order of microns, 10^4 times larger than the atomic spacing in a typical metal. And they are neutral, and so near-invisible to the primarily electromagnetic influence of the outside world. As such, the natural energy scale of these atoms - in KHz and MHz - is separated by ten orders of magnitude from the energy scales of the lasers and fields used to control them. Unintended interactions, external effects, and uncertainty - heating and temperature - can be reduced to unprecedented levels.

The same scales work to create atomic physics' other advantage, in the form of direct probes of our systems. Both the distances – microns – and time scales – fractions of seconds - at which our gases operate are nearly within the human range of perception, and the same separation that allows for a reduction of temperatures, allows for the use of scattered light to measure the properties of individual particles. From the aforementioned image, inferring of the momentum distribution of the particles from their position after flying away from the trap, to current experiments observing particles in situ [6, 116], we have gained access to an incredible wealth of information about these quantum systems.

And so we have the ability to set up and control quantum systems with high precision on the one hand, and to learn a great deal about the results of each intervention on the other. This is a perfect combination for a theorist, who is left to explain how we came from point A to point B. Like any physicist who has been working at it long enough, I have a set of explanations for my work ranging from the single sentence to the hour-colloquium, which are deployed in a modular fashion after gauging the listener's actual level of interest in the subject. My one-sentence version is, "I play games with quantum mechanics".

More specifically, my work, and this thesis, have focused on the study of many-body quantum systems, studying the emergent physics of the coherent interactions of many subatomic particles. The nature of theoretical research in our field is broad - there are many questions to be answered, and many questions that can be answered in a relatively concise fashion. This lends itself to an exciting mode of research, and has allowed me to work on a diverse range of subjects, using multiple techniques. It does not make for an entirely coherent dissertation. It is presented, instead, as a collection of studies of one of the fundamental systems

used in ultracold atomic physics, bosonic particles trapped on an optical lattice.

We begin, in Chapter 2, with an introduction to the underlying mathematics powering all of this work, the Bose Hubbard model. We also discuss the microscopic physics underpinning the model, and how to relate the it to experimental parameters. This introductory chapter is followed by five previously published works on the behavior of lattice bosons, divided into three topics.

The first of these, Chapter 3, is concerned with the physics of polarons. In a lattice with commensurate filling of two species of strongly interacting gas, we introduce a single impurity, in the form of a missing particle. We explore the ferromagnetic ordering this impurity induces.

In the following chapters, we discuss a field theoretical approach to calculating the superfluid density, the order parameter describing the superfluid state of low-temperature bosons. In Chapter 4 we calculate this order parameter in bosonic systems of one and two particle species. In making this calculation, we encounter a mathematical inconsistency brought on by the use of coherent states with the path integral formalism. In Chapter 5, we introduce and discuss a technique to correct this inconsistency.

Finally, the last two chapters focus on the dynamics of lattice bosons. In Chapter 6 we calculate the quantum effects of measurement as it is expressed in these systems, focusing on the reaction of lattice bosons to local density probes. Finally, in Chapter 7, we study the behavior of these systems as they undergo a phase transition between the Mott insulator and superfluid phase.

CHAPTER 2

THE BOSE HUBBARD MODEL

Much of the study of modern physics is driven by ideas of symmetry, and one of the defining features of a physical system is the symmetries that govern its behavior. From this point of view, the physics of condensed matter systems is driven by discrete translational symmetries associated with lattices [103].

The understanding of crystal systems, defined by such lattices, has evolved hand in hand with quantum mechanics over the last hundred years. Naturally, much of the initial focus was on the physics of individual particles, generally electrons, moving through a periodic system. This dissertation is concerned with the next step, the physics emerging from the interconnected behavior of many particles. This research is driven by the experimental breakthroughs in optical and atomic physics in the last two decades, as discussed in Chapter 1. It remains rooted in the efforts made in the understanding of condensed matter systems, and makes use of the breakthroughs of that field.

A crucial step in understanding the physics of periodic systems, as in any other field, is defining the problem in an accessible, clear way. We make use of the body of work on condensed matter systems by appropriating one of its most commonly used tools, the Hubbard model. It is an approach to periodic quantum systems that seeks to make maximal use of their symmetries, to present this complex problem in a manageable, transparent Hamiltonian form.

The Hubbard model was first proposed by its eponymous creator in 1963 [70] as a method of calculating electron correlations in metals. It has since been successful in predicting many results in condensed matter physics [149] and atomic physics

[17], for fermions and bosons [23,24,39,46,61,104,138,150]. Though much of what we present in this chapter is applicable to both Fermi-Hubbard and Bose-Hubbard systems, as the relevant models are called, our focus is on bosonic systems, and the results presented in later chapters are unique to those.

2.1 Many Body Physics in a Periodic Potential

In its most general formulation, the Hubbard model is simply a change of basis. We begin with a periodic potential, and a related set of $N_s \gg 1$ lattice vectors denoted by $\boldsymbol{R}_i$. We know, from Bloch's theorem [103], that the eigenfunctions of a single particle in such a potential can be written as

$$\psi_{n,k}(\boldsymbol{r}) = e^{-i\boldsymbol{k}\cdot\boldsymbol{r}} u_{n,k}(\boldsymbol{r}), \tag{2.1}$$

where the functions $u_{n,k}(\boldsymbol{r} + \boldsymbol{R}_i) = u_{n,k}(\boldsymbol{x})$ have the same periodicity as the potential, and $\boldsymbol{k}$ is a crystal momentum, defined up to a reciprocal lattice vector. Thus, we write the non-interacting Hamiltonian as

$$\hat{H}_1 = \tfrac{1}{N_s} \sum_k \sum_n \epsilon_{n,k} \hat{a}^\dagger_{n,k} \hat{a}_{n,k} \tag{2.2}$$

where $\hat{a}_{k,n}$ ($\hat{a}^\dagger_{k,n}$) are the annihilation (creation) operators for a particle with wavefunction $\psi_{n,k}(\boldsymbol{r})$:

$$\hat{a}^\dagger_{n,k} = \int \mathrm{d}\boldsymbol{r}\, e^{-i\boldsymbol{k}\cdot\boldsymbol{r}} u_{n,k}(\boldsymbol{r}) \hat{\psi}^\dagger_r \tag{2.3}$$

where $\hat{\psi}^\dagger_r$ is creation operator for a particle at position $\boldsymbol{r}$.

Next, we set to add an interaction term to the Hamiltonian. As these are often short-ranged on the scale of the lattice, it is useful to introduce a set of local creation operators, defining for for any lattice vector $\boldsymbol{R}_i$

$$\hat{a}^\dagger_{n,i} = \int \mathrm{d}\boldsymbol{r}\, \phi_n(\boldsymbol{r} - \boldsymbol{R}_i) \hat{\psi}^\dagger_r \equiv \tfrac{1}{\sqrt{N_s}} \sum_k e^{i\boldsymbol{k}\cdot\boldsymbol{R}_i} \hat{a}^\dagger_{n,k}. \tag{2.4}$$

The functions $\phi_n(\boldsymbol{r})$ used here are known as Wannier functions. They form are a localized basis for the single-particle wavefunctions.

With the addition of a two-particle interaction operator $\hat{V}_2$, the Hamiltonian takes on the most general Hubbard form,

$$\hat{H} = -\sum_{i,j} J_j^n \hat{a}_{n,i+j}^\dagger \hat{a}_{n,i} + \tfrac{1}{2} \sum_{\substack{i,j,\\ i',j'}} \sum_{\substack{m,n,\\ m',n'}} U_{i'-i,j,j'}^{m,n,m',n'} \hat{a}_{n',i+j}^\dagger \hat{a}_{m',i'+j'}^\dagger \hat{a}_{m,i'} \hat{a}_{n,i} \tag{2.5}$$

where

$$J_j^n = -\tfrac{1}{N_s} \sum_k \epsilon_{n,k} e^{-i\boldsymbol{k}\cdot\boldsymbol{R}_j} \tag{2.6}$$

$$\begin{aligned} U_{i'-i,j,j'}^{m,n,m',n'} = \int \mathrm{d}\boldsymbol{r}\mathrm{d}\boldsymbol{r}' \, \langle \boldsymbol{r} + \boldsymbol{R}_i, \boldsymbol{r}' + \boldsymbol{R}_{i'} | \hat{V}_2 | \boldsymbol{r} + \boldsymbol{R}_i, \boldsymbol{r}' + \boldsymbol{R}_{i'} \rangle \times \\ \phi_{n'}^*(\boldsymbol{r} - \boldsymbol{R}_j) \phi_{m'}^*(\boldsymbol{r}' - \boldsymbol{R}_{j'}) \phi_n(\boldsymbol{r}') \phi_m(\boldsymbol{r}). \end{aligned} \tag{2.7}$$

Here $|\boldsymbol{r}, \boldsymbol{r}'\rangle$ is a normalized two-particle wavefunction with particles at $\boldsymbol{r}$ and $\boldsymbol{r}'$.

The basis change of Eq. (2.5) is enlightening in itself, allowing us to view the problem in terms of the behavior of particles populating the discrete sites of lattice. As we will see in Section 2.2.2, Eqs. (2.6) and (2.7) allow us to easily transform microscopic potentials into this discrete Hamiltonian.

However, the real strength of the Hubbard model is in expediting relevant approximations, which make Eq. (2.5) amenable to analytical treatment. In particular, Wannier functions of bound states generally have exponentially decaying tails. Thus the magnitude of the parameters in Eqs. (2.6) and (2.7) generally falls off exponentially the relevant js.

For short-range interactions such the interatomic potentials that govern atomic experiments, the interaction strength in Equation (2.7) drops off quickly with the

distance $i - i'$, as well. In most experiments, it is only the on-site interaction that is relevant [75].

Finally, of the single-particle bands in the model, we often consider just one or a few. In many systems of interest, inter-particle interaction strength is weak enough that atoms are not scattered into the excited bands and the lowest-energy band can be considered by itself.

Under those simplifications, the single-band Hubbard model becomes, in an isotropic lattice,

$$\hat{H} = -J \sum_{\langle i,j \rangle} \left(\hat{a}_i^\dagger \hat{a}_j + \hat{a}_j^\dagger \hat{a}_i \right) + \frac{U}{2} \sum_i \hat{a}_i^\dagger \hat{a}_i^\dagger \hat{a}_i \hat{a}_i \tag{2.8}$$

where $\langle i, j \rangle$ counts over all nearest-neighbor pairs, and we have marked

$$J = J_1^1 \qquad U = U_{000}^{1111}. \tag{2.9}$$

An additional chemical potential term, of the form $\mu N = \mu \sum_i \hat{a}_i^\dagger \hat{a}_i$, is often incorporated into the Hamiltonian.

In momentum space, the Hamiltonian takes the form

$$\hat{H} = J \sum_k \varepsilon_k \hat{a}_k^\dagger \hat{a}_k + \frac{U}{2} \frac{1}{N_s} \sum_{p,k,q} \hat{a}_p^\dagger \hat{a}_{k+q}^\dagger \hat{a}_{p+q} \hat{a}_k. \tag{2.10}$$

where the kinetic energy is given by a sum over the lattice basis vectors $\boldsymbol{\Delta}$,

$$\varepsilon_k = -2 \sum_\Delta \cos(\boldsymbol{k} \cdot \boldsymbol{\Delta}). \tag{2.11}$$

2.1.1 Phase Diagram

The equilibrium properties of the simplified single-band Hubbard model of Eq. (2.8) have been studied extensively [23,24,39,46,61,104,138,149,150]. When the hopping

parameter dominates, $J/U \gtrsim 1$, a lattice gas behaves similarly to a free Bose gas. At low temperature, the atoms condense into the ground states, leading to superfluidity, while at high temperatures they behave like a thermal Boltzmann gas. In the weak hopping regime, $U \gg J$, a non-compressible Mott insulator state arises at low temperatures. Figure 2.1 shows the zero-temperature phase diagram of the single-band Bose Hubbard model.

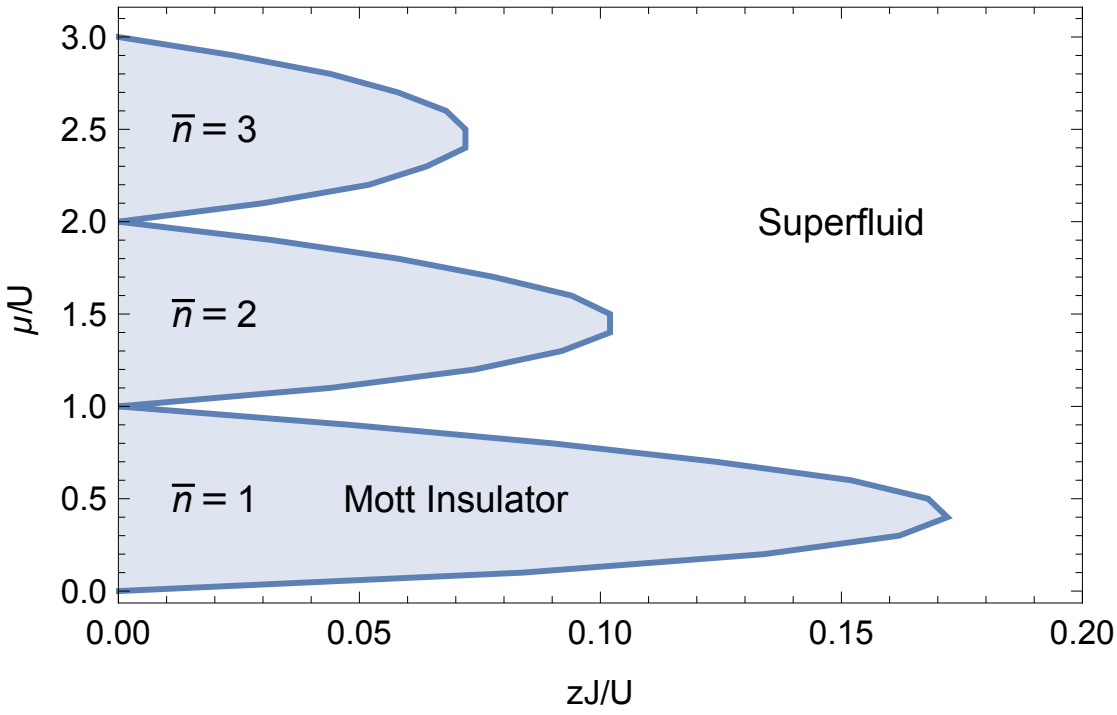

Figure 2.1: The zero-temperature mean-field phase diagram of the Bose Hubbard model of Eq. (2.8), as a function of the ratio of the hopping parameter to the interaction strength zJ/U, and the chemical potential, μ. Here $z = 2D$ is the number of nearest-neighbors for each site. The shaded area are an incompressible Mott-insulator state with an integer filling fraction, while the blank space is a superfluid state with a continuous change in mean occupation. This diagram was obtained by a Gutzwiller ansatz calculation (see Section 2.6.3). More precise methods of calculation yield qualitatively similar results but alter the shape of the Mott lobes.

2.2 Optical Lattices

The interest in the physics of periodic structures comes from our study of metals and the common crystal form that is found in nature. In atomic systems, periodic potentials are manufactured to simulate these systems.

The most common method of creating such lattices for neutral atoms are optical potentials [15]. An neutral atom interacts with an electromagnetic field via a dipole interaction of the form $V = -\boldsymbol{d}\cdot\boldsymbol{E}$. The electromagnetic Hamiltonian for an atom can be written in the hyperfine basis,

$$\begin{aligned}\hat{H}_{EM} = &\sum_{j,f}\epsilon_{j,f}|j,f\rangle\langle j,f| + \sum_{k}\hbar\omega_k\hat{c}_k^\dagger\hat{c}_k \\ &-\frac{1}{2}\sum_{j,f,j',f',k}\langle j',f'|(\boldsymbol{d}\cdot\boldsymbol{\mathcal{E}_k})|j,f\rangle\left(\hat{c}_k+\hat{c}_k^\dagger\right)|j',f'\rangle\langle j,f|\end{aligned} \tag{2.12}$$

where $|j,f\rangle$ is a hyperfine state, and $\hat{c}_k^\dagger$, $\hbar\omega_k$ and $\boldsymbol{\mathcal{E}_k}$ the photon creation operator, energy and field component for the photons with wavector k.

For a monochromatic laser, of energy $\hbar\omega_L$, that is far-detuned, so that $\left[\left(\epsilon^0_{j',f'}-\epsilon^0_{j,f}\right)-\hbar\omega_L\right]t \gg 1$ for any pair of hyperfine levels at the relevant time scales, the eigen-energies of the atom can be expanded perturbatively. We find

$$\begin{aligned}\epsilon_{j,f} = &\epsilon^0_{j,f} - \mathrm{Re}[\Omega]\langle j,f|(\boldsymbol{d}\cdot\boldsymbol{\mathcal{E}_k})|j,f\rangle \\ &-|\Omega|^2\sum_{j',f'}\frac{\left(\epsilon^0_{j',f'}-\epsilon^0_{j,f}\right)}{\left(\epsilon^0_{j',f'}-\epsilon^0_{j,f}\right)^2-(\hbar\omega_L)^2}|\langle j',f'|(\boldsymbol{d}\cdot\boldsymbol{\mathcal{E}_k})|j,f\rangle|^2\end{aligned} \tag{2.13}$$

where $\Omega = \langle\hat{c}_k\rangle$ is the intensity of the laser.

It is easy to see that the above becomes, for a standing wave, a periodic potential of the form $|\boldsymbol{\mathcal{E}_k}|^2 \propto \sin^2(\boldsymbol{k}\cdot\boldsymbol{r})$. The resonant structure allows experiments to be tuned to a specific virtual transition, while the depth of the lattice is easily controlled by tuning the intensity of the lasers.

2.2.1 Atomic interactions and Feshbach Resonances

At the scales relevant to atomic physics, interactions are governed entirely by the electromagnetic force. Interactions between electrically-neutral atoms, then, are inherently weak, and governed by higher order effects. At long distances, they generally take the form of a quickly vanishing $V(r) \propto -1/|\boldsymbol{r}|^n$, for some $n \geq 2$ [117], most typically $n = 6$ [77]. At short distances the potential increases exponentially at what is effectively the atomic radius, $V(r) \propto e^{-|\boldsymbol{r}|/r_0}$.

At the length scales we are concerned with, these interactions can be thought of as contact interactions, and their properties can be understood in terms of scattering parameters. The majority of relevant atom-atom interactions can be described by the potential form [15]

$$\hat{V}_2(\boldsymbol{r}) = \frac{4\pi\hbar^2 a}{m}\delta(\boldsymbol{r})\left(1 + |\boldsymbol{r}|\frac{\partial}{\partial|\boldsymbol{r}|}\right). \tag{2.14}$$

where a, the scattering length, depends on the atomic structure and the hyperfine state of the interacting particles. It may also be modified by the use of magnetic Feshbach resonances. It is often on the order of $1 - 100$ times Bohr radius, or $10^{-10} - 10^{-8}$ meters.

2.2.2 Optical Lattices and the Bose Hubbard Model

Having put optical lattices and the scattering potentials of atomic physics in mind, we will go on immediately do discard them and return to the abstract form of the Bose-Hubbard model. The remaining step along that path is to translate the microscopic description of Eqs. (2.13) and (2.14) into the energy parameters of Eq. (2.8).

We begin with the microscopic description of a single atom in an optical lattice. As we have seen, it can be described by

$$\hat{H}_1 = \frac{\hat{p}^2}{2m} + \sum_{\alpha=x,y,z} V_0^\alpha \sin^2(k_L r_\alpha) \tag{2.15}$$

where m is the atomic mass, and k_L is the wavenumber of the lattice lasers. Together, define the natural energy scale of the single-particle physics, given by the recoil energy, $E_R = \frac{\hbar^2 k_L^2}{2m}$.

From the single particle description we can obtain the energy bands that define the hopping term J, shown in Fig. 2.2. These nearly-sinusoidal bands yield long-range hoping coefficients that decay exponentially with distance, as shown in Fig. 2.3, justifying the approximations mentioned before. Also seen in Fig. 2.3, the nearest-neighbor hopping parameter drops exponentially as lattice depth increases.

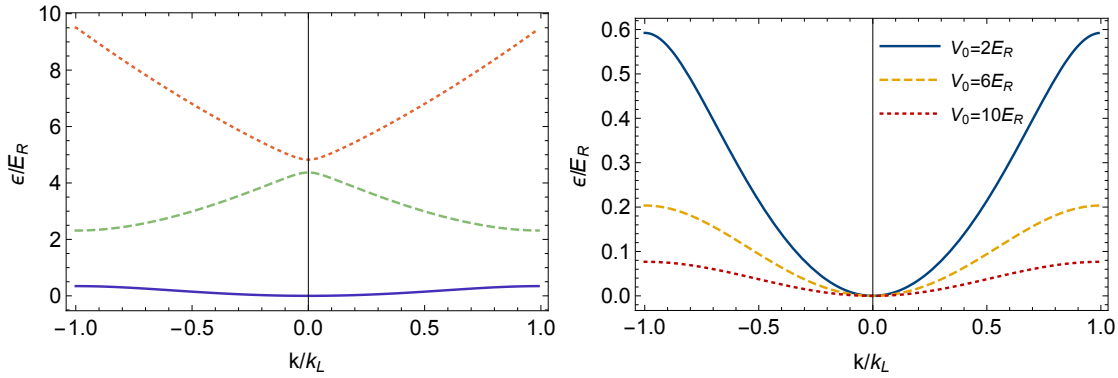

(a) $V_0 = 4$ (b) Lowest band

Figure 2.2: The single-particle energy spectrum of a neutral atom in an optical lattice potential of the form $V(x) = V_0 \sin^2(k_L x)$, in one dimension. (a) The complete bound energy spectrum for the potential at V_0 (two lower bands) as well as the bottom of the free-particle spectrum (upper curve). (b) The lowest energy band for different values of V_0.

Next, we add an interatomic interaction potential, of the form given in Eq. (2.14). We can calculate the interaction strength parameters of Eq. (2.7),

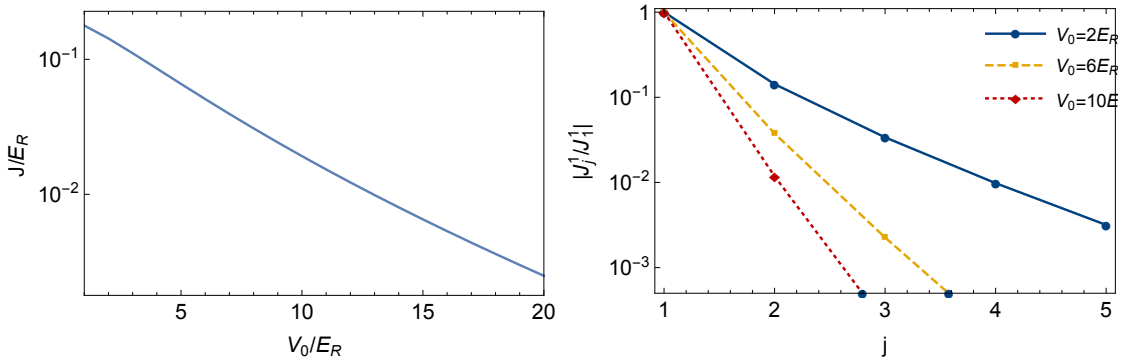

(a) Nearest-neighbor hopping (b) Long-range hopping

Figure 2.3: The effective hopping parameters of the Hubbard model for the lowest energy band of a neutral atom in an optical lattice. (a) The nearest neighbor hopping parameter $J = J_1^1$. The hopping strength drops exponentially with the depth of the lattice. (b) The relative strength of longer-range hopping strength parameters at selected lattice depths. They are suppressed, even at shallow lattice depths.

finding

$$U_{i'-i,j,j'}^{m,n,m',n'} = 8\pi E_R \frac{a}{k_L^2} \int \mathrm{d}\boldsymbol{r}\, \phi_{n'}^*(\boldsymbol{r} - \boldsymbol{R}_j)\phi_{m'}^*(\boldsymbol{r} - \boldsymbol{R}_{j'})\phi_n(\boldsymbol{r})\phi_m(\boldsymbol{r}). \tag{2.16}$$

The behavior of the on-site interaction parameter is show in Fig. 2.4. As we increase the lattice depth, the Wannier wavefunctions become more bunched, and the strength of the interaction increases. This is a slow, sub-linear, increase. However, the behavior of the Bose-Hubbard model depends only on the ratio U/J. As seen in Fig. 2.4(b), this parameter can be tuned over several orders of magnitude by a linear change in the intensity of the trapping lasers.

Figure 2.5 shows the role of interaction terms other than the on-site interaction term for the lowest energy band. As a rule, they are two or more orders of magnitude smaller than U, as well as much smaller than the energy gap between the lowest energy and first excited bands.

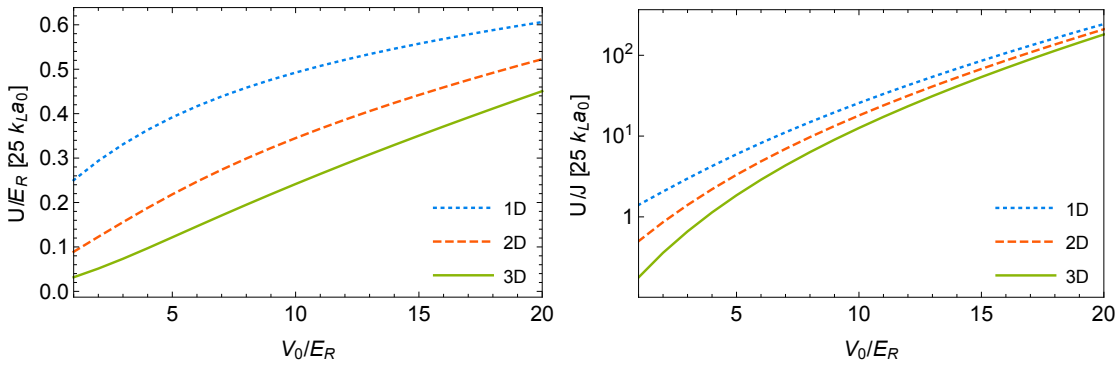

(a) Interaction Strength (b) Relative

Figure 2.4: Effective on-site interaction strength of the Hubbard model for the lowest energy band of a neutral atom in an optical lattice, as a function of lattice depth. Lower-dimensional setups are achieved by increasing the lattice depths in the remaining dimensions, so that $V(x) = \sum_{\alpha=1}^{D} V_0 \sin^2(k_L r_\alpha) + \sum_{\alpha=D+1}^{3} V_\perp \sin^2(k_L r_\alpha)$. Here we use $V_\perp = 30E_R$, so that the transverse hopping parameters is two orders of magnitude smaller than the active directions. (a) On-site interaction strengths in units of the recoil energy. The absolute strength of the interaction rises slowly with lattice depth, as the particle's wavefunction becomes narrower. (b) The ratio of the interaction and hopping parameter, U/J, determines the transition between Mott insulator and superfluid (see Section 2.1.1). It rises exponentially as the hopping parameter drops. The parameter $k_L a$, the ratio of the scattering length to the lattice parameter, is about $k_L a_0 \approx 0.04$ for ^{87}Rb atoms in a red laser trap, and of similar magnitude in other experimental setups.

2.3 Disorder Effects in Optical Lattices

The fundamental assumption in the analysis of lattice systems is periodicity, or discrete translational invariance. In particular, it allows for the use of Bloch's theorem, which stood at the foundation of the simplified Hubbard model introduced above. The overall periodic symmetry of the system is the source of many of its interesting qualities. In particular, it is essential to superfluidity in its various manifestations. In this chapter, we turn our attention to the breaking of this symmetry, by the introduction of disorder.

The addition of disorder is interesting for many reasons. The most apparent is

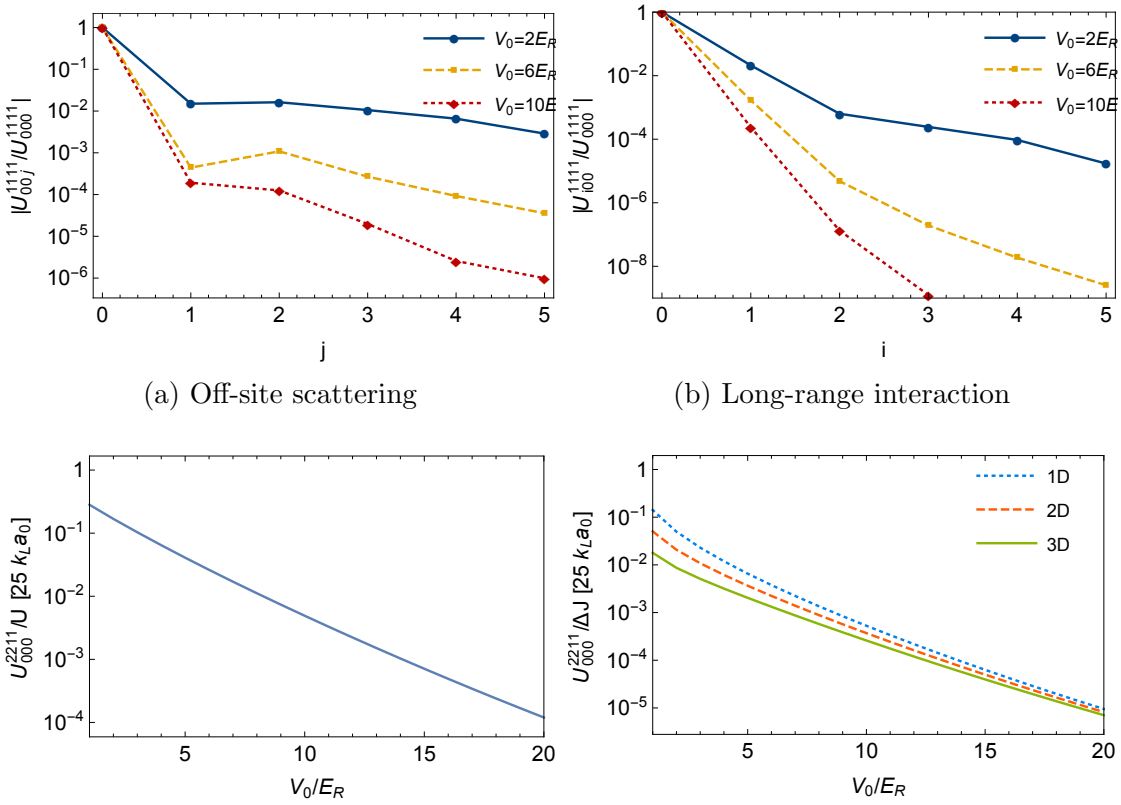

(a) Off-site scattering

(b) Long-range interaction

(c) Relative to Interaction Strength

(d) Relative to Band Gap

Figure 2.5: Secondary Hubbard model interaction terms for a neutral atom in an optical lattice, including (a),(b) long range interaction and (c),(d) inter-band scattering . (a) Off site scattering terms, U^{1111}_{00j}. (b) Inter-site interaction terms, U^{1111}_{i00}. All off-site terms are suppressed, even at shallow lattice depths. (c) The interband scattering term, U^{2211}_{000}, compared with the on-site interaction strength. (b) The interband scattering term relative to the band gap, $\Delta J = \min_k[\epsilon_{2,k}] - \max_k[\epsilon_{1,k}]$. Even in a shallow lattice, the bands are far detuned from each other.

the existence of disorder in real-life systems, and particularly in condensed matter systems. In atomic systems, the large energy scales involved make it easy to construct relatively perfect systems, but in material science and electronic systems imperfections are unavoidable. If we wish to use atomic systems as quantum simulators [16], we must learn to simulate disorder, as well.

A related motivation is the new physics that comes with the breaking of symmetries. Most famous of those are high-temperature superconductors relying on

doping by impurities of a Mott insulator [96]. More recently, there has been growing interest in the physics of many body localization [11,107], where the importance of disorder is seen not at the single-particle level but in the many-body wavefunction.

2.4 Realizations of Disorder in Optical Lattice Systems

As discussed in Section 2.2, the most common implementation of lattice systems in atomic physics is the optical lattice. The lattice itself, a standing laser wave, is entirely uniform, and there is no natural way to dope it. Disorder must be introduced intentionally. The chief techniques used are introduction of a secondary laser potential, either in the form of a laser speckle [158] or a secondary, incommensurate lattice [36, 41, 132] or the use of a secondary species of atoms at low density as a source of local potential [50].

Speckle Potentials

The earliest and most direct technique for the production of disorder is the use of a speckle field, simply a laser passed through a diffusing plate to produce a random optical field. Much like the beams of the optical lattice, it is kept detuned from the atomic resonances, and produces an effectively classical potential field. Often used with a one-dimensional or two-dimensional system, the speckle beam is aligned perpendicular or at an angle to the system, creating localized disorder.

This technique was used successfully in trapped gases and non-lattice experiments [14,28]. It is more difficult to use in lattice experiments, because the available speckle beams generally have wavelengths similar to those of lattice lasers, and so

the variation in potential is on scales as large or larger as a single lattice site. It is thus difficult to create variation in the strength of the disorder, but the speckle can be used to create a discrete random potential.

Incommensurate Lattices

An alternative optical route allows for the creation of quasiperiodic, or quasi-random, potentials. A secondary laser, with a non-rational multiple wavelength, is shined at a weaker intensity, creating a modulation of the primary optical lattice.

This technique creates a continuously distributed, quasi-randomly varying potential difference along the lattice. It is very useful for smaller lattices, which are common in atomic experiments. In longer lattices, the periodic structure of this potential may give rise to other effects.

Trapped Secondary Species

A final method of creating disorder involves the use of particle interaction. As previously, a secondary, incommensurate, optical lattice is used. However, in this case, its wavelength is selected to be off-resonant and invisible to the primary particles used. A second species of particle, generally a second hyperfine state, feels the effect of the second lattice, but not the first. The secondary lattice is tuned to the Mott regime, so that the second species is frozen in place for the duration of the experiment. Via interaction, it then serves as a static, random set of point potentials.

This technique creates a truly random potential. Its main disadvantage is that due to the very short range of particle interaction, the energy scale of the associated

disorder tends to be weaker.

2.5 Treatment within the Hubbard Model

Regardless of their experimental underpinning, we wish to describe effective disorder potentials in terms of the parameters Eq. (2.8). In adding disorder, we transform that uniform Hamiltonian into a local one of the same form,

$$\hat{H} = -\sum_{\langle i,j \rangle} J_{ij}\left(\hat{a}_i^\dagger \hat{a}_j + \hat{a}_j^\dagger \hat{a}_i\right) + \sum_i \left(\frac{U_i}{2}\hat{a}_i^\dagger \hat{a}_i^\dagger \hat{a}_i \hat{a}_i - \mu_i \hat{a}_i^\dagger \hat{a}_i\right). \tag{2.17}$$

In analyzing the effects of disorder, the parameters J_{ij}, U_i and μ_i are usually described as having some statistical distribution around the mean values J, U, μ.

To understand atomic experiments, we must connect the microscopic potentials, however they are created, to this model. In keeping with our simplifying assumptions, we neglect excited bound states to write an effective Hamiltonian for the N_s lowest-energy one-particle states.

2.5.1 Weak Disorder Potential

If the energy of the disorder potential remains small compared with the lattice depth, we may treat all disorder terms perturbatively. In this case, we continue to use the set of Wannier functions defined by the underlying lattice, Eq. (2.4) as our basis.

The effective Hamiltonian terms for a perturbation of the form $\mathcal{D}(\boldsymbol{r})$ are given

by

$$J_{ij} - J = -\int \mathrm{d}\boldsymbol{r}\, \phi^*(\boldsymbol{r} - \boldsymbol{R}_i)\mathcal{D}(\boldsymbol{r})\phi(\boldsymbol{r} - \boldsymbol{R}_j) \tag{2.18}$$

$$\mu_i = -\int \mathrm{d}\boldsymbol{r}\, \phi^*(\boldsymbol{r} - \boldsymbol{R}_i)\mathcal{D}(\boldsymbol{r})\phi(\boldsymbol{r} - \boldsymbol{R}_i) \tag{2.19}$$

while $U_i = U$ remains unchanged as our basis functions remain the same.

2.5.2 Strong Disorder Potential

If the scale of $\mathcal{D}(\boldsymbol{r})$ approaches that of the lattice potential, the approximation above begins to fail. In this case, the states of the system may simply not be captured by the vector space spanned by the lowest-band Wannier functions. Instead, we are must define a new set of basis functions.

To find this basis, we first make the simplifying assumption that the disorder potential is composed of a set of spatially separated impurities,

$$\mathcal{D}(\boldsymbol{r}) = \sum_m \mathcal{D}_m(\boldsymbol{r}) \tag{2.20}$$

where the summation is over some number of impurities less than N_s but on the same order. We take each local potential $\mathcal{D}_m$ to be centered around some $\boldsymbol{X}_m$, and assume it affects only the sites adjacent to it, $S_m^{(1)} = \{i \text{ s.t. } |\boldsymbol{R}_i - \boldsymbol{X}_m| \leq \Delta\}$.

Examining a particular impurity, we now restrict ourselves to a small subset of sites adjacent to it. We mark the set of nearest neighbors to $S_m^{(1)}$ by $S_m^{(2)} = \{i \text{ s.t. } i \notin S_m(1); \exists j \in S_m(1), |\boldsymbol{R}_i - \boldsymbol{R}_j| \leq \Delta\}$, and their union $S_m = S_m^{(1)} \cup S_m^{(2)}$. The single-particle Hamiltonian for these sites is given by

$$\hat{H}_m^{sp} = \sum_{\substack{\langle i,j \rangle \\ i,j \in S_m}} J_{ij}\left(\hat{a}_i^\dagger \hat{a}_j + \hat{a}_j^\dagger \hat{a}_i\right) - \sum_{i \in S_m} \mu_i \hat{a}_i^\dagger \hat{a}_i. \tag{2.21}$$

We obtain the parameters for this Hamiltonian by numerically integrating the single-particle wavefunction within the space it defines.

We first numerically diagonalize the free-space Hamiltonian,

$$\hat{H}_m^0 = \frac{\hat{p}^2}{2m} + \sum_{\alpha=x,y,z} V_0^\alpha \sin^2(k_L r_\alpha) \tag{2.22}$$

for the space around the basis vectors included in S_m. We obtain the Wannier function $\phi_m^{(0)}(\boldsymbol{r})$. As discussed in Section 2.1, the set of functions $\phi_m^{(0)}(\boldsymbol{r} - \boldsymbol{R}_i)$, for $i \in S_m$, forms a complete basis for the single-particle wavefunctions in the lowest energy band of $\hat{H}_m^0$. Next, we introduce the impurity, diagonalizing, for the same space,

$$\hat{H}_m^D = \frac{\hat{p}^2}{2m} + \sum_{\alpha=x,y,z} V_0^\alpha \sin^2(k_L r_\alpha) + \mathcal{D}_m(\boldsymbol{r}). \tag{2.23}$$

The 4^D lowest-energy wavefunctions of this Hamiltonian span the vector space the Ψ_m, defining its lowest energy band. We wish to find a local set of functions $\phi_{m,i}^{(1)}$ to span this space.

Next, we make use our assumption on the short-range effects of the impurity potential. We take the sites in $S_m^{(2)}$ to be unaffected by the impurity. Therefore we have $\phi_{m,i}^{(1)} = \phi_i^{(0)}$ for $i \in S_m^{(2)}$. The remaining subspace,

$$\Delta\Psi_m \equiv \Psi_m \setminus \mathrm{span}\Big\{ \phi_{\mathrm{i}}^{(0)} \text{ s.t. } \mathrm{i} \in \mathrm{S}_{\mathrm{m}}^{(2)} \Big\} \tag{2.24}$$

has dimensions 2^D. We choose a local basis, $\phi_{m,i}^{(1)}$, for $i \in S_m^{(1)}$, by rotating it to minimizing their overlap, $\sum_{i,j\in S_m^{(1)}} \int \mathrm{d}\boldsymbol{r} \left|\phi_{m,i}^{(1)}(\boldsymbol{r})\right|^2 \left|\phi_{m,j}^{(1)}(\boldsymbol{r})\right|^2$.

Therefore we have an effective Hamiltonian

$$\begin{aligned} \hat{H}_{m,\mathrm{eff}} = &\sum_{i,j\in S_m^{(2)}} \left|\phi_i^{(0)}\right\rangle \langle\phi_i|\hat{a}_i \hat{H}_m^D \left|\phi_j^{(0)}\right\rangle \left\langle\phi_j^{(0)}\right| \\ &+ \sum_{i,j\in S_m^{(1)}} \left|\phi_i^{(1)}\right\rangle \left\langle\phi_i^{(1)}\right| \hat{a}_i \hat{H}_m^D \left|\phi_j^{(1)}\right\rangle \left\langle\phi_j^{(1)}\right|, \end{aligned} \tag{2.25}$$

where $\left|\phi_i^{(0)}\right\rangle = \int \mathrm{d}\boldsymbol{r}\, \phi_m^{(0)}(\boldsymbol{r} - \boldsymbol{R}_i)\hat{\psi}_{\boldsymbol{r}}^\dagger|\mathrm{vac}\rangle$. The parameters of Eq. (2.23) are now extracted as described in Section 2.2.2. One example of this is seen in Fig. 2.6.

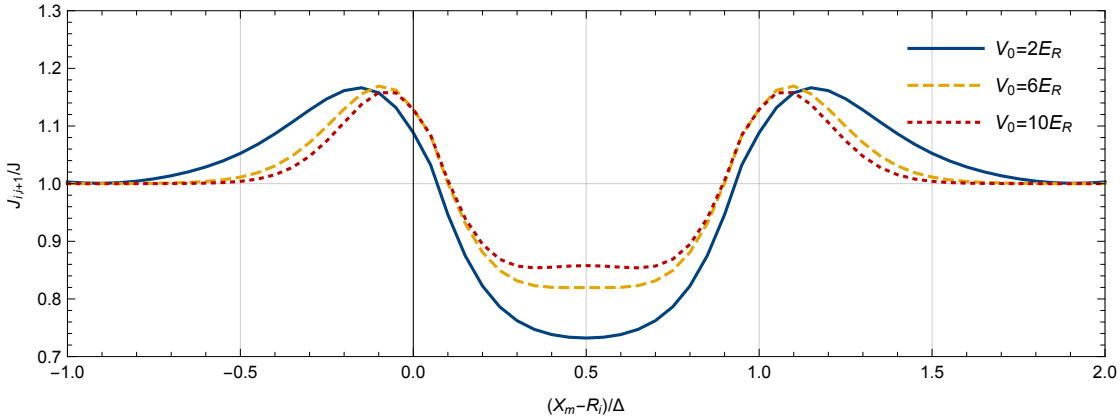

(a) Hopping Parameter

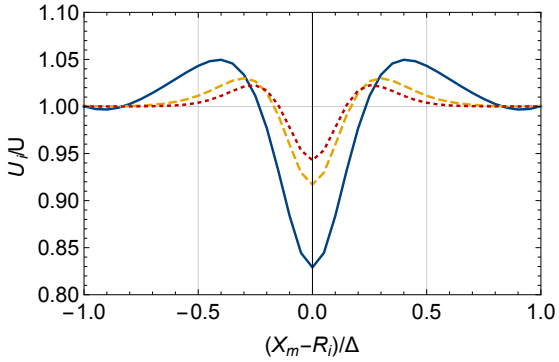

(b) Interaction Strength

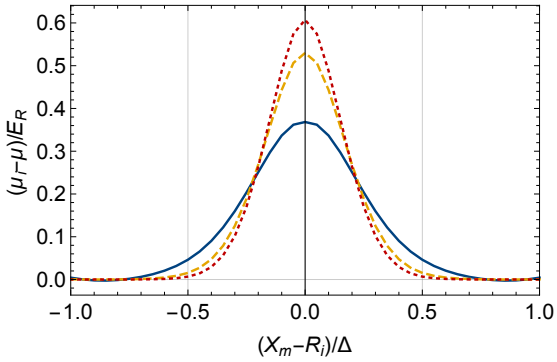

(c) Local Potential

Figure 2.6: The effect of a localized repulsive gaussian potential at position X_m on the adjacent parameters of the Hubbard model. They are shown for an effectively one-dimensional lattice (see Fig. 2.4) with lattice constant Δ, at various lattice depths. Here the impurity potential, $\mathcal{D}_m(x) \approx 1.2E_R e^{-72(x-X_m)^2}$, is a good approximation of a potential created by secondary particle species trapped in an auxiliary lattice (see Section 2.4). (a) The hopping parameter is suppressed for hopping through the impurity, but boosted for hopping away from the impurity, as the wavefunctions have a larger overlap. (b), (c) Similarly, an on-site impurity widens the local Wannier wavefunction, reducing on-site interaction strength, even as it increases the per-particle energy. An adjacent impurity bunches the wavefunction away from it, increasing interaction strength.

2.6 Many-Body Theoretical Methods

Though the simplified form of the Bose Hubbard Hamiltonian of Eq. (2.8) is easy to understand, its many body eigenstates are still difficult to solve. They are governed by a competition between the momentum-space form of the hopping term and the position-space form of the interaction term. Thus the eigenstates of free particles are simply the momentum-space states, while turning off hopping leaves us with a series of single sites described by simple number density states.

Theoretical treatment of each phase of the Hubbard model is inspired by these extreme situations. A perturbative expansion around the pure ground states – the condensate on the superfluid side or the number state on the Mott insulator side – gives a good picture of the ground state and low-lying excitations. Another common technique, which provides some results across the phase boundary, is the Gutzwiller ansatz. Here we give an overview of each of these methods.

2.6.1 Bogoliubov Superfluid Mean Field Theory

For non-interacting bosons, the Hubbard model is given by

$$\hat{H} = J \sum_k \varepsilon_k \hat{a}_k^\dagger \hat{a}_k. \tag{2.26}$$

The zero-temperature ground state of this Hamiltonian is

$$|\psi_G\rangle = \frac{\left(\hat{a}_0^\dagger\right)^{\bar{n}N_s}}{\sqrt{\bar{N}_s!}}|\text{vac}\rangle, \tag{2.27}$$

with $\left\langle \hat{a}_0^\dagger \hat{a}_0 \right\rangle = \bar{n}N_s$, $\left\langle \hat{a}_k^\dagger \hat{a}_{k\neq 0} \right\rangle = 0$. This wavefunction is described by

$$\hat{a}_0 = \sqrt{N_s \bar{n}} + O\Big(\tfrac{1}{N_s}\Big), \qquad \hat{a}_{k\neq 0} = 0. \tag{2.28}$$

Inspired by this state, we add interactions as a perturbation. We demote the condensate density to a scalar

$$\hat{a}_0 \to \sqrt{N_s n_0} = \sqrt{N_s \bar{n} - \sum_{k\neq 0} \hat{a}_k \hat{a}_k} \tag{2.29}$$

to find for all other momenta

$$\begin{aligned}\hat{H}_{Bog} = &\sum_k \left[J\Delta\varepsilon_k + \frac{U}{2}\left(2\bar{n} - \frac{1}{N_s}\sum_p \hat{a}_p^\dagger \hat{a}_p\right)\right]\hat{a}_k^\dagger \hat{a}_k \\ &+ \frac{U}{2}\sum_k \left[\bar{n} - \frac{1}{N_s}\sum_p \hat{a}_p^\dagger \hat{a}_p\right]\left(\hat{a}_k \hat{a}_{-k} + \hat{a}_k^\dagger \hat{a}_{-k}^\dagger\right) + \frac{U}{2}\sum_{p,k} \hat{a}_p^\dagger \hat{a}_{-p}^\dagger \hat{a}_k \hat{a}_{-k} \\ &U\sqrt{\frac{n_0}{N_s}}\sum_{(p,k)}\left(\hat{a}_p^\dagger \hat{a}_{p-k}\hat{a}_k + \hat{a}_k \hat{a}_{p-k}\hat{a}_p^\dagger\right) + \frac{U}{2}\frac{1}{N_s}\sum_{(p,k,q)} \hat{a}_p^\dagger \hat{a}_{k-q}^\dagger \hat{a}_{p-q}\hat{a}_k,\end{aligned} \tag{2.30}$$

where $\Delta\varepsilon_k = \varepsilon_k - \varepsilon_0$ and the summations marked (p,k) have no repeated indices.

We diagonalize the quadratic portion via a Bogoliubov transformation,

$$\begin{aligned}\hat{a}_k &= \cosh\theta_k \tilde{a}_k + \sinh\theta_k \tilde{a}_{-k}^\dagger \\ \tilde{a}_k &= \cosh\theta_k \hat{a}_k - \sinh\theta_k \hat{a}_{-k}^\dagger\end{aligned} \tag{2.31}$$

with $\theta_k = \theta_{-k}$. This construction maintains canonical commutation relations,

$$[\tilde{a}_k, \tilde{a}_q] = 0, \qquad \left[\tilde{a}_k, \tilde{a}_q^\dagger\right] = \delta_{k,q}. \tag{2.32}$$

Taking the creation operators as a small parameter $\hat{a}_k \sim U/J$, the Hamiltonian is diagonalized by setting

$$\tanh 2\theta_k = -\frac{Un_0}{J\Delta\varepsilon_k + Un_0}. \tag{2.33}$$

self-consistently with $\frac{1}{N_s}\sum_k \sinh^2\theta_k = \bar{n} - n_0$. The Hamiltonian is then diagonal,

$$\hat{H}_{Bog} = J\sum_k \sqrt{\Delta\varepsilon_k\left(\Delta\varepsilon_k + \frac{2Un_0}{J}\right)}\tilde{a}_k^\dagger \tilde{a}_k. \tag{2.34}$$

2.6.2 Doublon-Holon Expansion

When the hopping parameter is turned off, the Hubbard model decomposes into an array of single sites,

$$\hat{H} = \frac{U}{2} \sum_i \hat{a}_i^\dagger \hat{a}_i^\dagger \hat{a}_i \hat{a}_i. \tag{2.35}$$

For an integer particle density $\bar{n}$, the ground state takes on a parallel form to that of Eq. (2.27),

$$|\psi_G\rangle = \prod_i \frac{\left(\hat{a}_i^\dagger\right)^{\bar{n}}}{\sqrt{\bar{n}}} |\text{vac}\rangle. \tag{2.36}$$

As weak hopping is turned on, the wish to allow coherence between neighboring sites. Expecting the state to remain close to the ground state of Eq. (2.36), we consider that it will be spanned well by limiting the single-site occupation to $n_i \in \{\bar{n}-1, \bar{n}, \bar{n}+1\}$. The lattice become an array of spin-1 spins. We then think of the vacuum state as defined by equal occupation $\bar{n}$ at all sites, while excitations in the form of "doublons" (occupation $\bar{n}+1$) and "holons" (occupation $\bar{n}-1$) - the names are inspired by the case $\bar{n}=1$ - can form and move on the lattice.

We define the creation operators, by their action on the spinor $\chi_i = \begin{pmatrix} |\bar{n}+1\rangle_i & |\bar{n}\rangle_i & |\bar{n}-1\rangle_i \end{pmatrix}^T$

$$\hat{d}_i^\dagger = \begin{pmatrix} 0 & 1 & 0 \\ 0 & 0 & 0 \\ 0 & 0 & 0 \end{pmatrix}, \qquad \hat{h}_i = \begin{pmatrix} 0 & 0 & 0 \\ 0 & 0 & 0 \\ 0 & 1 & 0 \end{pmatrix}. \tag{2.37}$$

Transforming

$$\hat{a}_i^\dagger \hat{a}_j \to (\bar{n}+1)\hat{d}_i^\dagger \hat{d}_j + \bar{n}\hat{h}_i \hat{h}_j^\dagger + \sqrt{\bar{n}(\bar{n}+1)}\left(\hat{d}_i^\dagger \hat{h}_j^\dagger + \hat{h}_i \hat{d}_j\right) \tag{2.38}$$

$$\hat{a}_i^\dagger \hat{a}_i^\dagger \hat{a}_i \hat{a}_i \to \bar{n}(\bar{n}-1) + (2\bar{n}-1)\Big(\hat{d}_i^\dagger \hat{d}_i - \hat{h}_i^\dagger \hat{h}_i\Big) + \hat{d}_i^\dagger \hat{d}_i + \hat{h}_i^\dagger \hat{h}_i \tag{2.39}$$

we find

$$\begin{aligned}\hat{H}_{DH} = \sum_k \Big(\frac{U}{2} + J(\bar{n}+1)\varepsilon_k\Big)\hat{d}_k^\dagger \hat{d}_k + \Big(\frac{U}{2} + J\bar{n}\varepsilon_k\Big)\hat{h}_k^\dagger \hat{h}_k \\ + J\varepsilon_k\sqrt{\bar{n}(\bar{n}+1)}\Big(\hat{d}_k \hat{h}_{-k} + \hat{d}_k^\dagger \hat{h}_{-k}^\dagger\Big).\end{aligned} \tag{2.40}$$

We have used here that the difference between the total number of doublons and holons, $\sum_i \Big(\hat{d}_i^\dagger \hat{d}_i - \hat{h}_i^\dagger \hat{h}_i\Big)$, is fixed.

Though this Hamiltonian is quadratic, it is not trivial to solve. The new excitations are hard-core particles, and $\hat{d}_k, \hat{h}_k$ are not simple bosonic operators, having instead the commutation relations

$$\begin{aligned}\Big[\hat{d}_k, \hat{d}_q^\dagger\Big] &= \delta_{k,q} - 2\hat{n}_{q-k}^d - \hat{n}_{q-k}^h, \qquad \Big[\hat{d}_k, \hat{h}_q^\dagger\Big] = -\hat{\nu}_{q-k}^\dagger, \\ \Big[\hat{h}_k, \hat{h}_q^\dagger\Big] &= \delta_{k,q} - 2\hat{n}_{q-k}^h - \hat{n}_{q-k}^d, \qquad \Big[\hat{h}_k, \hat{d}_q^\dagger\Big] = -\hat{\nu}_{q-k}\end{aligned} \tag{2.41}$$

with

$$\begin{aligned}\hat{n}_k^d &= \frac{1}{N_s}\sum_p \hat{d}_{p+k}^\dagger \hat{d}_p \quad \hat{\nu}_k^\dagger = \frac{1}{N_s}\sum_p \hat{h}_{p+k}^\dagger \hat{d}_p, \\ \hat{n}_k^h &= \frac{1}{N_s}\sum_p \hat{h}_{p+k}^\dagger \hat{h}_p \quad \hat{\nu}_k = \frac{1}{N_s}\sum_p \hat{d}_p^\dagger \hat{h}_{p+k}.\end{aligned} \tag{2.42}$$

However, in the regime where $J \ll U$, we expect the number of excitations to be small. As these operations are proportional to the doublon and holon densities, they can be neglected, and the quasiparticles can be treated as regular bosons. The quadratic Hamiltonian of Eq. (2.40) then becomes immediately solvable by yet another Bogoliubov transformation, taking the form now

$$\begin{aligned}\hat{d}_k &= \cosh\theta_k \tilde{d}_k + \sinh\theta_k \tilde{h}_{-k}^\dagger \qquad \hat{h}_k = \cosh\theta_k \tilde{h}_k + \sinh\theta_k \tilde{d}_{-k}^\dagger \\ \tilde{d}_k &= \cosh\theta_k \hat{d}_k - \sinh\theta_k \hat{h}_{-k}^\dagger \qquad \tilde{h}_k = \cosh\theta_k \hat{h}_k + \sinh\theta_k \hat{d}_{-k}^\dagger.\end{aligned} \tag{2.43}$$

Taking

$$\tanh 2\theta_k = -\frac{2J\sqrt{\bar{n}(\bar{n}+1)}\varepsilon_k}{U + J(2\bar{n}+1)\varepsilon_k}, \tag{2.44}$$

the Hamiltonian takes the diagonal form

$$\begin{aligned}\hat{H}_{DH} = \frac{U}{2}\sum_k \sqrt{1 + 2(2\bar{n}+1)\tfrac{J\varepsilon_k}{U} + \left(\tfrac{J\varepsilon_k}{U}\right)^2}\left(\tilde{d}_k^\dagger \tilde{d}_k + \tilde{h}_k^\dagger \tilde{h}_k\right) \\ + \tfrac{J\varepsilon_k}{U}\left(\tilde{d}_k^\dagger \tilde{d}_k - \tilde{h}_k^\dagger \tilde{h}_k\right).\end{aligned} \tag{2.45}$$

2.6.3 Gutzwiller Ansatz

As seen in Eqs. (2.27) and (2.36), the ground states many-body wave-function decomposes into a product state on both sides of the phase diagram. It is natural to propose, then, a product state ansatz to span the whole range. The Gutzwiller variational wavefunction [62] expands the form of Eq. (2.36) to suggest

$$|\psi_G\rangle = \prod_i \left(\sum_n \alpha_n \tfrac{\left(\hat{a}_i^\dagger\right)^n}{\sqrt{n!}}\right)|\text{vac}\rangle. \tag{2.46}$$

The factors α are constrained by normalization and by the particle number,

$$\sum_n |\alpha_n|^2 = 1, \qquad \sum_n n|\alpha_n|^2 = \bar{n}. \tag{2.47}$$

Here,

$$\left\langle \hat{a}_i^\dagger \hat{a}_j \right\rangle = \left|\sum_n \sqrt{n}\alpha_n\alpha_{n-1}\right|^2, \qquad \left\langle \hat{a}_i^\dagger \hat{a}_i^\dagger \hat{a}_i \hat{a}_i \right\rangle = \sum_n n(n-1)|\alpha_n|^2 \tag{2.48}$$

and so the energy is given by

$$\tfrac{1}{N_s}\left\langle \hat{H} \right\rangle = -2DJ\left|\sum_n \sqrt{n}\alpha_n\alpha_{n-1}\right|^2 + \frac{U}{2}\sum_n n(n-1)|\alpha_n|^2. \tag{2.49}$$

The values of α_n can generally be determined numerically, taking a number of terms around $\alpha_{\bar{n}}$. An estimate can also be made of the phase transition point. If

we restrict the ansatz, to three terms returning essentially to the doublon-holon model, the conditions of Eq. (2.47) eliminate all but one degree of freedom. Finding

$$|\psi_G\rangle = \prod_i \Big(\sqrt{1-\theta^2}|\bar{n}\rangle_i + \theta|\bar{n}+1\rangle_i + \theta|\bar{n}-1\rangle_i \Big), \tag{2.50}$$

we find that the energy is minimized by $\theta = 0$ for

$$U \leq U_c = 2D\Big(2\bar{n} + 1 + 2\sqrt{\bar{n}(\bar{n}+1)}\Big)J. \tag{2.51}$$

A slightly more general, numerical, approach produces similar results, which can be seen in Fig. 2.1.

Part I

Displacement

CHAPTER 3

MAGNETIC POLARONS IN TWO-COMPONENT HARD CORE BOSONS

In the mid 1960's, Thouless and Nagaoka studied the two-component Fermi system on a bipartite lattice with very strong on-site repulsion [105, 151]. They found that in the presence of a single hole the ground state was a fully polarized ferromagnet. These and further studies showed that at finite temperatures the system is not fully polarized: near the hole there is a ferromagnetic "bubble", while far away the spins are uncorrelated [4, 66]. On such bipartite lattices, the statistics are irrelevant for the single-hole problem, and the same physics should be seen in the bosonic case as in the fermionic system. Thus the bosonic ground state is the Nagaoka state, and at finite temperature, ferromagnetic correlations are found near the hole. Here we calculate these correlations in a two-component gas of hard core lattice bosons. We find that at experimentally relevant temperatures these correlations are measurable using a quantum gas microscope [6].

This is the simplest example of emergent physics in a strongly correlated system. Variants of it are also highly nontrivial: for example the ground state of two component fermions on a non-bipartite lattice with a single hole is unknown. A qualitative picture of this ferromagnetism can be developed by imagining a child's puzzle where tiles slide on a square grid. One tile is missing. By moving this "hole" one can rearrange the tiles. Here we have a quantum mechanical version of this puzzle. The motion of the hole from one location to another involves summing all possible paths. If the tiles are in a symmetric superposition of all possible arrangements (corresponding to ferromagnetism) then these paths will add constructively, allowing the hole to move over large distances. This ferromagnetic arrangement

thereby minimizes the zero-point energy of the hole.

Borrowing the term from how electronic motion couples to lattice distortions, the elementary excitation consisting of a hole dressed by a ferromagnetic cloud is referred to as a "polaron". Other cold-atom polaron problems include the behavior of a single down-spin atom in a Fermi sea of up-spins [100, 120, 128, 143].

Even far from the strong-coupling hard-core limit studied here the physics of two-component bosons is quite rich. This physics has been explored in theoretical works [30, 42, 80, 92, 93], and in cold gas experiments [26, 51]. The components can be different hyperfine states [51], or different atomic species [26]. In the most ordered state there will be two independent order parameters, and it costs energy to twist the phase ϕ_1, ϕ_2, of either condensate. Depending on interaction parameters one can also find states where only some linear combination of the two phases has a finite stiffness. For example, with sufficiently strong attraction between the species there will be a condensate of "pairs" but no single particle condensate [112]: One then has a stiffness to twisting $\phi_1 + \phi_2$, but not $\phi_1 - \phi_2$. Even more exotic is the "counter-superfluid" phase formed when the interspecies repulsion becomes strong: One then has a stiffness to twisting $\phi_1 - \phi_2$. Under these circumstances trying to drive a current of species 1 to the right creates a current of species 2 to the left. Identifying the two components as the $\pm z$-component of a pseudospin-1/2 object – the counter-superfluid state corresponds to an $x - y$ ferromagnet. If the in-species interactions are not sufficiently strong, either of these exotic states can be preempted by phase separation or collapse. [115] In the single hole limit, the phase stiffnesses scale as the inverse of the system size.

Here we use a high temperature expansion to calculate the correlations between spins bordering a single hole in a two-component hard-core Bose system on the

square lattice. Using the techniques in [6, 47, 56, 72, 78, 111], these correlations can be directly measured, giving a signature of this interesting physics.

The temperature scale at which these correlations become significant is of order the hopping energy t. In physical units, this energy is on the order of $t \sim k_B \times (1\,\mathrm{nK})$ for ^{87}Rb atoms trapped by $\lambda = 820\,\mathrm{nm}$ lasers [145], but using lighter atoms such as ^{7}Li would increase the hopping energy energy and corresponding temperature by a factor of ten. Similarly, using a shorter wavelength lattice would also increase this scale.

Our study assumes hard-core interactions, where double occupancy is forbidden. In most experiments, the strength of on-site interactions U is fixed and the hard-core regime is achieved by increasing the height of the potential barrier between neighboring sites so that $t \ll U$. Corrections to the hard-core results scale as t/U. Spielman et al. [145] report results with $t/U \sim 0.001$.

Another relevant experimental detail is most cold atom systems are confined in harmonic traps. Local physics, such as the correlations we study, are unaffected by such confinement, as long as one restricts attention to regions where the polarons are dilute.

The physics of Nagaoka ferromagnetism is relevant for a number of other cold atom systems [113, 156].

This chapter is based on previously published work [163].

3.1 Analysis

We model the two-component Bose system via the single band Bose-Hubbard Hamiltonian

$$\hat{H} = -t \sum_{\langle i,j \rangle} \sum_{\sigma=\uparrow,\downarrow} \left(a^{\dagger}_{\sigma,i} a_{\sigma,j} + a^{\dagger}_{\sigma,j} a_{\sigma,i} \right) \tag{3.1}$$

where $a_{\sigma,i}$ ($a^{\dagger}_{\sigma,i}$) is the bosonic annihilation (creation) operator for a particles of type ("spin") σ at lattice site i, and $\langle i,j \rangle$ are all nearest-neighbor pairs and we limit ourselves to a two-dimensional square lattice. The single-particle spectrum has band-width of $8t$. We work in the canonical ensemble, with fixed particle number, and do not need to include a chemical potential.

The Bose-Hubbard model is a good description of the system as long as the band-spacing E_b is large compared with the other relevant energy scales. We require $t \ll E_b$ so that the (single-particle) bands are distinct, while $T \ll E_b$ is required so that all bosons are in the lowest band. In addition, we will be analyzing Eq. (3.1) within a high temperature expansion, requiring that the ratio T/t is not too small.

For a cold-atoms experiment described by the single-band Hubbard model, the band spacing varies with microscopic parameters as $E_b \sim \sqrt{V_0 E_R}$, where V_0 is the height of the potential barriers between lattice sites, $E_R = \hbar^2 k^2 / 2m$: $k = 2\pi/\lambda$ being the laser wavenumber and m the particle mass. The tunneling t depends exponentially on V_0 and is typically $t \sim 0.1 - 0.01 E_R$ for $V_0 \gtrsim E_R$ [75]. There is therefore a separation of scales, allowing $t \sim T \ll E_b$. Deeper lattices accentuate this separation, at the cost of requiring lower temperatures.

Strong interactions imply a hard-core constraint

$$a^{\dagger}_{\sigma,i} a^{\dagger}_{\tau,i} = 0, \tag{3.2}$$

which is valid when the on-site interactions are large compared to t.

We examine the case of a single hole in an infinite system and calculate the finite temperatures expectation values of an observable operator $\hat{X}$ by

$$\langle X \rangle = \frac{1}{Z} \operatorname{Tr} \hat{X} e^{-\beta \hat{H}}; \quad Z = \operatorname{Tr} e^{-\beta \hat{H}} \tag{3.3}$$

where $\beta = (k_B T)^{-1}$ is the inverse temperature; we take $k_B = 1$. The trace is most readily calculated in a basis given by placing the hole on the site r_h, and specifying the pseudospin $\sigma_i = \uparrow / \downarrow$ on all remaining sites $i \neq r_h$. We will look at the correlations between spins on positions which are fixed relative to r_h. For observables of that form, denoting by ζ a spin state with the hole at the origin, we have

$$\langle X \rangle = \frac{N_s}{Z} \sum_{\zeta} X(\zeta) \langle \zeta | e^{-\beta \hat{H}} | \zeta \rangle \tag{3.4}$$

where the factor N_s comes from summation over all N_s possible locations of r_h, and $\hat{X}|\zeta\rangle = X(\zeta)|\zeta\rangle$.

To perform the calculation we use a high-temperature expansion, $e^{-\beta \hat{H}} = \sum_{n=0}^{\infty} \frac{1}{n!} \left(-\beta \hat{H} \right)^n$. Each power of H corresponds to a single "hop" of the hole, and the moments can be calculated from the sum of all closed paths of length n ("$n - paths$") starting at the origin,

$$\langle \zeta | \left(-\beta \hat{H} \right)^n | \zeta \rangle = (\beta t)^n \sum_{p \in n-paths} \langle \zeta \mid \mathcal{P}_p(\zeta) \rangle. \tag{3.5}$$

Here $\mathcal{P}_p(\zeta)$ is the spin permutation that results from moving the hole through the path p. Any open paths, that do not take the hole back to the origin, do not

contribute to the sum, and the expectation value is zero if the path leads to a non-equivalent spin configuration. This requirement also restricts the sum to even values of n.

Although the number of closed paths grows exponentially with n, we are able to exhaustively enumerate them for small $n \leq 2M$, and calculate a high temperature approximant

$$\begin{aligned} \left\langle \hat{X} \right\rangle &\approx \frac{N_s}{Z} \sum_{n=0}^{M} \frac{(\beta t)^{2n}}{(2n)!} \sum_{p \in 2n-paths} \sum_{\zeta} X(\zeta) \delta(\zeta = \mathcal{P}_p(\zeta)) \\ Z &\approx N_s \sum_{n=0}^{M} \frac{(\beta t)^{2n}}{(2n)!} \sum_{p \in 2n-paths} \sum_{\zeta} \delta(\zeta = \mathcal{P}_p(\zeta)). \end{aligned} \tag{3.6}$$

We use $M = 6$.

Estimating the error of cutting off such series to be on the order of the last term calculated, the correlation functions for spins around the hole are accurate to about 10% down to $T/t \sim 0.4$ for $M = 6$. To investigate lower temperatures, one would need to resort to more sophisticated methods of summing the series, such as the Monte-Carlo approach of Raghavan and Elser [129]. Lower temperatures are difficult to achieve experimentally.

3.2 Vacancy-Induced Ferromagnetism

The tendency towards ferromagnetism is apparent in the structure of Eq. (3.6). Ferromagnetic configurations ζ automatically have $\mathcal{P}(\zeta) = \zeta$, regardless of the path p. A further insight is that it is only paths with loops in them that favor ferromagnetism. Paths p which retrace themselves have $\mathcal{P}(\zeta) = \zeta$ regardless of ζ.

To measure the polarization around the hole we define

$$\hat{S}_8 = \sum_{i \in n.n.n} \hat{S}_z^i \tag{3.7}$$

where S_z^i is the spin operator applied to the site i and the summation is over the eight nearest-neighbor and next-nearest neighbor sites of the hole. The ground state of our system possesses a spontaneously broken symmetry. In an infinite system with an infinitesimal magnetic field along z, $\hat{S}_8$ will have a finite expectation value. This expectation value vanishes as $T \to \infty$ and approaches 4 as $T \to 0$. If there is no symmetry breaking field, then the spontaneous symmetry breaking occurs in a random direction. In a typical cold-atoms experiment, every time a new sample is created, this symmetry-breaking direction will be different. Under those circumstances, one can model the ensemble measurement by taking expectation values in zero field. By symmetry, in zero field $\left\langle \hat{S}_8 \right\rangle = 0$, at all T, but the temperature dependence of its distribution will be non-trivial. At $T \to \infty$ when all states are equally likely we expect a binomial distribution around zero. At $T \to 0$, the distribution is uniform. This may be understood in several ways; in a quantum mechanical treatment, one would attribute this to the fact that each projection m of the spin multiplet is equally likely. Classically the z-component of a uniformly distributed random 3D unit vector is uniformly distributed. These distributions are shown in Fig. 3.1.

To quantify these distributions, we examine the variance of $\hat{S}_8$. We define

$$\begin{aligned} \hat{C}_8 &= \frac{3}{14}\left[\left(\hat{S}_8\right)^2 - 2\right], \\ &= \frac{3}{14}\left[\left(\sum_{i \in n.n.n.} \hat{S}_z^i\right)^2 - \sum_{i \in n.n.n.} \left(\hat{S}_z^i\right)^2\right], \end{aligned} \tag{3.8}$$

which is normalized and offset so that $\langle C_8 \rangle$ goes to unity when the hole is maximally polarized and to zero when all sites are uncorrelated. Note that individual

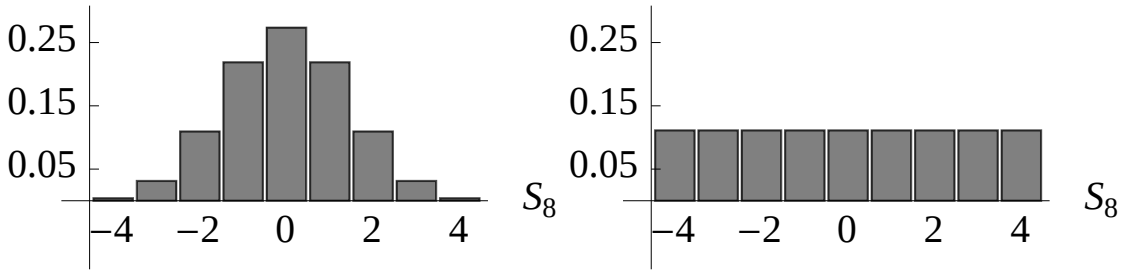

(a) $T \to \infty$ (b) $T = 0$

Figure 3.1: The probability distribution of $\langle S_8 \rangle$, the total spin of the bosons around the hole, at (a) $T \to \infty$ and (b) $T \to 0$.

measurements of $\hat{C}_8$ can be negative or greater than one.

We have calculated for a range of temperatures $\langle C_8 \rangle$ and the uncertainty $\Delta C_8 = \sqrt{\langle {C_8}^2 \rangle - \langle C_8 \rangle^2}$ and they are shown in Fig. 3.2. In particular, at temperatures corresponding to $T/t = 0.4$ we predict $\langle C_8 \rangle = 0.05$ and $\Delta C_8 = 0.62$. This compares with a $T \to \infty$ result of $\langle C_8 \rangle = 0$ and $\Delta C_8 = \sqrt{9/28} \approx 0.57$. Both the non-zero mean of this quantity and the increase in variance are indicative of the ferromagnetic correlations present around the hole. About 5000 measurements would be needed to determine the mean to within 20% of the predicted value. A given sample will contain multiple holes, so each experimental run can contribute multiple independent measurements.

3.3 Fixed Magnetization

In a cold atom experiment the number of ↑-spin and ↓-spin atoms are fixed, requiring a slightly different ensemble. This difference only matters when the correlation length becomes of the same order as the system size. For the temperatures described in Fig. 3.2, the correlation length is of order the lattice spacing, and these subtleties are irrelevant.

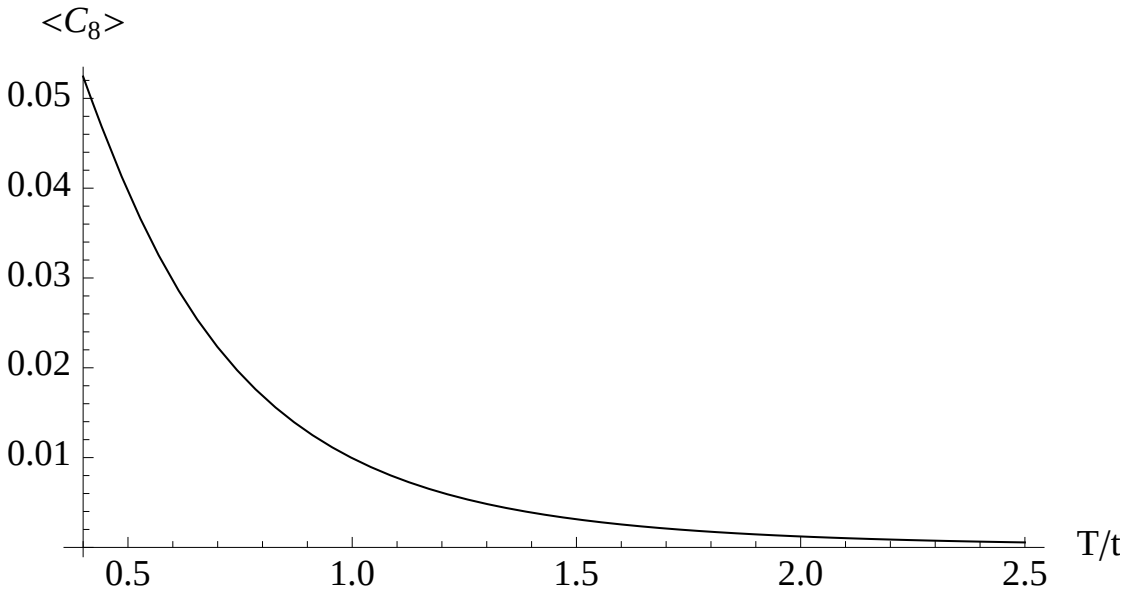

(a) Polarization around the hole

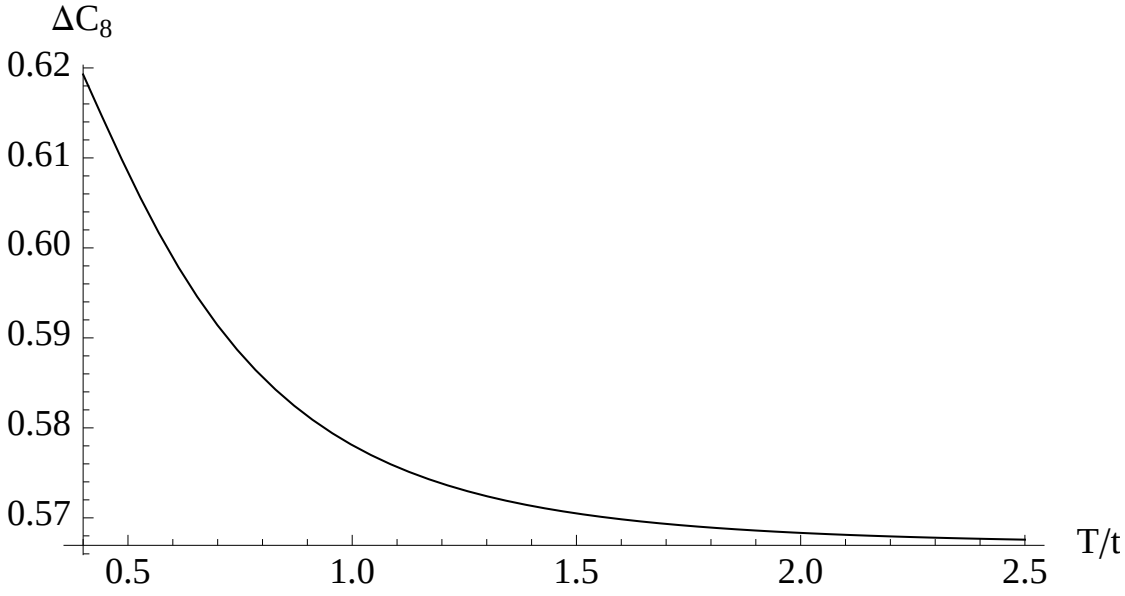

(b) Variation in the polarization around the hole

Figure 3.2: (a) $\langle C_8 \rangle$, the measure of polarization around the hole, and (b) $\Delta C_8 = \sqrt{\langle {C_8}^2 \rangle - \langle C_8 \rangle^2}$, as a function of the relative temperature T/t. Note that ΔC_8 goes to $\sqrt{9/28}$ as $T \to \infty$.

By using exact diagonalization on a small system we can, however, show that at an order of magnitude lower temperature one must consider these finite size effects. We consider a system of 5×3 sites described by the Hamiltonian in Eq. 3.1 with periodic boundary conditions, 7 $\uparrow$-spins, 7 $\downarrow$-spins and a single hole. We define a similar operator to the one used before

$$\hat{C}_8^f = \frac{3}{14}\left[\left(\hat{S}_8\right)^2 - 2 - 56C_2^\infty\right], \tag{3.9}$$

The constant $C_2^\infty = \langle S_z^1 S_z^2 \rangle$ is the infinite temperature two-spin correlation caused by the finite number of spins: $C_2^\infty = \frac{1}{4}\frac{1}{2-N_{\text{sites}}} = -\frac{1}{52}$ for an equal number of $\uparrow$ and $\downarrow$-spins.

The results are shown in Fig. 3.3. At high temperatures, one sees behavior indistinguishable from Fig. 3.2, while at low temperatures the expectation value is suppressed. This suppression can be attributed to the ferromagnetic order parameter being forced to lie in the $x - y$ plane.

3.4 Outlook

The problem of how charge and spin degrees of freedom interact with one another is key to a number of important condensed matter systems, most notably high temperature superconductors. More importantly, conceptually clean examples of strongly correlated phenomena, such as the two component Bose system one, are essential to developing new paradigms for many-body physics.

In a cold gas experiment the quantities $\langle S_8 \rangle$ and $\langle C_8 \rangle$ can be measured by a variant of the quantum gas microscope technique pioneered by Bakr et al. [6] and extended to spinor gases by Fukuhara et al [47]. An image is taken of the optical

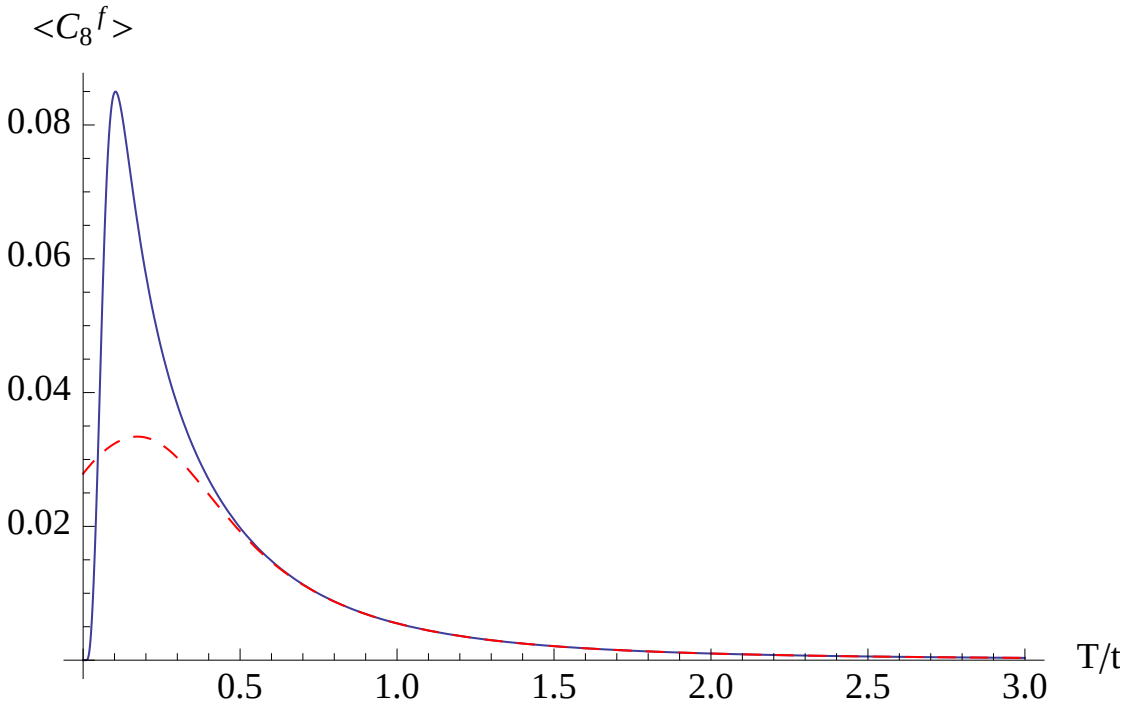

Figure 3.3: $\left\langle \hat{C}_8^f \right\rangle$ for a system of 3×5 sites with an equal number of $\uparrow$ and $\downarrow$ particles, as a function of temperature T/t. (solid blue line) Results from exact diagonalization, (dashed red line) result from high-temperature expansion taken to the same order as in Fig. 3.2. The two match well to about $T/t \sim 0.4$.

lattice, which shows the location of all particles, and their spin projection along a fixed axis. One would locate an isolated hole in this picture, and add up the spin projections of its neighbors to produce a single realization of S_8 or C_8. The experiment would be repeated many times. A histogram similar to Fig. 3.1 can be produced for S_8. The ensemble average can be compared with our prediction for the quantum mechanical expectation value $\langle C_8 \rangle$.

While the single-hole problem studied here is already interesting, the many-hole problem is even more rich. At zero temperature, the system is both superfluid and ferromagnetic. Kuklov et al. [80,92,93] have used Monte-Carlo methods to explore the relative strengths of superfluid and magnetic stiffnesses. Although no finite temperature studies have been done, both orders will disappear as one heats the

system. It would be interesting to know if magnetism or superfluidity vanish first, or if the two orders vanish simultaneously [109]. This question could be largely answered by studying the interaction between two polarons.

Part II

Density

CHAPTER 4

A PATH-INTEGRAL APPROACH TO THE SUPERFLUID DENSITY OF BOSONS IN OPTICAL LATTICES

4.1 Introduction

Superfluidity is one of the most profound collective manifestations of quantum mechanics [94, 98]. It is characterized by dissipation-less flow and is analogous to the vanishing resistivity seen in superconductors. The phenomenology of superfluidity is largely contained in Landau's two fluid model: one component, the normal fluid, responds to the motion of the container walls, while the other component, the superfluid, does not. The total density $\rho = \rho_n + \rho_s$ is the sum of the density of each component. Leggett showed that at zero temperature, in a translationally invariant system, either $\rho_s = 0$ or $\rho_n = 0$ [97]. In a lattice, however, even at $T = 0$, ρ_s/ρ_n can be finite. Here we calculate the superfluid fraction for an interacting Bose lattice gas in the large filling limit. Our study complements continuum calculations of superfluid densities [32, 42, 99, 127].

We are largely motivated by experiments of cold bosonic atoms in optical lattices [59]. These systems are well described by the Bose-Hubbard model described in Chapter 2 , which can be studied using mean field theories [138] and Quantum Monte Carlo methods [91, 157]. Further motivated by experiments where two bosonic species are trapped on a lattice [26, 51, 142], we also calculate the superfluid density of a two-component system. Such mixtures have rich behavior, including exotic phases such as paired superflow and counter-superflow [80, 93].

To calculate the superfluid fraction we use a functional integral approach, in-

cluding quadratic fluctuations about a coherent state which makes the action stationary. This method becomes exact in the weakly-interacting, low-temperature, high-density limit. We give finite temperature results and compare with exact numerical diagonalization on small systems.

Our calculation involves coherent state path integrals. As was previously established [159] there are difficulties with the continuous time limit of these objects. In the process of calculating the behavior of lattice bosons, we developed a formalism correcting these difficulties. We discuss the technical terms of this formalism in Chapter 5.

This chapter is structured as follows. In Section 4.2 we introduce the physical meaning and thermodynamic definition of the superfluid density. In Section 4.3 we present the results of the calculation in the case of a single species of bosons on a lattice, and in Section 4.4 we explore the superfluid properties of two-component bosons. Section 4.5 demonstrates the technical details of calculating thermodynamic quantities in this formalism.

This chapter is based on previously published material [160].

4.2 Superfluid Density

To define the superfluid density ρ_s we follow [98] and introduce a new thermodynamic variable $\boldsymbol{v}_s$ via a thought experiment. We imagine a fluid at rest within an infinitely long cylinder that is itself at rest. This defines the lab frame. We now give the cylinder an infinitesimal velocity $-\boldsymbol{v}_s$ along its axis. After we have allowed the container and fluid to reach equilibrium, the mass current as observed

in the *cylinder* frame of reference is

$$\boldsymbol{j} = \rho_s \boldsymbol{v}_s, \tag{4.1}$$

which defines ρ_s, the superfluid density. A normal fluid will move as a rigid body with the container and so have $\rho_s = 0$; an entirely superfluid liquid will feel no drag and remain at rest in the lab frame, yielding $\rho_s = \rho$. It is also convenient to define the remaining fraction of the particles as the normal density,

$$\rho = \rho_s + \rho_n. \tag{4.2}$$

Formally, we may calculate the superfluid density as the second derivative of the free energy density $\mathcal{F}$ with respect to $\boldsymbol{v}_s$,

$$\rho_s = \left. \frac{\partial^2 \mathcal{F}}{\partial v_s^2} \right|_{\boldsymbol{v}_s = 0}. \tag{4.3}$$

In a more technical language, this indicates that the superfluid density is the low-frequency, long wavelength limit of a transverse current-current correlation function [12].

In a translationally invariant system, for a fluid with well-defined quasiparticles, one can express Eq. (4.3) as a sum over the excitation spectrum, [117]

$$\rho_n = \int \frac{\mathrm{d}^3\mathrm{p}}{(2\pi\hbar)^3} \left(\frac{\boldsymbol{p} \cdot \boldsymbol{v}_s}{|\boldsymbol{v}_s|} \right)^2 \left(-\frac{\partial n_b}{\partial \epsilon_p} \right)_{\boldsymbol{v}_s = 0} \tag{4.4}$$

where $n_b = \left[e^{\beta \mathcal{E}_k} - 1 \right]^{-1}$ is the Bose-Einstein distribution function and ϵ_p is the energy of an excitation of momentum $\boldsymbol{p}$.

In three dimensions, the microscopic understanding of superfluidity involves condensation into a single macroscopically-occupied quantum state. If the wave-function of that condensed state is given by $\psi(\boldsymbol{r}, t) = \sqrt{\rho_c(\boldsymbol{r}, t)} e^{i\chi(\boldsymbol{r}, t)}$, then the

superfluid velocity v_s is directly related to the phase χ,

$$\boldsymbol{v}_s = \frac{\hbar}{m}\boldsymbol{\nabla}\chi(\boldsymbol{r}, t). \tag{4.5}$$

The variable ρ_c defines the condensate fraction, ρ_c/ρ, the portion of the system that is condensed into the ground state. This fraction is not, in general, equal to the superfluid fraction ρ_s/ρ.

4.2.1 Experimental probes of ρ_s

To measure ρ_s in a gas of cold atoms we propose the following experiment. One begins with an equilibrated Bose gas in an optical lattice, confined by an additional harmonic trap. The dimensionality can be controlled by adjusting the intensity of the lattice beams in the relevant directions. The harmonic trap is then turned off, and the lattice accelerated to velocity v_s by chirping the frequency of one of the lattice beams. One then turns off the lattice and uses time-of-flight expansion to measure the momentum p of the cloud. In the limit that all steps are adiabatic, the mass contained in the normal component is p/v_s. Converting this to a density or a superfluid fraction is trivial.

Gadway et al [50] have implemented a related protocol, but did not emphasize the fact that they were measuring the superfluid density. Alternate theoretical proposals involve rotation or artificial gauge fields. Ho and Zhou [67] showed that the superfluid density can be extracted from images of rotating clouds. John, Hadzibabic and Cooper [76] identified a global spectroscopic measure of superfluidity, while Carusotto and Castin [25] investigated a local probe.

4.3 The Superfluid Density in a Single Species

4.3.1 Model

We begin by analyzing the case of a single species of weakly-interacting bosons on an optical lattice. We begin with the single-band Bose-Hubbard Hamiltonian of Chapter 2, defined by the Hamiltonian of Eq. (2.8),

$$\hat{H} = -J \sum_{\langle i,j \rangle} \left(\hat{a}_i^\dagger \hat{a}_j + \hat{a}_j^\dagger \hat{a}_i \right) + \frac{U}{2} \sum_i \hat{a}_i^\dagger \hat{a}_i^\dagger \hat{a}_i \hat{a}_i - \mu \sum_i \hat{a}_i^\dagger \hat{a}_i. \tag{4.6}$$

As we are dealing with thermodynamic calculations, we have incorporated a chemical potential, μ. In this paper we focus on the case of a cubic D-dimensional lattice, taking the lattice spacing to be a_0 and the volume to be $V = N_s a_0^D$.

The Bose Hubbard model is a good description of the atomic system as long as the band spacing E_b is greater than all relevant energy scales in the system, $E_b \gg J, U, T$. Under these conditions, excitation into higher bands can be neglected. In cold atom experiments this spacing scales as $E_b \approx \sqrt{4 V_0 E_R}$ where $E_R = \frac{\hbar^2 k^2}{2m}$ is the recoil energy for particles of mass m trapped by lasers of wavenumber $k = 2\pi/\lambda$, and V_0 is the optical lattice depth, which is typically of order $V_0 \sim 10 - 100 \times E_R$. For near-optical lasers and particles lighter than $m \lesssim 100\,\text{amu}$ the single band approximation works up to $T \lesssim 10^{-6} K$ [75].

We introduce the velocity v_s into our model by applying a phase twist $\boldsymbol{\Delta}\Theta$ to the hopping term,

$$\hat{a}_i^\dagger \hat{a}_j \to e^{-i \boldsymbol{\Delta\Theta} \cdot (\boldsymbol{R}_i - \boldsymbol{R}_j)/a_0} \hat{a}_i^\dagger \hat{a}_j \tag{4.7}$$

or equivalently, $\hat{a}_j \to e^{i \boldsymbol{\Delta\Theta} \cdot \boldsymbol{R}_j / a_0} \hat{a}_j$, where $\boldsymbol{R}_i$ is the position of lattice site i. This

phase is related to the lattice velocity by

$$\boldsymbol{v}_s = \frac{\hbar}{m a_0} \boldsymbol{\Delta\Theta} \tag{4.8}$$

and so we obtain the relation

$$\rho_s^{\Delta\Delta'} = \frac{m^2 a_0^2}{\hbar^2} \left[\frac{\partial^2 \mathcal{F}}{\partial \Delta\Theta_\Delta \partial \Delta\Theta_{\Delta'}} \right]_{\boldsymbol{\Delta\Theta}=0} \tag{4.9}$$

where $\Delta, \Delta' = 1, \ldots, D = x, y, z$ are the lattice directions. In principle, the superfluid density on a lattice may be a symmetric rank 2 tensor, but for the cubic lattice one has $\rho_s^{\Delta\Delta'} = \delta_{\Delta,\Delta'} \rho_s$.

Like all thermodynamic quantities, the free energy density can be derived from the partition function,

$$\mathcal{F} = -\frac{1}{V} \frac{1}{\beta} \ln Z, \tag{4.10}$$

given by

$$Z = \mathrm{Tr}\, e^{-\beta \hat{H}} = \sum_{|\psi\rangle} \langle \psi | e^{-\beta \hat{H}} | \psi \rangle \tag{4.11}$$

where $\beta = 1/T$ is the inverse temperature and the sum is over a complete set of states $|\psi\rangle$. Introducing the overcomplete coherent state basis, $\hat{a}_i |\rho_i, \varphi_i\rangle = \sqrt{\rho_i} e^{i\varphi_i} |\rho_i, \varphi_i\rangle$, we break up the operator $e^{-\beta \hat{H}}$ into N_t slices and express the partition function as a path integral of the Euclidean action over the classical fields [1],

$$Z = \oint \mathcal{D}\rho \mathcal{D}\varphi \exp[-S_E]. \tag{4.12}$$

As discussed in Chapter 5, the overcomplete basis necessitates the use of the discrete time formulation of the action,

$$S_E = \sum_{t=0}^{N_t - 1} L_E^t \tag{4.13}$$

with

$$
\begin{aligned}
L_E^t &= \sum_i \left[-\log[\langle \rho_{i,t}, \varphi_{i,t} \mid \rho_{i,t+1}, \varphi_{i,t+1} \rangle] + \frac{\beta}{N_t} \frac{\langle \rho_{i,t}, \varphi_{i,t} | \hat{H} | \rho_{i,t+1}, \varphi_{i,t+1} \rangle}{\langle \rho_{i,t}, \varphi_{i,t} \mid \rho_{i,t+1}, \varphi_{i,t+1} \rangle} \right] \\
&= \sum_i \left[\frac{\rho_{i,t} + \rho_{i,t+1}}{2} - \sqrt{\rho_{i,t}\rho_{i,t+1}} e^{i(\varphi_{i,t+1} - \varphi_{i,t})} \right] \\
&\quad - J\Delta t \sum_{\langle i,j \rangle} \left[\sqrt{\rho_{i,t}\rho_{j,t+1}} e^{i(\varphi_{j,t+1} - \varphi_{i,t} - \Delta\Theta_{ji})} + \sqrt{\rho_{j,t}\rho_{i,t+1}} e^{i(\varphi_{i,t+1} - \varphi_{j,t} - \Delta\Theta_{ij})} \right] \\
&\quad + \frac{U\Delta t}{2} \sum_i \rho_{i,\tau}\rho_{i,\tau+1} e^{2i(\varphi_{i,\tau+1} - \varphi_{i,\tau})} - \mu\Delta t \sum_i \sqrt{\rho_{i,\tau}\rho_{i,\tau+1}} e^{i(\varphi_{i,\tau+1} - \varphi_{i,\tau})}
\end{aligned}
\tag{4.14}
$$

where $\Delta\Theta_{ij} = \boldsymbol{\Delta\Theta} \cdot (\boldsymbol{R}_i - \boldsymbol{R}_j)/a_0$ and $\Delta t = \beta/N_t$ is the discrete time step. We take the number of time steps to be large, $N_t \to \infty$.

4.3.2 Saddle-point Approximation

We expand the fields ρ_i, φ_i around the mean density $\bar{\rho}$ and mean phase twist $\boldsymbol{\Delta\Phi} = \sum_\Delta \Delta\Phi_\Delta \boldsymbol{\Delta}$, with $\boldsymbol{\Delta}$ the set of cubic lattice vectors. For any site i and its nearest neighbors along $\boldsymbol{\Delta}$, $i_{+\Delta}$ and $i_{-\Delta}$, we have

$$
\begin{aligned}
\rho_{i,t} &= \bar{\rho} + \delta\rho_{i,t} \\
\varphi_{i,t} &= \frac{1}{a_0} \boldsymbol{R}_i \cdot \boldsymbol{\Delta\Phi} + \phi_{i,t} \\
\varphi_{i_{+\Delta},t} - \varphi_{i,t} &= \Delta\Phi_\Delta + \phi_{i_{+\Delta},t} - \phi_{i,t} \\
\varphi_{i,t} - \varphi_{i_{-\Delta},t} &= \Delta\Phi_\Delta + \phi_{i,t} - \phi_{i_{-\Delta},t}.
\end{aligned}
\tag{4.15}
$$

We take these perturbations to be small, $\delta\rho_{i,t} \ll \bar{\rho}$, $\left|\phi_{i_{\pm\Delta},t} - \phi_{i,t}\right| \ll 1$, $|\phi_{i,t+1} - \phi_{i,t}| \ll 1$. The validity of these assumptions is examined below, in Section 4.3.5. In particular, when $T, U \lesssim \bar{\rho}J$ one finds $\left\langle \delta\rho_{i,t}^2 \right\rangle \sim \rho$ and $\left\langle (\phi_{x+1} - \phi_x)^2 \right\rangle \lesssim 1/\bar{\rho}$. Thus if $\bar{\rho} \gg 1$ this expansion is well behaved.

Although we assume $\left(\phi_{i_{\pm\Delta},t} - \phi_{i,t}\right)$ and $(\phi_{i,t+1} - \phi_{i,t})$ are small, we make no

assumption that $\phi_{i,t}$ itself is small. Consequently our calculation is valid even in low dimensions, where the condensate fraction vanishes and there is no long range order.

Equation (4.14) expanded around the mean values reads

$$L_E^t = \sum_i \mathcal{L}_0 + \mathcal{L}_1^{i,t} + \mathcal{L}_2^{i,t} + \mathcal{L}_{int}^{i,t}, \tag{4.16}$$

where each subsequent term involves higher powers of the fluctuations.

The first term is a constant,

$$\mathcal{L}_0 = \left[-\textstyle\sum_\Delta 2\bar{\rho} J \cos(\Delta\Phi_\Delta - \Delta\Theta_\Delta) + \frac{U}{2}\bar{\rho}^2 - \mu\bar{\rho} \right] \Delta t. \tag{4.17}$$

Keeping only this term gives the mean-field Gross-Pitaevskii approximation where $\rho_s = \bar{\rho} = \rho$.

The second term, linear in the perturbation, is

$$\mathcal{L}_1^{i,t} = \left[-2J \textstyle\sum_\Delta \cos(\Delta\Phi_\Delta - \Delta\Theta_\Delta) + U\bar{\rho} - \mu \right] \Delta t \delta\rho_{i,t}. \tag{4.18}$$

The saddle-point mean values minimizing $\mathcal{L}_0$ are

$$\begin{aligned} \Delta\Phi &= \Delta\Theta \\ \bar{\rho} &= \frac{1}{U}\left(\mu + 2J \sum_\Delta \cos(\Delta\Phi_\Delta) \right). \end{aligned} \tag{4.19}$$

Setting $\bar{\rho}$ to this value makes $\mathcal{L}_1$ vanish. Such a structure is generic, as minimizing the zeroth-order action causes the first order action to vanish. To calculate the superfluid density, we take $\mathbf{\Delta\Theta} = 0$ but keep $\mathbf{\Delta\Phi}$ finite, giving the bosons velocity $\frac{\hbar}{ma_0}\mathbf{\Delta\Phi}$ relative to the lattice. The superfluid density becomes $\rho_s = \frac{m^2 a_0^2}{\hbar^2}\left[\frac{\partial^2 \mathcal{F}}{\partial \Delta\Phi_d^2}\right]_{\mathbf{\Delta\Phi}=0}$.

The "interaction" term, which we neglect in our calculations, consists of terms of third order or higher in the perturbation fields,

$$\mathcal{L}^i_{int}/\bar{\rho} = O(\delta\rho/\bar{\rho}, \phi_j - \phi_i)^3 = O\big(1/\sqrt{\bar{\rho}}\big)^3. \tag{4.20}$$

Our non-trivial results come from the the quadratic term, which is best expressed in momentum space,

$$S_E = \sum_n \int \frac{\mathrm{a_0^D d^D k}}{(2\pi)^{\mathrm{D}}} \left[\frac{V}{{a_0}^D} \mathcal{L}_0 + \mathcal{L}_2^{\boldsymbol{k},\omega_n} + \mathcal{L}_{int}^{\boldsymbol{k},\omega_n} \right] \tag{4.21}$$

where summation is over $n = -\frac{N_t-1}{2} \ldots \frac{N_t-1}{2}$ with frequencies given by $\omega_n = \frac{2\pi}{\beta} n$, and the integration is over the first Brillouin zone $|k_d| \leq \pi/a_0$.

Section 4.5 provides details on the explicit form of $\mathcal{L}_2^{\boldsymbol{k},\omega}$ and the calculation of propagators. However, all significant physical results rely only on the behavior of the propagators and action at two regimes: $\omega\Delta t \ll 1$ (superscript p for pole behavior) and $\omega\Delta t = \pi e^{i\chi}$ (superscript $\circ$ for contour behavior). These are given, at $\Delta\Phi = 0$, by

$$\begin{aligned}
\langle \delta\rho\delta\rho \rangle^p_{\boldsymbol{k},\omega} &= \frac{V}{a_0^D} \bar{\rho} \left[\frac{1}{\Delta t} \frac{2\mathcal{E}_{1k}}{\omega^2 + {\mathcal{E}_k}^2} + O(\Delta t)^0 \right], \\
\langle \delta\rho\phi \rangle^p_{\boldsymbol{k},\omega} &= \frac{V}{a_0^D} \left[-\frac{1}{\Delta t} \frac{\omega}{\omega^2 + {\mathcal{E}_k}^2} + O(\Delta t)^0 \right], \\
\langle \phi\phi \rangle^p_{\boldsymbol{k},\omega} &= \frac{V}{a_0^D} \frac{1}{4\bar{\rho}} \left[\frac{1}{\Delta t} \frac{2\mathcal{E}_{2k}}{\omega^2 + {\mathcal{E}_k}^2} + O(\Delta t)^0 \right],
\end{aligned} \tag{4.22}$$

$$\begin{aligned}
\langle \delta\rho\delta\rho \rangle^\circ_{\boldsymbol{k},\omega} &= \frac{V}{a_0^D} \bar{\rho} \left[1 + \frac{\mathcal{E}_{1k}\Delta t}{1 - \cos(\pi e^{i\chi})} + O(\Delta t)^2 \right], \\
\langle \delta\rho\phi \rangle^\circ_{\boldsymbol{k},\omega} &= \frac{V}{a_0^D} \left[-\frac{1}{2} \frac{\sin(\pi e^{i\chi})}{1 - \cos(\pi e^{i\chi})} + O(\Delta t)^2 \right], \\
\langle \phi\phi \rangle^\circ_{\boldsymbol{k},\omega} &= \frac{V}{a_0^D} \frac{1}{4\bar{\rho}} \left[1 + \frac{\mathcal{E}_{2k}\Delta t}{1 - \cos(\pi e^{i\chi})} + O(\Delta t)^2 \right],
\end{aligned} \tag{4.23}$$

where we use the notation $\langle XY \rangle_{\boldsymbol{k},\omega} = \langle X_{\boldsymbol{k},\omega} Y_{-\boldsymbol{k},-\omega} \rangle$ and on the right it is under-

stood $\omega = \frac{\pi}{\Delta t} e^{i\chi}$. The energies appearing in these expressions are

$$\begin{aligned} \mathcal{E}_{1k} &= 4J \sum_{\Delta} \sin^2(\boldsymbol{k} \cdot \boldsymbol{\Delta}/2), \qquad \mathcal{E}_{2k} = 2\bar{\rho}U + \left(4J \sum_{\Delta} \sin^2(\boldsymbol{k} \cdot \boldsymbol{\Delta}/2) \right), \\ {\mathcal{E}_k}^2 &= \left[4J \sum_{\Delta} \sin^2(\boldsymbol{k} \cdot \boldsymbol{\Delta}/2) \right] \left[2\bar{\rho}U + \left(4J \sum_{\Delta} \sin^2(\boldsymbol{k} \cdot \boldsymbol{\Delta}/2) \right) \right]. \end{aligned} \tag{4.24}$$

In the continuum limit, one has $\mathcal{E}_{1k} \to \frac{\hbar^2 \boldsymbol{k}^2}{2m}$ and $\mathcal{E}_{2k} \to \frac{\hbar^2 \boldsymbol{k}^2}{2m} + 2g\rho$, where $g = U a_0^D / m$, $\rho = m\bar{n}/a_0^D$. The excitation spectrum $\mathcal{E}_k$ then corresponds to the familiar Bogoliubov result. These is the same spectrum of the Bogoliubov expansion of Section 2.6.1.

4.3.3 Calculation of the Superfluid Density

The superfluid density is given by

$$\rho_s = \frac{m^2 a_0^2}{\hbar^2} \left(-\frac{1}{\beta V} \right) \left[\frac{\partial^2 \ln Z}{\partial \Delta \Phi_x^2} \right]_{\boldsymbol{\Delta\Phi}=0}. \tag{4.25}$$

As mentioned above, it is generally a tensor, but reduces to a scalar for a cubic lattice. One may equally take the derivative in another direction of $\Delta\Phi$.

Some insight may be gained by inserting the path integral expressions for the free energy density and the partition function into this equation. We find that the superfluid density, to order $O(1/\bar{\rho})^0$, can be decomposed into three terms,

$$\rho_s = \frac{2ma_0^2 J}{\hbar^2} \frac{m}{a_0^D} \left[n_0 - n_n^U - n_n^{\rho\phi} \right]. \tag{4.26}$$

The first term is identified below as the total density, from which two normal-density terms are subtracted.

The densities defined by Eq. (4.26) are

$$\frac{2J}{a_0^D} n_0 = -\frac{1}{\beta V} \frac{N_t V}{a_0^D} \left\langle \left. \frac{\partial^2 \mathcal{L}_0}{\partial \Delta \Phi_x^2} \right|_{\bar{\rho}} \right\rangle - \frac{1}{\beta V} \sum_n \int \frac{\mathrm{a_0^D d^D k}}{(2\pi)^{\mathrm{D}}} \frac{\partial^2 \bar{\rho}}{\partial \Delta \Phi_x^2} \left\langle \left. \frac{\partial \mathcal{L}_2^{\boldsymbol{k},\omega_n}}{\partial \bar{\rho}} \right|_{\Delta\Phi} \right\rangle, \tag{4.27}$$

$$\frac{2J}{a_0^D} n_n^U = \frac{1}{\beta V} \sum_n \int \frac{\mathrm{a_0^D d^D k}}{(2\pi)^{\mathrm{D}}} \left\langle \frac{\partial^2 \mathcal{L}_2^{\boldsymbol{k},\omega_n}}{\partial \Delta \Phi_x^2} \right|_{\bar{\rho}} \Bigg\rangle, \tag{4.28}$$

$$\begin{aligned} &\frac{2J}{a_0^D} n_n^{\rho\phi} = \\ &\frac{1}{\beta V} \sum_{m,n} \int \frac{\mathrm{a_0^D d^D k}}{(2\pi)^{\mathrm{D}}} \frac{\mathrm{a_0^D d^D q}}{(2\pi)^{\mathrm{D}}} \left[\left\langle \frac{\partial \mathcal{L}_2^{\boldsymbol{k},\omega_n}}{\partial \Delta \Phi_x} \right|_{\bar{\rho}} \frac{\partial \mathcal{L}_2^{\boldsymbol{q},\omega_m}}{\partial \Delta \Phi_x} \Big|_{\bar{\rho}} \Bigg\rangle - \left\langle \frac{\partial \mathcal{L}_2^{\boldsymbol{k},\omega_n}}{\partial \Delta \Phi_x} \right|_{\bar{\rho}} \Bigg\rangle \left\langle \frac{\partial \mathcal{L}_2^{\boldsymbol{q},\omega_m}}{\partial \Delta \Phi_x} \right|_{\bar{\rho}} \Bigg\rangle \right]. \end{aligned} \tag{4.29}$$

Here, $\langle X \rangle = \frac{1}{Z} \oint \mathcal{D}\rho \mathcal{D}\varphi X \exp[S_E]$ is a thermodynamic average; on the right-hand side of the equations, derivatives in $\Delta\Phi_x$ and $\bar{\rho}$ are to be taken at a constant $\bar{\rho}$ and $\boldsymbol{\Delta\Phi}$, respectively, and then evaluated at $\boldsymbol{\Delta\Phi} = 0$; and we have omitted multiple vanishing terms. This is similar to the calculation shown explicitly in Section 4.5.

Using Eq. (4.27) in combination with Eqs. (4.17) and (4.19) we find $n_0 = -\frac{\partial \mathcal{F}}{\partial \mu}$, the total average occupation number. Explicitly,

$$n_0 = \bar{\rho} + \frac{1}{2} \int \frac{\mathrm{a_0}^{\mathrm{D}} \mathrm{d^D k}}{(2\pi)^{\mathrm{D}}} \left(1 - \frac{\mathcal{E}_{1k}}{\mathcal{E}_k} \coth(\beta \mathcal{E}_k / 2) \right). \tag{4.30}$$

At $T = 0$, one finds $n_0 \to (\mu + 2DJ)/U$ as $U/J \to 0$, and $n_0 \to \mu/U + \frac{1}{2}$ as $U/J \to \infty$. These correspond to the correct occupation numbers in the non-interacting and the no-hopping regimes. The explicit calculation of this term is given in Section 4.5. The chemical potential μ may be set to given the occupation number $\bar{\mu}$.

The term $n_n^{\rho\phi}$ is given by

$$n_n^{\delta\rho\phi} = \int \frac{\mathrm{a_0}^{\mathrm{D}} \mathrm{d^D k}}{(2\pi)^{\mathrm{D}}} 2J \sin^2(k_x a_0/2) \left(-\frac{\partial n_b}{\partial \mathcal{E}_k} \right)_{\Delta\Phi=0}. \tag{4.31}$$

This expression is reminiscent of the form of the normal density in the continuum case, given in Eq. (4.4), and it likewise vanishes at $T = 0$.

The additional term, n_n^U, can be understood to come from density-density and phase-phase correlations created by the interaction term in the hamiltonian.

$$n_n^U = \int \frac{\mathrm{a_0{}^D d^D k}}{(2\pi)^{\mathrm{D}}} \sin^2(k_x a_0/2) \left[\frac{(\mathcal{E}_{1k} + \mathcal{E}_{2k})}{2\mathcal{E}_k} \coth(\beta \mathcal{E}_k/2) - 1 \right]. \tag{4.32}$$

At $T = 0$, $U = 0$, this term vanishes and the superfluid fraction becomes one; at non-zero values of U this term is finite even at $T = 0$.

The resulting superfluid fraction, ρ_s/ρ, is plotted in Fig. 4.1 at zero temperature as a function of U/J and in Fig. 4.2 for set values of U/J as a function of temperature. In Fig. 4.3 we show the curve $U(T)$ where ρ_s vanishes, suggesting a phase transition.

The limits of validity of these results will be discussed in Section 4.3.5.

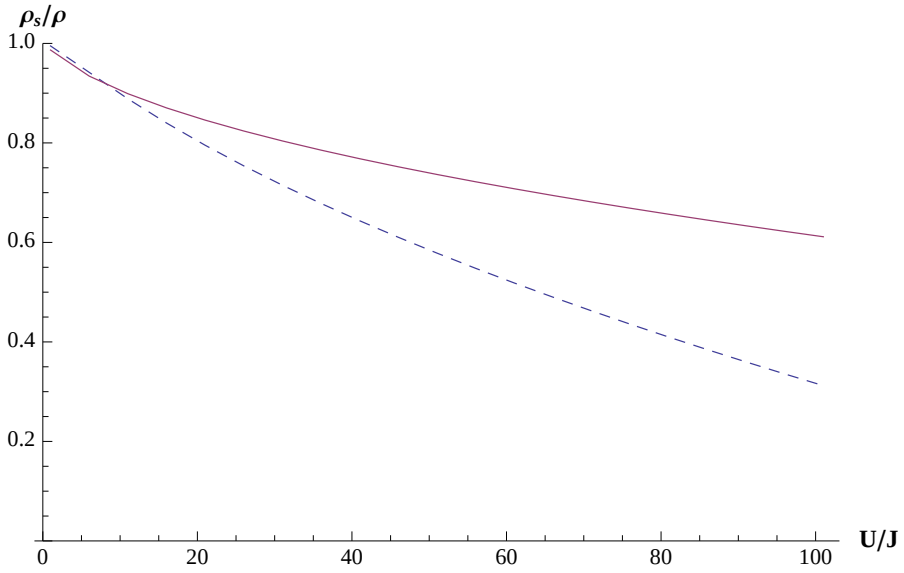

Figure 4.1: The superfluid fraction ρ_s/ρ as function of U/J in an infinite 3D cubic lattice, for $\bar{n} = 10$ (solid red line) and $\bar{n} = 1$ (dashed blue line), calculated to leading order in a $1/\bar{n}$ expansion. As discussed in the text, the results are not expected to be quantitatively accurate above $U/J \gtrsim \bar{n}$.

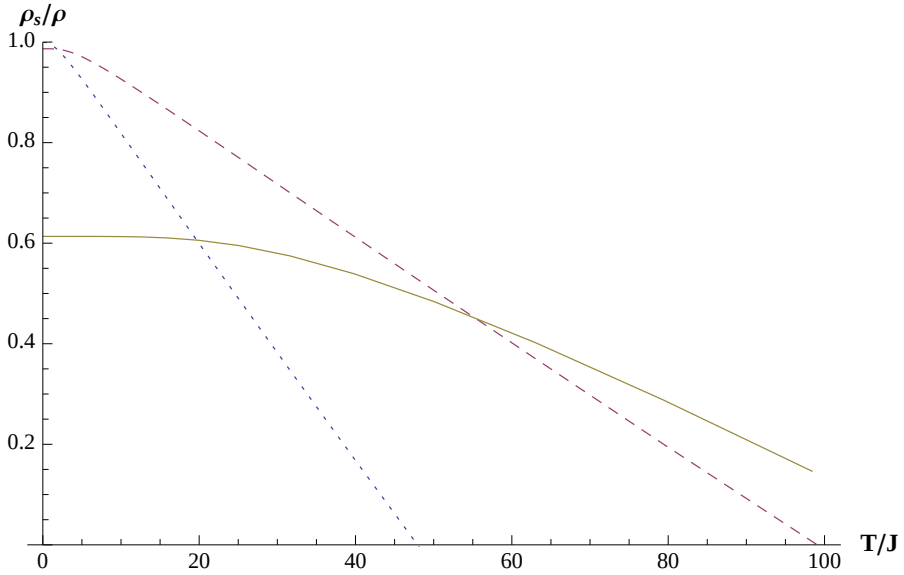

Figure 4.2: The superfluid fraction ρ_s/ρ as function of T/J in an infinite 3D cubic lattice, for $\bar{n} = 10$, at $U/J = 0.01$ (dotted blue line), $U/J = 1$ (dashed red line) and $U/J = 100$ (solid yellow line). At $U = 0$, ρ_s vanishes at $T/J = 41.5$, the ideal gas transition temperature. As discussed in the text, the results are not expected to be quantitatively accurate at $T/\sqrt{J(J + \bar{\rho}U)} \gtrsim \langle n \rangle$.

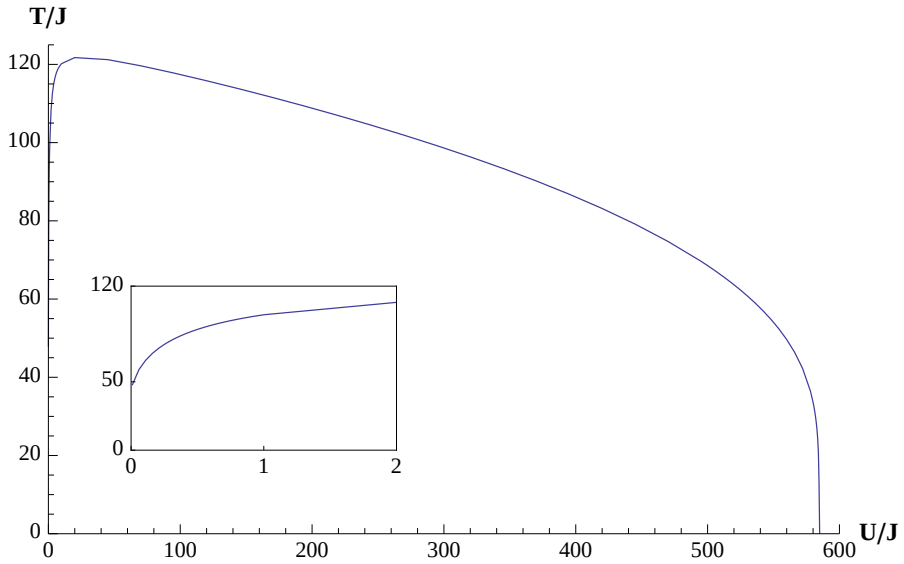

Figure 4.3: The values of $U/J, T/J$ at the intercept $\rho_s = 0$, suggesting a superfluid-Mott insulator transition. The calculation is performed for an infinite 3D cubic lattice, with $\bar{n} = 10$. The inset shows the form of the curve at small T/J. As discussed in the text, the results are not expected to be quantitatively accurate at values of $U/J \gtrsim \bar{n}$ or $T/\sqrt{J(J + \bar{\rho}U)} \gtrsim \bar{n}$, but the form is qualitatively similar to curves generated by quantum Monte Carlo methods [23].

4.3.4 Analytical Limits

Here we examine the behavior of Eq. (4.26) in several limiting cases.

First we compare our result to the continuum limit by taking $a_0 \to 0, J \to \infty$ so that Ja_0^2 is constant. In this case, the second term Eq. (4.32) vanishes. This can be seen by separately considering the contributions from $k \sim 1/a_0$ and $k \ll 1/a_0$; in both cases the integrand vanishes. The first part of the normal density, Eq. (4.31), has contribution only from finite momenta, and becomes

$$\frac{m}{a_0^D} n_n^{\delta\rho\phi} \to 2mJa_0^2 \int \frac{\mathrm{d^D k}}{(2\pi)^{\mathrm{D}}}\, k_d^2 \left(-\frac{\partial n_b}{\partial \mathcal{E}_k^c}\right)_{\Delta\Phi=0}, \tag{4.33}$$

with $\mathcal{E}_k^c$ the continuum spectrum. Identifying $2mJa_0^2/\hbar^2 \to 1$, this is precisely the known continuum result seen in Eq. (4.4).

Another important limit is zero temperature and large $\bar{\rho}$. If $U \sim J$, then $\bar{\rho}U \gg J$ and to first order $\mathcal{E}_k \approx \sqrt{8UJ\bar{\rho}\big(\sum_\Delta \sin^2(\boldsymbol{k}\cdot\boldsymbol{\Delta}/2)\big)}$, $\mathcal{E}_{1k} + \mathcal{E}_{2k} \approx 2\bar{\rho}U$ and the normal density becomes

$$n_n^U \approx \int \frac{\mathrm{a_0^D d^D k}}{(2\pi)^{\mathrm{D}}} \sin^2(k_x a_0/2) \frac{(\bar{\rho}U)}{\mathcal{E}_k} - 1 \approx \bar{\rho}\left[\sqrt{\frac{1}{f_D}\frac{U}{J\bar{\rho}}}\right] - \frac{1}{2} \tag{4.34}$$

where

$$\frac{1}{\sqrt{f_D}} = \int \frac{\mathrm{d^D}\theta}{(2\pi)^{\mathrm{D}}} \frac{\sin^2(\theta_x/2)}{\sqrt{8\big(\sum_\Delta \sin^2(\theta_\Delta/2)\big)}} \tag{4.35}$$

has $f_D \approx 20, 35, 51$ in one, two and three dimensions respectively. This expression is suggestive of a phase transition from superfluid to Mott insulator at a critical $U = U_c \sim f_D \bar{\rho} J$. In two and three dimensions, the values for f_D are about double the mean-field result of $U_c \sim 2D \times 4\big(\bar{n} + \frac{1}{2}\big)$ [154]. More comparisons along these lines are made in Section 4.3.6. As discussed in Section 4.3.5, these estimates are beyond the range of U/J where our approximations are quantitatively valid. It is nonetheless appealing to see the Mott transition appearing within this formalism.

Finally we consider the free particle case, $U = 0$. There, a function of T,

$$\begin{aligned} n_n &= n_n^U + n_n^{\rho\phi} = \\ &\int \frac{{\mathrm{a_0}}^{\mathrm{D}}\mathrm{d}^{\mathrm{D}}\mathrm{k}}{(2\pi)^{\mathrm{D}}}\,\frac{1}{2}(\coth(\beta\mathcal{E}_k/2)-1) \\ &+\int \frac{{\mathrm{a_0}}^{\mathrm{D}}\mathrm{d}^{\mathrm{D}}\mathrm{k}}{(2\pi)^{\mathrm{D}}}\,\frac{1}{2}\left[\cos(k_x a_0)(1-\coth(\beta\mathcal{E}_k/2)) + \tfrac{\beta J\sin^2(k_x a_0)}{\sinh^2(\beta\mathcal{E}_k/2)}\right]. \end{aligned} \tag{4.36}$$

The integrand in the first line $\frac{1}{2}(\coth(\beta\mathcal{E}_k/2)-1) = n_b(\mathcal{E}_k)$ and the one in the second is a total derivative that vanishes at $k_x a_0 = 0, 2\pi$, and so $n_n = n_{ex}$, the total occupation of excited states. ρ_s vanishes at $\bar{n} = n_{ex}$, corresponding to the ideal gas transition temperature.

4.3.5 Realm of Validity

Though the formulation of the action in Eq. (4.14), Eq. (4.21) is exact, our calculations are performed by neglecting the infinite series of terms in $\mathcal{L}_{int}^{\boldsymbol{k},\omega}$. We can place bounds on the realms of validity of this approximation by requiring that the perturbations from the mean values $\bar{\rho}$, $\Delta\Phi$ be small,

$$\begin{aligned} \langle\delta\rho_{i,t}\delta\rho_{i,t}\rangle &\lesssim \bar{\rho}^2 \\ \left\langle\left(\phi_{i_{+d},t}-\phi_{i,t}\right)^2\right\rangle &\lesssim 1 \\ \left\langle\left(\phi_{i,t+1}-\phi_{i,t}\right)^2\right\rangle &\lesssim 1. \end{aligned} \tag{4.37}$$

We do not require the phases themselves to be small, only the deviation from one site to another and from one time step to another.

These fluctuations can be calculated by the use of the propagators in Eq. (4.22),

$$\left\langle\left(\phi_{i,t+1}-\phi_{i,t}\right)^2\right\rangle = \frac{1}{2\bar{\rho}}, \tag{4.38}$$

$$\left\langle \left(\phi_{i_{+d},t} - \phi_{i,t}\right)^2 \right\rangle = \frac{1}{4\bar{\rho}}\left[2 + \int \frac{\mathrm{a_0^D d^D k}}{(2\pi)^{\mathrm{D}}} \frac{\mathcal{E}_k}{J} \coth(\beta\mathcal{E}_k/2)\right], \tag{4.39}$$

$$\frac{\langle \delta\rho_i \delta\rho_i \rangle}{\bar{\rho}^2} = \frac{1}{\bar{\rho}}\left[1 + \int \frac{\mathrm{a_0^D d^D k}}{(2\pi)^{\mathrm{D}}} \frac{\mathcal{E}_{1k}}{\mathcal{E}_k} \coth(\beta\mathcal{E}_k/2)\right]. \tag{4.40}$$

Examination of the integrals in the latter two inequalities implies that to to keep these parameters small we must have

$$\begin{aligned} \bar{\rho} &\gtrsim 1 \\ U/J &\lesssim \bar{\rho} \\ T/J &\lesssim \bar{\rho} \\ T/\sqrt{J(J+\bar{\rho}U)} &\lesssim \bar{\rho}, \end{aligned} \tag{4.41}$$

where the first constraint is universally required, the second stems from the density fluctuations in Eq. (4.40) and the last two from the phase fluctuations in Eq. (4.39).

4.3.6 Gutzwiller Ansatz

At zero temperature, an alternative approach to calculating the superfluid density is to use the Gutzwiller ansatz, described in Section 2.6.3 [90]. We use it here as a point of comparison for our results.

Beginning with the Gutzwiller ansatz of Eq. (2.46), we transform hopping terms as in Eq. (4.7). The superfluid density is then given by

$$\begin{aligned} \rho_s &= \frac{m^2 a_0^2}{\hbar^2} \frac{1}{V}\left[\frac{\partial^2}{\partial \Delta\Phi_x^2} \langle \psi_G | \hat{H} | \psi_G \rangle\right]_{\mathbf{\Delta\Phi}=0} \\ &= \frac{2ma_0^2 J}{\hbar^2} \frac{m}{a_0^D}\left(\sum_m \sqrt{m+1}\alpha^{m+1}\alpha^m\right)^2. \end{aligned} \tag{4.42}$$

We calculated the parameters α^m numerically by cutting off the sum at $m = 20$. We compare the results with those of Eqs. (4.26) to (4.32), in Fig. 4.4.

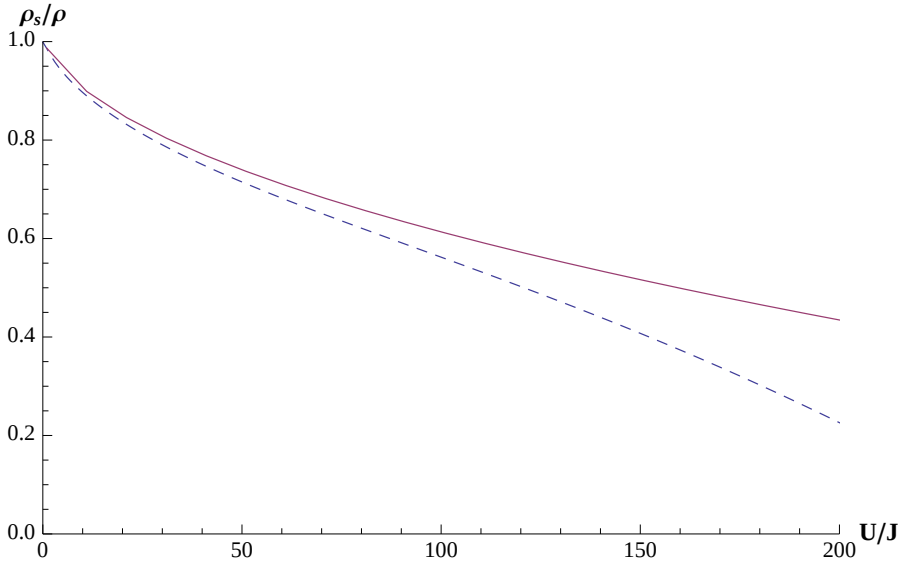

Figure 4.4: The superfluid fraction ρ_s/ρ for an infinite three-dimensional cubic lattice with $\bar{n} = 10$, at $T = 0$. The dashed blue line shows the result of the Gutziller ansatz calculation and the solid red line shows result as calculated using Eqs. (4.26) to (4.32).

4.3.7 Numerical Comparison

We also compared the results of Eqs. (4.26) to (4.32) to an exact numerical calculation of the superfluid density for a variety of small lattices in one and two dimensions. For a finite lattice and fixed number of particles, we can represent the Hamiltonian in Eq. (2.8) as a finite matrix. We diagonalized this matrix, finding all eigenstates and eigenvalues. We calculated the superfluid density by performing the full weighted trace over all eigenstates.

Some comparisons are shown in Fig. 4.5. We find that at zero temperature the approximate analytic expressions for the superfluid density match the numerical

result well even at a relatively small number of particles per site, $\bar{n} = 4$. Moreover the agreement persists to relatively large U. One such example is shown in Fig. 4.5(a). The finite temperature values do not agree as well with the numerical result, except for very large values of $\bar{n}$, but they follow the same trend as the numerically calculated results (see Figs. 4.5(b) and 4.5(c)). Overall the numerical results confirm the limits of validity in Eq. (4.41).

For these comparisons we replaced the integrals in Eqs. (4.30) and (4.32) with sums, corresponding to the finite size system.

4.4 Two-Component Systems

4.4.1 Model

We apply the same path integral method to a system of two species of bosons on a lattice. The Hamiltonian for this system is given by

$$\hat{H} = \hat{H}_{\uparrow} + \hat{H}_{\downarrow} + \hat{H}_{\uparrow\downarrow} \tag{4.43}$$

where $\hat{H}_{\sigma}$ for $\sigma = \uparrow, \downarrow$ are the single-particle Hamiltonians for particle species $\uparrow, \downarrow$ respectively, identical to Eq. (4.6) except with constants $J_{\sigma}, U_{\sigma}, \mu_{\sigma}$ and operators $\hat{a}_i^{\sigma}, (\hat{a}_i^{\sigma})^{\dagger}, \hat{n}_i^{\sigma}$ as appropriate. The final term

$$\hat{H}_{\uparrow\downarrow} = \sum_i U_{\uparrow\downarrow} \hat{n}_i^{\uparrow} \hat{n}_i^{\downarrow} \tag{4.44}$$

is the inter-species interaction Hamiltonian.

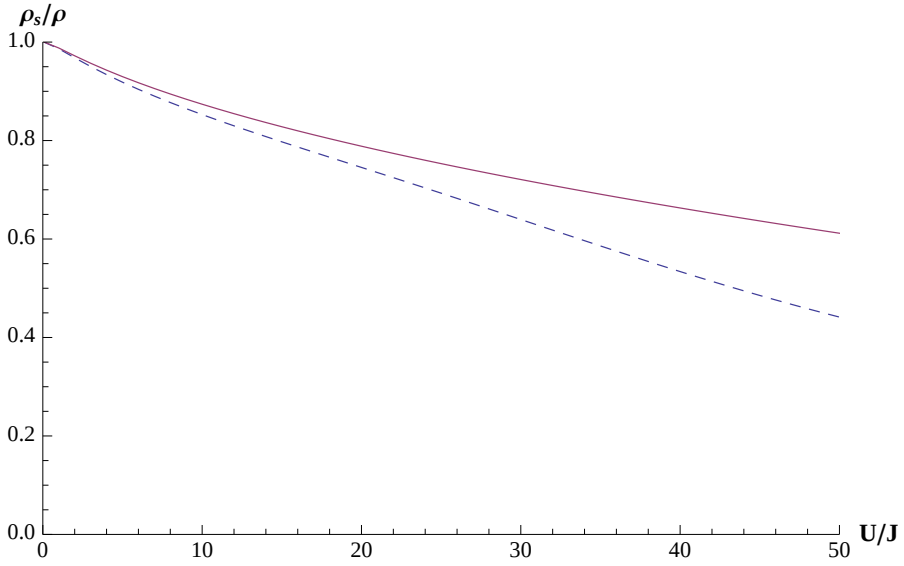

(a) $T = 0$

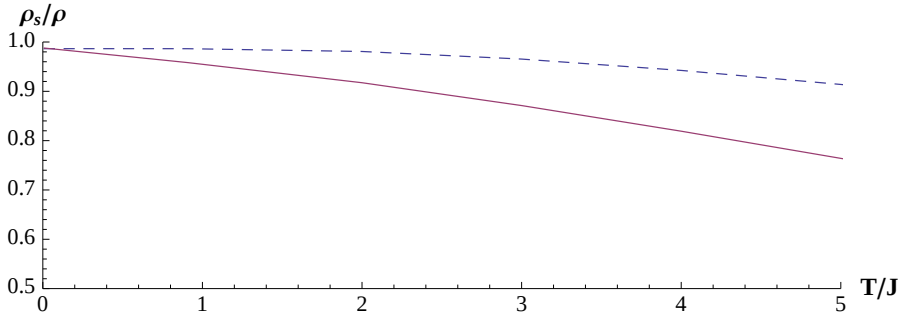

(b) $U/J = 1$

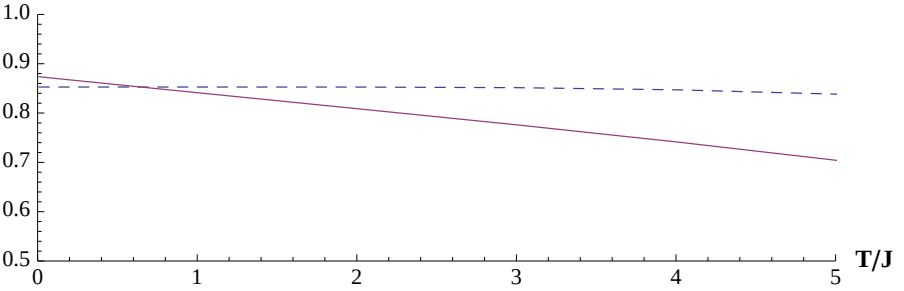

(c) $U/J = 10$

Figure 4.5: The superfluid fraction ρ_s/ρ, for a two-dimensional two-by-two lattice with 16 particles. The dashed blue line shows the numerically exact result and the solid red line shows the analytic approximation as calculated using Eqs. (4.26) to (4.32). (a) At $T = 0$, for varying interaction strength, (b), (c) as a function of temperature, for $U/J = 1, 10$, respectively.

The action for this Hamiltonian given by

$$S_E = \sum_n \left(\frac{a_0}{2\pi}\right)^D \int \mathrm{d^D k} \left[\sum_\sigma \left(\frac{V}{{a_0}^D}{}_\sigma\mathcal{L}_0 + {}_\sigma\mathcal{L}_2^{\boldsymbol{k},\omega_n} + {}_\sigma\mathcal{L}_{int}^{\boldsymbol{k},\omega_n}\right)\right] + {}_{\uparrow\downarrow}\mathcal{L}_2^{\boldsymbol{k},\omega_n} + {}_{\uparrow\downarrow}\mathcal{L}_{int}^{\boldsymbol{k},\omega_n} \tag{4.45}$$

where ${}_\sigma\mathcal{L}_{0,2,int}$ are again identical to those defined in Eqs. (4.17), (4.20) and (4.56), with mean densities and phase twists $\bar{\rho}_\sigma$, $\Delta\Phi_d^\sigma$ substituted for the one-component equivalents as appropriate, and the saddlepoint relation

$$\mu_\sigma = U_\sigma\bar{\rho}_\sigma + U_{\uparrow\downarrow}\bar{\rho}_{\bar{\sigma}} - 2J_\sigma\sum_\Delta \cos(\Delta\Phi_\Delta^\sigma) \tag{4.46}$$

used, with $\bar{\sigma}$ indicating the non-σ species, so that $\bar{\uparrow} = \downarrow, \bar{\downarrow} = \uparrow$. The additional terms are

$${}_{\uparrow\downarrow}\mathcal{L}_2^{\boldsymbol{k},\omega} = 2\times\frac{1}{2}U_{\uparrow\downarrow}\Delta t\times \left[\begin{array}{c}\left(\frac{1+\cos(\omega\Delta t)}{2}\right)\delta\rho^\uparrow_{\boldsymbol{k},\omega}\delta\rho^\downarrow_{-\boldsymbol{k},-\omega} - 2\bar{\rho}_\uparrow\bar{\rho}_\downarrow(1-\cos(\omega\Delta t))\phi^\uparrow_{\boldsymbol{k},\omega}\phi^\downarrow_{\boldsymbol{k},\omega} \\ +\sin(\omega\Delta t)\bar{\rho}_\downarrow\delta\rho^\uparrow_{\boldsymbol{k},\omega}\phi^\downarrow_{-\boldsymbol{k},\omega} + \sin(\omega\Delta t)\bar{\rho}_\uparrow\delta\rho^\downarrow_{\boldsymbol{k},\omega}\phi^\uparrow_{-\boldsymbol{k},\omega}\end{array}\right], \tag{4.47}$$

and the higher order terms scale as ${}_{\uparrow\downarrow}\mathcal{L}_{int}^{\omega_n,\boldsymbol{k}} = \bar{\rho}_\uparrow\bar{\rho}_\downarrow U_{\uparrow\downarrow}\times O(1/\sqrt{\bar{\rho}})^3$.

The in-species propagators are now, at $\omega\Delta t \ll 1$,

$$\begin{aligned}
\langle\delta\rho^\sigma\delta\rho^\sigma\rangle^p_{\boldsymbol{k},\omega} &= \frac{V}{a_0^D}\bar{\rho}_\sigma\left[\frac{1}{\Delta t}\frac{2\mathcal{E}_{\sigma 1k}\left(\omega^2+{\mathcal{E}_{\bar{\sigma}k}}^2\right)}{\left(\omega^2+{\mathcal{E}_{+k}}^2\right)\left(\omega^2+{\mathcal{E}_{-k}}^2\right)} + O(\Delta t)^0\right] \\
\langle\delta\rho^\sigma\phi^\sigma\rangle^p_{\boldsymbol{k},\omega} &= \frac{V}{a_0^D}\left[-\frac{1}{\Delta t}\frac{\omega\left(\omega^2+{\mathcal{E}_{\bar{\sigma}k}}^2\right)}{\left(\omega^2+{\mathcal{E}_{+k}}^2\right)\left(\omega^2+{\mathcal{E}_{-k}}^2\right)} + O(\Delta t)^0\right] \\
\langle\phi^\sigma\phi^\sigma\rangle^p_{\boldsymbol{k},\omega} &= \frac{V}{a_0^D}\frac{1}{4\bar{\rho}}\left[\frac{1}{\Delta t}\frac{2\mathcal{E}_{2k}\left(\omega^2+{\mathcal{E}_{\bar{\sigma}k}}^2\right) - 8\bar{\rho}_\uparrow\bar{\rho}_\downarrow{U_{\uparrow\downarrow}}^2\mathcal{E}_{\bar{\sigma}1k}}{\left(\omega^2+{\mathcal{E}_{+k}}^2\right)\left(\omega^2+{\mathcal{E}_{-k}}^2\right)} + O(\Delta t)^0\right]
\end{aligned} \tag{4.48}$$

while the contour pieces are identical to the single-component case. $\mathcal{E}_{\sigma k}, \mathcal{E}_{\sigma 1k}, \mathcal{E}_{\sigma 1k}$ are the single-particle dispersion relations given in Eq. (4.24), and the new dispersion relations are given by

$${\mathcal{E}_{\pm k}}^2 = \frac{{\mathcal{E}_{\uparrow k}}^2 + {\mathcal{E}_{\downarrow k}}^2}{2} \pm \sqrt{\left(\frac{{\mathcal{E}_{\uparrow k}}^2 - {\mathcal{E}_{\downarrow k}}^2}{2}\right)^2 + 4\bar{\rho}_\uparrow\bar{\rho}_\downarrow{U_{\uparrow\downarrow}}^2\mathcal{E}_{\uparrow 1k}\mathcal{E}_{\downarrow 1k}}. \tag{4.49}$$

The interspecies propagators are given by

$$\begin{aligned}
\left\langle \delta\rho^{\uparrow}\delta\rho^{\downarrow}\right\rangle^{p}_{\boldsymbol{k},\omega} &= \frac{V}{a_0^D}U_{\uparrow\downarrow}\left[-\frac{1}{\Delta t}\frac{4\bar{\rho}_{\uparrow}\bar{\rho}_{\downarrow}\mathcal{E}_{1\uparrow}\mathcal{E}_{1\downarrow}}{\left(\omega^2+{\mathcal{E}_{+}}^2\right)\left(\omega^2+{\mathcal{E}_{-}}^2\right)}+O(\Delta t)^0\right],\\
\left\langle \delta\rho^{\sigma}\phi^{\bar{\sigma}}\right\rangle^{p}_{\boldsymbol{k},\omega} &= \frac{V}{a_0^D}U_{\uparrow\downarrow}\left[\frac{1}{\Delta t}\frac{2\bar{\rho}_{\sigma}\mathcal{E}_{1\sigma}\omega}{\left(\omega^2+{\mathcal{E}_{+}}^2\right)\left(\omega^2+{\mathcal{E}_{-}}^2\right)}+O(\Delta t)^0\right],\\
\left\langle \phi^{\uparrow}\phi^{\downarrow}\right\rangle^{p}_{\boldsymbol{k},\omega} &= \frac{V}{a_0^D}U_{\uparrow\downarrow}\left[\frac{1}{\Delta t}\frac{\omega^2}{\left(\omega^2+{\mathcal{E}_{+}}^2\right)\left(\omega^2+{\mathcal{E}_{-}}^2\right)}+O(\Delta t)^0\right],
\end{aligned} \tag{4.50}$$

$$\begin{aligned}
&\left\langle \delta\rho^{\uparrow}\delta\rho^{\downarrow}\right\rangle^{\circ}_{\boldsymbol{k},\omega} = \frac{V}{a_0^D}U_{\uparrow\downarrow}\left[O(\Delta t)^2\right], \qquad \left\langle \delta\rho^{\sigma}\phi^{\bar{\sigma}}\right\rangle^{\circ}_{\boldsymbol{k},\omega} = \frac{V}{a_0^D}U_{\uparrow\downarrow}\left[O(\Delta t)^2\right],\\
&\left\langle \phi^{\uparrow}\phi^{\downarrow}\right\rangle^{\circ}_{\boldsymbol{k},\omega} = \frac{V}{a_0^D}U_{\uparrow\downarrow}\left[\frac{1}{2}\frac{\sin^2\left(\frac{\pi}{2}e^{i\chi}\right)\Delta t}{\left(1-\cos(\pi e^{i\chi})\right)^2}+O(\Delta t)^2\right].
\end{aligned} \tag{4.51}$$

4.4.2 Calculation of the Superfluid Density

In the presence of two species there are now three superfluid densities,

$$\rho_s^{\sigma\tau} = \frac{m_\sigma m_\tau a_0^2}{\hbar^2}\left[\frac{\partial^2\mathcal{F}}{\partial\Delta\Phi_x^{\sigma}\partial\Delta\Phi_x^{\tau}}\right]_{\boldsymbol{\Delta\Phi^{\sigma}=\Delta\Phi^{\tau}=0}}, \tag{4.52}$$

where $\rho_s^{\sigma\tau}$ is the superfluid response of species σ to the twisting of the phase of species τ. The diagonal terms $\rho_s^{\sigma\sigma}$ are the superfluid densities of species σ, while the off-diagonal term $\rho_s^{\uparrow\downarrow}=\rho_s^{\downarrow\uparrow}$ is the cross-stiffness.

The full expressions for all three terms may be calculated in a similar manner to the single-species case, as described in Section 4.5. At zero temperature, the superfluid densities are given by

$$\rho_s^{\sigma} = \frac{2m_\sigma a_0^2 J_\sigma}{\hbar^2}\frac{m_\sigma}{a_0^D}\left[\bar{n}^{\sigma}-n_n^{\sigma U}\right] \tag{4.53}$$

where the number of normal atoms per site is given by

$$n_n^{\sigma U} = \int\frac{\mathrm{a_0^D d^D k}}{(2\pi)^{\mathrm{D}}}\sin^2(k_x a_0/2)\left[\frac{(\mathcal{E}_{\sigma 1k}+\mathcal{E}_{\sigma 2k})\left(\mathcal{E}_{+k}\mathcal{E}_{-k}+\mathcal{E}_{\bar{\sigma}k}{}^2\right)-4\bar{\rho}_{\uparrow}\bar{\rho}_{\downarrow}{U_{\uparrow\downarrow}}^2\mathcal{E}_{\sigma 1k}}{2\mathcal{E}_{+k}\mathcal{E}_{-k}(\mathcal{E}_{+k}+\mathcal{E}_{-k})}-1\right]. \tag{4.54}$$

The cross-stiffness at $T = 0$ is

$$\rho_s^{\uparrow\downarrow} = \frac{2\sqrt{m_\uparrow m_\downarrow}a_0^2\sqrt{J_\uparrow J_\downarrow}}{\hbar^2}\frac{\sqrt{m_\uparrow m_\downarrow}}{a_0^D}\times \int \frac{\mathrm{a_0^D d^3k}}{(2\pi)^3}\,\sin^2(k_x a_0)\frac{4\sqrt{J_\uparrow J_\downarrow}\bar{\rho}_\uparrow\bar{\rho}_\downarrow U_{\uparrow\downarrow}^2\mathcal{E}_{1\uparrow}\mathcal{E}_{1\downarrow}}{\mathcal{E}_+\mathcal{E}_-(\mathcal{E}_+ + \mathcal{E}_-)^3}. \tag{4.55}$$

While the cross-stiffness is expected to be substantial in hard-core bosons [80] it is negligible in the weak-interaction case, as illustrated in Fig. 4.6.

A more dramatic effect can be seen in the superfluid densities. At zero temperature, a strong coupling to a second species of particles can replenish the superfluid fraction, as long as the superfluid has an equal or larger hopping parameter. This is seen in Fig. 4.7.

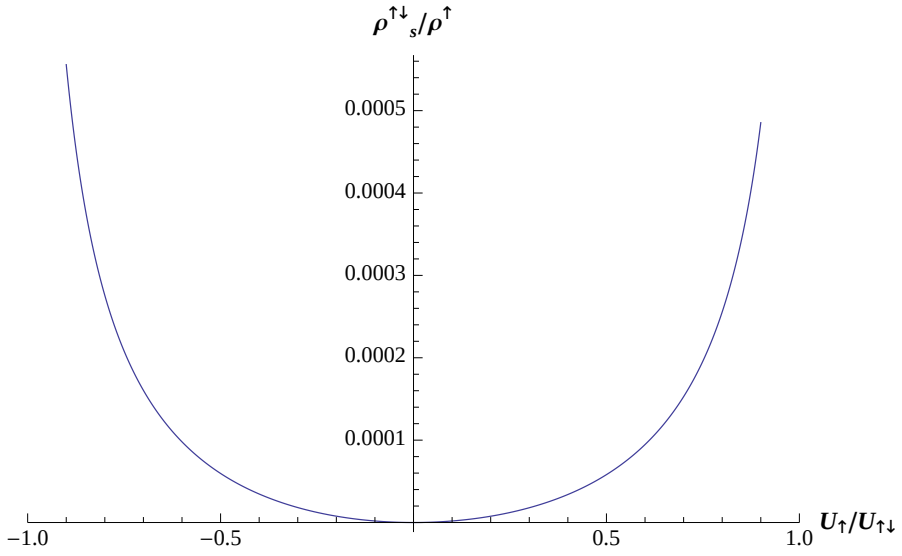

Figure 4.6: The superfluid cross-stiffness $\rho_s^{\uparrow\downarrow}/\rho^\uparrow$ as function of the interspecies interaction $U_{\uparrow\downarrow}/U_\uparrow$ for a two-component Bose gas on an infinite 3D cubic lattice. Here $\langle n^\uparrow\rangle = \langle n^\downarrow\rangle = 10$, with $U_\downarrow = U_\uparrow = 10J_\downarrow = 10J_\uparrow$, calculated to leading order in a $1/\langle n\rangle$ expansion.

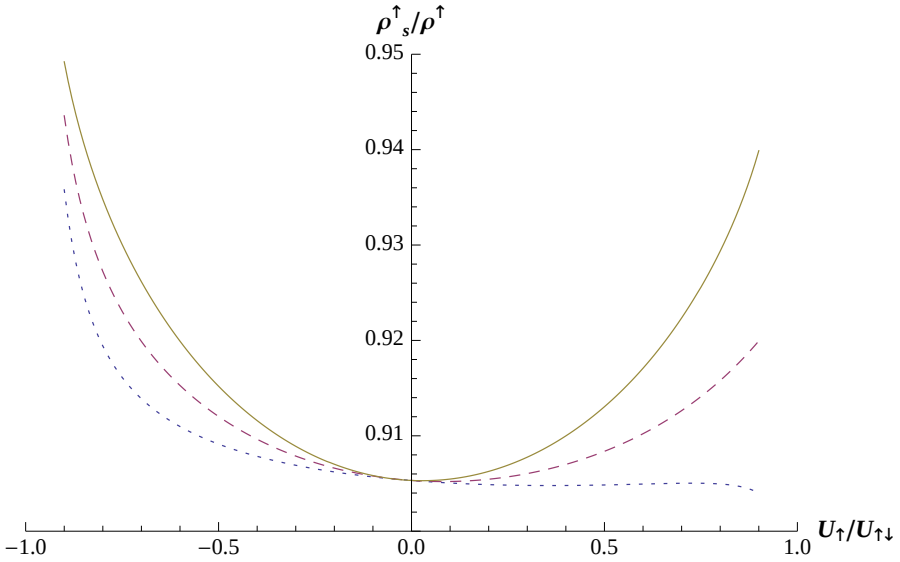

Figure 4.7: The superfluid fraction of the one component $\rho_s^{\uparrow}/\rho^{\uparrow}$ as function of the interspecies interaction $U_{\uparrow\downarrow}/U_{\uparrow}$ for a two-component Bose gas on an infinite 3D cubic lattice. Here $\langle n^{\uparrow}\rangle = \langle n^{\downarrow}\rangle = 10$, $U_{\downarrow} = U_{\uparrow} = 10J_{\uparrow}$, and the second component has hopping parameter $J_{\downarrow}/J_{\uparrow} = 0.1$ (dotted blue line), $J_{\downarrow}/J_{\uparrow} = 1$ (dashed red line) and $J_{\downarrow}/J_{\uparrow} = 10$ (solid yellow line).

4.5 Explicit Path Integral Calculations

We provide here a further explicit example of a calculation in the discrete time step path integral formalism. For a more elementary example see Chapter 5.

Our starting point is Eq. (4.21). Explicitly, the quadratic term is

$$\mathcal{L}_2 = \frac{1}{2}\begin{pmatrix} \frac{\delta\rho_{\boldsymbol{k},\omega}}{2\sqrt{\bar{\rho}}} & \sqrt{\bar{\rho}}\phi_{\boldsymbol{k},\omega}\end{pmatrix}\mathcal{G}^{-1}_{\boldsymbol{k},\omega}\begin{pmatrix} \frac{\delta\rho_{-\boldsymbol{k},-\omega}}{2\sqrt{\bar{\rho}}} \\ \sqrt{\bar{\rho}}\phi_{-\boldsymbol{k},-\omega}\end{pmatrix}, \tag{4.56}$$

where $\mathcal{G}^{-1}$ is an inverse Green's function matrix,

$$\begin{aligned}
\left[\mathcal{G}^{-1}_{\boldsymbol{k},\omega}\right]_{1,1} &= 2(1-\cos(\omega\Delta t)) + 2(1+\cos(\omega\Delta t))\bar{\rho}U\Delta t \\
&\quad + 4J\Delta t \sum_{\Delta} \begin{bmatrix} (1-\cos(\boldsymbol{k}\cdot\boldsymbol{\Delta}))\cos(\Delta\Phi_\Delta)\cos(\omega\Delta t) \\ +i\sin(\boldsymbol{k}\cdot\boldsymbol{\Delta})\sin(\Delta\Phi_\Delta)\sin(\omega\Delta t) \end{bmatrix} \\
\left[\mathcal{G}^{-1}_{\boldsymbol{k},\omega}\right]_{1,2} &= -2\sin(\omega\Delta t)(1-\bar{\rho}U\Delta t) \\
&\quad + 4J\Delta t \sum_{\Delta} \begin{bmatrix} (1-\cos(\boldsymbol{k}\cdot\boldsymbol{\Delta}))\cos(\Delta\Phi_\Delta)\sin(\omega\Delta t) \\ -i\Delta t\cos(\omega\Delta t)\sin(\boldsymbol{k}\cdot\boldsymbol{\Delta})\sin(\Delta\Phi_\Delta) \end{bmatrix} \\
\left[\mathcal{G}^{-1}_{\boldsymbol{k},\omega}\right]_{2,1} &= 2\sin(\omega\Delta t)(1-\bar{\rho}U\Delta t) \\
&\quad - 4J\Delta t \sum_{\Delta} \begin{bmatrix} (1-\cos(\boldsymbol{k}\cdot\boldsymbol{\Delta}))\cos(\Delta\Phi_\Delta)\sin(\omega\Delta t) \\ -i\sin(\boldsymbol{k}\cdot\boldsymbol{\Delta})\sin(\Delta\Phi_\Delta)\cos(\omega\Delta t) \end{bmatrix} \\
\left[\mathcal{G}^{-1}_{\boldsymbol{k},\omega}\right]_{2,1} &= 2(1-\cos(\omega\Delta t))(1-\bar{\rho}U\Delta t) \\
&\quad + 4J\Delta t \sum_{\Delta} \begin{bmatrix} (1-\cos(\boldsymbol{k}\cdot\boldsymbol{\Delta}))\cos(\Delta\Phi_\Delta)\cos(\omega\Delta t) \\ +i\sin(\boldsymbol{k}\cdot\boldsymbol{\Delta})\sin(\Delta\Phi_\Delta)\sin(\omega\Delta t) \end{bmatrix}
\end{aligned} \tag{4.57}$$

The propagators are obtained by inverting $\mathcal{G}^{-1}$, and are given by

$$\begin{aligned}
&\langle \delta\rho_{\boldsymbol{k},\omega}\delta\rho_{\boldsymbol{q},\eta}\rangle = \frac{\delta^{(D)}(\boldsymbol{q}+\boldsymbol{k})\delta_{\omega,-\eta}}{(a_0/2\pi)^D}\times \\
&\left[\bar{\rho}\frac{2(1-\cos(\omega\Delta t)) + [(\mathcal{E}_{1k}+\mathcal{E}_{2k})\cos(\omega\Delta t) + (\mathcal{E}_{1k}-\mathcal{E}_{2k})]\Delta t}{2(1-\cos(\omega\Delta t))\left(1-\frac{1}{2}(\mathcal{E}_{1k}+\mathcal{E}_{2k})\Delta t\right) + {\mathcal{E}_k}^2\Delta t^2} + O(\Delta\Phi)\right] \\
&\langle \delta\rho_{\boldsymbol{k},\omega}\phi_{\boldsymbol{q},\eta}\rangle = \frac{\delta^{(D)}(\boldsymbol{q}+\boldsymbol{k})\delta_{\omega,-\eta}}{(a_0/2\pi)^D}\times \\
&\left[-\sin(\omega\Delta t)\frac{1-\frac{1}{2}(\mathcal{E}_{1k}+\mathcal{E}_{2k})\Delta t}{2(1-\cos(\omega\Delta t))\left(1-\frac{1}{2}(\mathcal{E}_{1k}+\mathcal{E}_{2k})\Delta t\right) + {\mathcal{E}_k}^2\Delta t^2} + O(\Delta\Phi)\right] \\
&\langle \phi_{\boldsymbol{k},\omega}\phi_{\boldsymbol{q},\eta}\rangle = \frac{\delta^{(D)}(\boldsymbol{q}+\boldsymbol{k})\delta_{\omega,-\eta}}{(a_0/2\pi)^D}\times \\
&\left[\frac{1}{4\bar{\rho}}\frac{2(1-\cos(\omega\Delta t)) + [(\mathcal{E}_{1k}+\mathcal{E}_{2k})\cos(\omega\Delta t) + (\mathcal{E}_{2k}-\mathcal{E}_{1k})]\Delta t}{2(1-\cos(\omega\Delta t))\left(1-\frac{1}{2}(\mathcal{E}_{1k}+\mathcal{E}_{2k})\Delta t\right) + {\mathcal{E}_k}^2\Delta t^2} + O(\Delta\Phi)\right].
\end{aligned} \tag{4.58}$$

As explained below, the only important features of these functions are their

$\omega\Delta t \to 0$ structures and their values at $|\omega\Delta t| = \pi$. We illustrate this result by calculating the average occupation number via

$$\frac{\langle n\rangle}{a_0^D} = -\frac{\partial \mathcal{F}}{\partial \mu} = \frac{1}{\beta V}\frac{1}{Z}\frac{\partial Z}{\partial \mu} = \\ -\frac{1}{\beta V}\Big(\frac{a_0}{2\pi}\Big)^D \int \mathrm{d^D k} \sum_{\omega_n}\left[\frac{V}{{a_0}^D}\left\langle \frac{\partial \mathcal{L}_0}{\partial \mu}\right\rangle + \left\langle \frac{\partial \mathcal{L}_2^{\boldsymbol{k},\omega_n}}{\partial \mu}\right\rangle + \left\langle \frac{\partial \mathcal{L}_{int}^{\boldsymbol{k},\omega_n}}{\partial \mu}\right\rangle\right]. \tag{4.59}$$

As we have assigned $\bar{\rho} = \frac{1}{U}(\mu + 2J\sum_\Delta \cos(\Delta\Phi_\Delta))$, the derivatives are given by

$$\frac{\partial}{\partial \mu} = \frac{\partial}{\partial \mu}\bigg|_{\bar{\rho}} + \frac{\partial \bar{\rho}}{\partial \mu}\frac{\partial}{\partial \bar{\rho}}\bigg|_{\mu}. \tag{4.60}$$

We calculate this quantity at $\boldsymbol{\Delta\Phi} = 0$.

The saddle point contribution comes from the constant

$$\frac{\partial \mathcal{L}_0}{\partial \mu} = -\bar{\rho}\Delta t. \tag{4.61}$$

The contribution from this term to Eq. (4.59) is

$$-\frac{1}{\beta V}\Big(\frac{a_0}{2\pi}\Big)^D \int \mathrm{d^D k} \sum_{\omega_n} \frac{V}{{a_0}^D}\left\langle \frac{\partial \mathcal{L}_0}{\partial \mu}\right\rangle = \frac{\bar{\rho}}{a_0^D}. \tag{4.62}$$

The nontrivial part of the calculation comes from the term involving $\mathcal{L}_2^{\boldsymbol{k},\omega}$,

$$\frac{\partial \mathcal{L}_2^{\boldsymbol{k},\omega_n}}{\partial \mu} = \\ \frac{1}{\mu}(1-\cos(\omega\Delta t) + \mathcal{E}_{1k}\Delta t\cos(\omega\Delta t))\left(\bar{\rho}\phi_{\boldsymbol{k},\omega}\phi_{-\boldsymbol{k},-\omega} - \frac{\delta\rho_{\boldsymbol{k},\omega}\delta\rho_{-\boldsymbol{k},-\omega}}{4\bar{\rho}}\right) \\ + \sin(\omega\Delta t)\Delta t\delta\rho_{\boldsymbol{k},\omega}\phi_{-\boldsymbol{k},-\omega} - (1-\cos(\omega\Delta t))2\Delta t\bar{\rho}\phi_{\boldsymbol{k},\omega}\phi_{-\boldsymbol{k},-\omega}. \tag{4.63}$$

We perform the summation over the frequencies ω_n by taking a contour integral. The same trick is used in the continuous time approach, but the contour here is slightly different. As illustrated in Fig. 4.8, the integration is performed over a circle of finite radius $\frac{2\pi}{\beta}\frac{N_t-1}{2} < |\omega| < \frac{2\pi}{\beta}\frac{N_t+1}{2}$. In terms of the integral over this contour γ, the summation over frequencies can be expressed as

$$\frac{1}{\beta}\sum_{\omega_n} F(\omega) = \frac{1}{2\pi}\oint_\gamma \mathrm{d}\omega \frac{F(\omega)}{e^{i\beta\omega}-1} - i\sum_{\omega_F}\mathrm{Res}\left[\frac{\mathrm{F}(\omega)}{\mathrm{e}^{\mathrm{i}\beta\omega}-1}, \omega_\mathrm{F}\right]. \tag{4.64}$$

The sum on the left hand side is over the frequencies $\omega_n = -\frac{2\pi}{\beta}\frac{N_t-1}{2} \ldots \frac{2\pi}{\beta}\frac{N_t-1}{2}$, the sum on the right is over the poles ω_F of $F(\omega)$ inside the contour γ, and γ is the complex circle defined by $|\omega| = \frac{2\pi}{\beta}\frac{N_t}{2} = \frac{\pi}{\Delta t}$. The notation $\mathrm{Res}(\mathrm{X}(\omega), \omega_\mathrm{F})$ refers to the residue of $X(\omega)$ at $\omega = \omega_F$.

In a continuous time calculation, one takes the contour γ to infinity. Assuming $F(\omega)$ is well behaved, the integral on the right-hand side of Eq. (4.64) then vanishes. In our case we must explicitly include this term. To calculate the contour integral, we take $\omega = \frac{\pi}{\Delta t}e^{i\chi}$, with $\chi = 0 \ldots 2\pi$. As $\Delta t \to 0$, the Bose factor is

$$\left(e^{i\pi(\beta/\Delta t)e^{i\chi}} - 1\right)^{-1} \to \begin{cases} -1 & 0 < \chi < \pi \\ 0 & \pi < \chi < 2\pi \end{cases} \tag{4.65}$$

and so the integral of Eq. (4.64) becomes

$$\oint_\gamma \mathrm{d}\omega \frac{F(\omega)}{e^{i\beta\omega} - 1} = -i\frac{\pi}{\Delta t}\int_0^\pi \mathrm{d}\chi\, e^{i\chi} F\Big(\frac{\pi}{\Delta t}e^{i\chi}\Big). \tag{4.66}$$

In the limit $\Delta t \to 0$, the poles of the functions in Eq. (4.58) converge to finite values of ω. Hence $\omega_F \Delta t \ll 1$, and the sum over ω_F accesses only information about the low-energy structure of Eqs. (4.58) and (4.63).

Thus, the summation of functions of the propagators in Eq. (4.58) requires only the form of their low-frequency poles, at $\omega\Delta t \ll 1$ (marked with superscript p) and their values on the contour γ, at $\omega = \frac{\pi}{\Delta t}e^{i\chi}$ (marked by superscript $\circ$). For our particular case, the summand Eq. (4.63) is composed of

$$\begin{aligned} \left\langle \frac{\partial \mathcal{L}_2^{\boldsymbol{k},\omega_n}}{\partial \mu} \right\rangle^p &= \frac{\mathcal{E}_{1k}\Delta t}{\mu}\left(\bar{\rho}\langle\phi\phi\rangle^p_{\boldsymbol{k},\omega} - \frac{\langle\delta\rho\delta\rho\rangle^p_{\boldsymbol{k},\omega}}{4\bar{\rho}}\right) \\ &\quad + O(\Delta t)^2 \times (\langle\delta\rho\delta\rho\rangle, \langle\delta\rho\phi\rangle, \langle\phi\phi\rangle), \end{aligned} \tag{4.67}$$

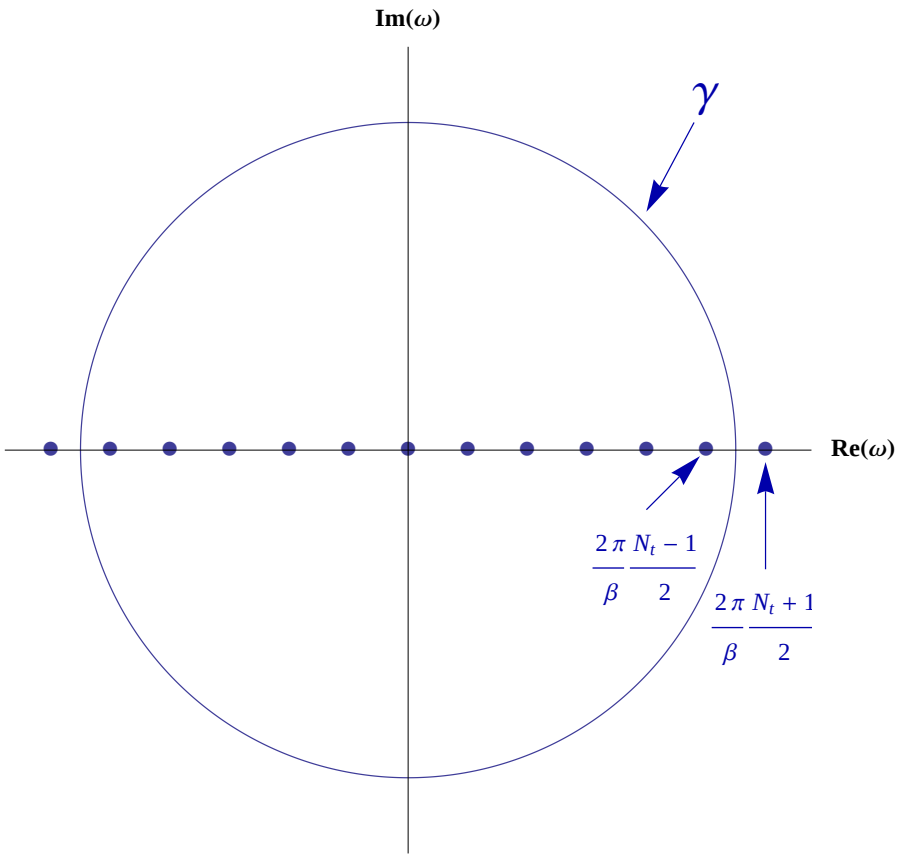

Figure 4.8: The contour γ used to perform the summation over $\omega = -\frac{2\pi}{\beta}\frac{N_t-1}{2}\ldots\frac{2\pi}{\beta}\frac{N_t-1}{2}$ as in Eq. (4.64). The contour is given by $\omega = \frac{\pi}{\Delta t}e^{i\chi}$, $\chi = 0\ldots 2\pi$. As one goes to the continuous time case with $\Delta t \to 0$, the radius of the contour goes to infinity.

and

$$\begin{aligned}\left\langle \frac{\partial \mathcal{L}_2^{\boldsymbol{k},\omega_n}}{\partial \mu} \right\rangle^{\circ} &= \sin\left(\pi e^{i\chi}\right)\Delta t\langle\delta\rho\phi\rangle^{\circ}_{\boldsymbol{k},\omega} - \left(1-\cos\left(\pi e^{i\chi}\right)\right)2\Delta t\bar{\rho}\langle\phi\phi\rangle^{\circ}_{\boldsymbol{k},\omega} \\ &+ \frac{1}{\mu}\left(1-\cos\left(\pi e^{i\chi}\right)+\mathcal{E}_{1k}\Delta t\cos\left(\pi e^{i\chi}\right)\right)\left(\bar{\rho}\langle\phi\phi\rangle^{\circ}_{\boldsymbol{k},\omega} - \frac{\langle\delta\rho\delta\rho\rangle^{\circ}_{\boldsymbol{k},\omega}}{4\bar{\rho}}\right).\end{aligned} \tag{4.68}$$

Thus we do not need the full structure given in Eq. (4.58) but rather just the pole and contour values given in Eq. (4.22).

We now explicitly calculate the contribution of $\frac{\partial}{\partial\mu}\mathcal{L}_2^{\boldsymbol{k},\omega_n}$ to $\langle n\rangle$. The low-

frequency behavior is

$$\left\langle \frac{\partial \mathcal{L}_2^{\boldsymbol{k},\omega_n}}{\partial \mu} \right\rangle^p = \frac{V}{a_0^D} \frac{\mathcal{E}_{1k}}{\omega^2 + \mathcal{E}_k^2} \tag{4.69}$$

with poles at $\omega_F = \pm i\mathcal{E}_k$, so that

$$-i \sum_{\omega_F} \mathrm{Res} \left[\left\langle \frac{\partial \mathcal{L}_2^{\boldsymbol{k},\omega}}{\partial \mu} \right\rangle^p \left(e^{i\beta\omega} - 1\right)^{-1}, \omega_F \right] = \frac{V}{a_0^D} \frac{1}{2} \frac{\mathcal{E}_{1k}}{\mathcal{E}_k} \coth(\beta \mathcal{E}_k/2), \tag{4.70}$$

while the contour value is

$$\begin{aligned} \left\langle \frac{\partial \mathcal{L}_2^{\boldsymbol{k},\omega_n}}{\partial \mu} \right\rangle^\circ &= -\frac{V}{a_0^D} \frac{1}{2} \Delta t \\ \frac{1}{2\pi} \oint_\gamma \mathrm{d}\omega \left\langle \frac{\partial \mathcal{L}_2^{\boldsymbol{k},\omega_n}}{\partial \mu} \right\rangle^\circ \left(e^{i\beta\omega} - 1\right)^{-1} &= -\frac{1}{2} \frac{V}{a_0^D}. \end{aligned} \tag{4.71}$$

Hence

$$-\frac{1}{\beta V} \left(\frac{a_0}{2\pi}\right)^D \int \mathrm{d^D k} \sum_{\omega_n} \left\langle \frac{\partial \mathcal{L}_2^{\boldsymbol{k},\omega_n}}{\partial \mu} \right\rangle = \frac{1}{2} \int \frac{\mathrm{d^D k}}{(2\pi)^{\mathrm{D}}} \left(1 - \frac{\mathcal{E}_{1k}}{\mathcal{E}_k} \coth(\beta \mathcal{E}_k/2)\right). \tag{4.72}$$

Combining this result with the zeroth-order contribution in Eq. (4.62) we find

$$\bar{n} = \bar{\rho} + \frac{1}{2} \int \frac{\mathrm{a_0^D d^D k}}{(2\pi)^{\mathrm{D}}} \left(1 - \frac{\mathcal{E}_{1k}}{\mathcal{E}_k} \coth(\beta \mathcal{E}_k/2)\right) \tag{4.73}$$

where $\bar{\rho} = (\mu + 2JD)/U$.

4.6 Outlook

The $T = 0$ normal density, ρ_n, for lattice bosons is generally non-zero. As discussed in Section 4.3, this property, and the temperature dependence of the superfluid density, can be experimentally studied using cold atoms. Here we calculated ρ_n, and proposed comparing our results with experiment.

For our calculation we extended the standard saddle-point functional integral approach. When using a coherent state basis, the discrete time path integral contains extra terms over the continuous time limit version. We explicitly derived those corrections for the Bose Hubbard model. Similar issues appear in spin models, and our techniques could be applied there.

Our results are applicable at high density, low temperature, and weak interaction. One could envision extending them to strong interaction by using a different set of coherent states. For example, in the hard core limit it would be natural to use $|\theta, \varphi\rangle_i = \cos\theta|0\rangle_i + e^{i\varphi}\sin\theta|1\rangle_i$, where $|0\rangle_i, |1\rangle_i$ are the states with no particles or one particle on site i respectively. The other approach to extending the validity of our results would be to include perturbative corrections. In particular, one might envision summing an infinite set of these corrections using Feynman diagram techniques.

We also present results for the superfluid properties of two-component lattice bosons. These are an active area of research, and there are rich possibilities for exploring our formalism in those systems. One experiment [51] has seen hints of the impact of one bosonic species on the superfluid properties of another. Those results appear to be in the opposite direction from our predictions - however they are in a stronger interacting regime, near the superfluid-to-Mott insulator transition and the quantitative applicability of our results to their experiment is questionable. We also neglect any processes which involve higher bands.

CHAPTER 5

CORRECTIONS TO THE CONTINUOUS TIME SEMICLASSICAL COHERENT STATE PATH INTEGRAL

5.1 Introduction

Path integrals convert the difficult problem of diagonalizing a Hamiltonian into the potentially simpler one of summing over a set of all possible paths, weighted by the classical action [82, 84]. They are particularly powerful for making semiclassical approximations, where only a few classical paths dominate. Often the natural variables for describing the path are conjugate. For example, one would like to describe a spin system in terms of paths on the Bloch sphere, even though the different components of spin do not commute [83]. Coherent states are often used in such cases, and can yield useful results [85, 87, 95, 121, 165, 166].

Most path integral formulations involve a continuous imaginary time limit [1]. This limit, however, leads to the rise of well-known anomalies [88, 141, 148] that were clearly described most recently by Wilson and Galitski [159]. One example they consider is a path integral calculation of the partition function Z'_{ss} of the single site Bose Hubbard model, $\hat{H}_{ss} = \frac{U}{2}\hat{n}(\hat{n}-1) - \mu\hat{n}$, where $\hat{n} = \hat{a}^\dagger\hat{a}$ represents the number of Bosons, U parameterizes their interaction and μ is the chemical potential. This is a sufficiently simple model that one can calculate the exact partition function Z_{ss}, and find $Z_{ss} \neq Z'_{ss}$. In particular, at zero temperature, the mean occupation number calculated from Z'_{ss} is $\langle n' \rangle = \left[\left[\frac{\mu}{U}\right]\right]$, while the exact result derived from Z_{ss} is $\langle n \rangle = \left[\left[\frac{\mu}{U} + \frac{1}{2}\right]\right]$. Here $[[x]]$ is the integer closest to x.

We analyze here the structure of the discrete, exact, path integral, and de-

rive an algorithm for correcting the continuous time result for the free energy $F = -\frac{1}{\beta}\log Z$. To do so, we restrict ourselves to the semiclassical path integral, expanding the action in quadratic quantum fluctuations around a classical path, which is known be valid in the discrete formalism [48]. Our correction is given by

$$F = F^{CPI} - i\frac{1}{4\Delta t}\int_0^\pi \mathrm{d}\chi\, e^{i\chi}\log\left[\frac{\det G_\omega^{-1}}{\det \bar{G}_\omega^{-1}}\right]_{\omega=\frac{\pi e^{i\chi}}{\Delta t}} \tag{5.1}$$

where F^{CPI} is the free energy obtained from the continuous-time path integral (CPI) while the matrices $[G_\omega]_{ij} = \langle \psi^i_\omega \psi^j_{-\omega}\rangle$, $\left[\bar{G}_\omega\right]_{ij} = \left\langle \psi^i_\omega \psi^j_{-\omega}\right\rangle_{CPI}$ are composed of perturbation field propagators in frequency space for a discrete-time and CPI calculation, respectively. We precisely define all these terms below as we derive Eq. (5.1) and discuss techniques for calculating the correction terms. The key feature of Eq. (5.1) is that it is of the form of the continuous time result plus a correction. This allows it to be easily integrated into the wide body of work that makes use of that formalism [7, 13, 40, 49, 54, 139].

This chapter is based on previously published work [162].

5.2 Path Integral Formulation

The formulation of partition function as a path integral in imaginary time involves the expansion

$$\begin{aligned} Z = \mathrm{Tr}\, e^{-\beta\hat{H}} &= \sum_{\mathbf{\Psi}_0}\langle \mathbf{\Psi}_0|e^{-\beta\hat{H}}|\mathbf{\Psi}_0\rangle \\ &= \sum_{\mathbf{\Psi}_1,\ldots,\mathbf{\Psi}_{N_t}}\prod_{t=1}^{N_t}\langle \mathbf{\Psi}_{t-1}|e^{-\hat{H}\Delta t}|\mathbf{\Psi}_t\rangle. \end{aligned} \tag{5.2}$$

Here $\beta = 1/T$ is the inverse temperature. $\{|\mathbf{\Psi}_t\rangle\}$ is any complete basis of the states, characterized by a set of parameters $\mathbf{\Psi}_t$, e.g. $\mathbf{\Psi}_t = \left(n, \varphi\right)$ so that $\hat{a}\left|\left(n, \varphi\right)\right\rangle =$

$\sqrt{n}e^{i\varphi}\left|\left(n,\varphi\right)\right\rangle$ in the coherent state basis of the Bose-Hubbard model. The sum $\sum_{\mathbf{\Psi}_t}|\mathbf{\Psi}_t\rangle\langle\mathbf{\Psi}_t| = \mathcal{I}$ is the identity operator, of which we insert $N_t - 1 \equiv \beta/\Delta t - 1$ copies into the operator. We are now summing over all N_t-point paths in $\mathbf{\Psi}$-space, with $\mathbf{\Psi}_0 = \mathbf{\Psi}_{N_t}$. In the limit of small Δt one can approximate $e^{-\hat{H}\Delta t} \approx 1 - \hat{H}\Delta t$ and thus write the partition function in the form of a discrete time path integral $Z = \int \mathcal{D}\mathbf{\Psi}\, e^{-\sum_t L_t}$, where the Lagrangian is

$$L_t = -\log[\langle \mathbf{\Psi}_t \mid \mathbf{\Psi}_{t+1}\rangle] + \Delta t \frac{\langle \mathbf{\Psi}_t|\hat{H}|\mathbf{\Psi}_{t+1}\rangle}{\langle \mathbf{\Psi}_t \mid \mathbf{\Psi}_{t+1}\rangle}. \tag{5.3}$$

5.3 Coherent State Anomaly

As emphasized by Wilson and Galitski [159], the anomalies they discuss are not related to ambiguities of operator ordering or geometric phases. Rather, they arise from the over-completeness of coherent states. When the basis $\{|\mathbf{\Psi}\rangle\}$ is orthogonal, the first term in this expansion can be taken to be arbitrarily small, and one can approximate $|\mathbf{\Psi}_{t+1}\rangle \approx (1 + \Delta t\partial_t)|\mathbf{\Psi}_t\rangle$, and by taking $\Delta t \to 0$ convert the problem into the traditional CPI form [1]. As noted by Solari [141], this approximation breaks down when expanding in an overcomplete basis; the overlap between the wavefunctions at consecutive time steps remains finite even when the parameters describing those wavefunctions are not infinitesimally close. The consequences for typical paths are illustrated in Fig. 5.1, where we show representative contributions to the partition function of a harmonic oscillator.

Multiple previous studies have been made of this anomaly. They proceed by returning to the valid discrete time formulation of Eq. (5.3). The approach first used by Solari [141] involves an iterative evaluation of the simple integrals for each time step. The resulting recursion relations, in the large N_t limit, become differential

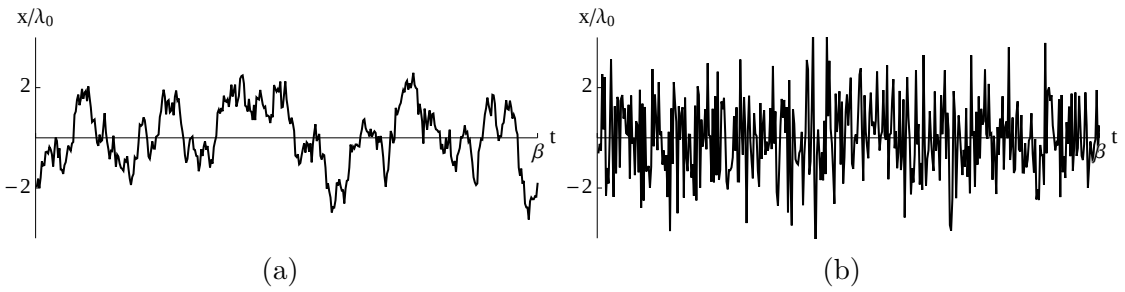

Figure 5.1: Typical paths in imaginary time space path integral of a harmonic oscillator. Position x is measured in units of $\lambda_0 = \sqrt{\frac{\hbar}{m\omega}}$. Here the inverse temperature is $\beta\hbar\omega = 20$ and imaginary time is discretized into $N_t = 400$ steps. In (a) we show a path in standard configuration space, while (b) shows a coherent state path with the momentum coordinate integrated out. The configuration space paths are continuous in the limit $N_t \to \infty$, but the coherent paths are not.

equations that may be solved to obtain the semiclassical propagator or the partition function. Similar formalisms have been applied to the case of the harmonic oscillator [7, 19], any number of interacting spins [20], and finally any number of interacting harmonic oscillators [155]. Kochetov, meanwhile, demonstrated that in the case of the a single spin-half system knowledge of the symmetries of the system, related to the recursion relations of the previous methods, can be used to write a CPI action that produces the correct propagator [88].

5.4 Low Frequency Correction

Our approach to the problem differs from Solari's approach and the related antecedents. We return, as they do, to the mathematically exact discrete action, but transpose our view to the Fourier domain, where discrete time steps determine the high-frequency portions of the action. As the low-frequency action remains identical to what is seen in the continuous formalism, we are able to express our result in terms of a correction to the results of the continuous-time formalism. In

addition, the technique we present may be used with any overcomplete basis, and the approach may be readily used in higher-order calculations.

We begin by following the standard procedure [140] to characterize the states in terms of a saddle point solution $\bar{\mathbf{\Psi}}$ satisfying $\left[\frac{\delta L_t}{\delta \mathbf{\Psi}_t}\right]_{\mathbf{\Psi}_t=\bar{\mathbf{\Psi}}} = 0$, and a fluctuation $\boldsymbol{\psi}_t$, writing $\mathbf{\Psi}_t = \bar{\mathbf{\Psi}} + \boldsymbol{\psi}_t$. We then expand to quadratic order in the fluctuations $L_t = L_0 + \boldsymbol{\psi}_t \cdot L_2 \cdot \boldsymbol{\psi}_t + \boldsymbol{\psi}_t \cdot L_{2\Delta} \cdot \boldsymbol{\psi}_{t+1} + O(|\psi_t|)^3$ where the classical energy L_0 and matrices $L_2, L_{2\Delta}$ are independent of time. This saddle point approximation becomes exact as the number of local degrees of freedom become large. For example, in the Bose Hubbard Model, it is the leading correction in a $1/n$ expansion, where n is the average number of particles per site. Similarly, in a spin system, the total spin S plays the role of n. In terms of the Fourier components $\boldsymbol{\psi}_\omega = \frac{1}{\sqrt{N_t}} \sum_t e^{-i\omega t} \boldsymbol{\psi}_t$, the partition function reads

$$Z = \int \mathcal{D}\psi \, \exp\left[-\beta F_0 - \frac{1}{2} \sum_{\omega=\omega_n} \boldsymbol{\psi}_\omega \cdot G_\omega^{-1} \cdot \boldsymbol{\psi}_\omega\right] \tag{5.4}$$

where summation is over the frequencies $\omega_n = \frac{2\pi}{\beta} n$ for $n = -\frac{N_t-1}{2} \ldots \frac{N_t-1}{2}$, yielding the free energy

$$F = F_0 + \frac{1}{\beta} \sum_{n=-\frac{N_t-1}{2}}^{\frac{N_t-1}{2}} \frac{1}{2} \log\left[\frac{\det G_{\omega_n}^{-1}}{2\pi}\right]. \tag{5.5}$$

This compares with the free energy given by the continuous-time formalism, $F^{CPI} = F_0^{CPI} + \frac{1}{\beta} \sum_{n=-\infty}^{\infty} \frac{1}{2} \log\left[\frac{\det \bar{G}_{\omega_n}^{-1}}{2\pi}\right]$ where $\bar{G}_{\omega_n}^{-1}$ is the CPI fluctuation matrix. As we take $\Delta t \to 0$, generically we expect the classical free energy to converge to the continuous result $F_0 \to F_0^{CPI}$, and the sum $\sum_{|n|>\frac{N_t-1}{2}} \frac{1}{2} \log\left[\frac{\det \bar{G}_{\omega_n}^{-1}}{2\pi}\right] \to 0$.

The difference in energies is given then by

$$F - F^{CPI} = \frac{1}{\beta} \sum_{n=-\frac{N_t-1}{2}}^{\frac{N_t-1}{2}} \frac{1}{2} \log\left[\frac{\det G_{\omega_n}^{-1}}{\det \bar{G}_{\omega_n}^{-1}}\right]. \tag{5.6}$$

We can replace this sum with a contour integral, using the identity

$$\begin{aligned}\frac{1}{2\pi}\oint_\gamma \mathrm{d}\omega \frac{f(\omega)}{e^{i\beta\omega}-1} \\ = \frac{1}{\beta}\sum_{\omega=\omega_n} f(\omega) + i\sum_{\omega_f}\mathrm{Res}\left[\frac{f(\omega)}{e^{i\beta\omega}-1},\omega_f\right].\end{aligned} \tag{5.7}$$

Here the last sum is over the poles ω_f of $f(\omega)$ inside the contour γ, and γ is the complex circle defined by $|\omega| = \frac{2\pi}{\beta}\frac{N_t}{2} = \frac{\pi}{\Delta t}$. The notation $\mathrm{Res}[f(\omega),\omega_f]$ refers to the residue of $f(\omega)$ at $\omega = \omega_f$ and here $f(\omega) = \frac{1}{2}\log\left[\frac{\det G_\omega^{-1}}{\det \bar{G}_\omega^{-1}}\right]$.

The last term of Eq. (5.7) vanishes: for any fixed ω, $\lim_{\Delta t\to 0} G_\omega^{-1} = \bar{G}_\omega^{-1}$. Thus the function $f(\omega)$ is analytic inside γ, and the set $\{\omega_f\}$ of singularities is empty. For $|\omega\Delta t| > \pi$, the matrices G_ω^{-1} and $\bar{G}_\omega^{-1}$ are no longer simply related, and $f(\omega)$ has branch cut singularities outside of γ.

Once the residue term is eliminated, we are left with the contour integral. This integral involves fluctuations of frequency $\omega_{\max} = \frac{\pi}{\Delta t}$, corresponding to the time scale separating consecutive time steps. When the basis $|\mathbf{\Psi}_t\rangle$ is orthogonal these fluctuations are vanishingly small, but for an overcomplete basis they are finite, and the contour integral does not vanish. Straightforward algebra then reduces Eqs. (5.6) and (5.7) to the expression in Eq. (5.1).

5.5 Discrete Time Corrections

5.5.1 The Bose Hubbard Model

A clear example of this calculation is provided by the single-site Bose-Hubbard Hamiltonian. Using the coherent state basis and the field $\boldsymbol{\psi}_t = \Big(\delta n_t, \phi_t\Big)$, the

components of the quadratic Lagrangian are

$$L_0 = \frac{1}{2}\frac{\mu^2}{U}\Delta t$$
$$L_2 = \begin{pmatrix} \frac{U}{4\mu}(1+\mu\Delta t) & 0 \\ 0 & \frac{\mu}{U}(1-\mu\Delta t) \end{pmatrix} \tag{5.8}$$
$$L_{2\Delta} = -[1-\mu\Delta t]\begin{pmatrix} \frac{U}{4\mu} & \frac{i}{2} \\ -\frac{i}{2} & \frac{\mu}{U} \end{pmatrix}$$

and so

$$\det G_\omega^{-1} = 2(1-\cos(\omega\Delta t))(1-\mu\Delta t). \tag{5.9}$$

This compares with the CPI result $\det \bar{G}_\omega^{-1} = (\beta\omega)^2$, and indeed the ratio of the two is finite everywhere for $|\omega| \leq \pi/\Delta t$. By performing the contour integral one finds the difference between the free energies $F - F^{CPI} = \frac{\mu}{2}$ up to an irrelevant constant.

The power of this approach is more readily apparent in the multisite Bose Hubbard model. Consider a D-dimensional cubic lattice of N_s sites with lattice constant a_0. There momentum is a good quantum number and one can consider $G_{\omega,\boldsymbol{k}}$. The large ω structure takes on the simple form

$$\frac{\det G_{\omega,\boldsymbol{k}}^{-1}}{\det \bar{G}_{\omega,\boldsymbol{k}}^{-1}} = \frac{2(1-\cos(\omega\Delta t))(1+\epsilon_k\Delta t)}{\beta^2\omega^2} \tag{5.10}$$

where $\epsilon_k = 4J\sum_{j=1}^{D}\sin^2(k_j a_0/2) - \mu$. By performing the contour integral one finds simply,

$$F - F^{CPI} = \frac{1}{2}(\mu - 2J\times D)N_s \tag{5.11}$$

plus a constant. This is the same μ dependence as the single-site problem.

This correction to the free energy has allowed us to calculate the superfluid density of lattice bosons [160] within the validity range of the semiclassical approximation.

5.5.2 Spin System

For completeness sake, we present the second system explored by Wilson and Galitski in [159]. We examine the Hamiltonian $\hat{H} = \hat{S}_z^2$ for a spin S system. The difference in free energies between the exactly-calculated and the CPI results is given, at $T \to 0$, by $\Delta F = -\frac{S}{2}$. Using the semiclassical formalism presented here, one finds

$$\frac{\det G_\omega^{-1}}{\det \bar{G}_\omega^{-1}} = \frac{2(1-\cos(\omega\Delta t))\left(1-\left(S-\frac{1}{2}\right)\Delta t\right)}{\beta^2\omega^2} \tag{5.12}$$

leading to a correction of $F = F^{CPI} - \left(\frac{S}{2} - \frac{1}{4}\right)$. Our finite time-step correction accounts for most of the discrepancy, while the remaining $O(S)^0$ term arises from the semiclassical approximation.

Part III

Dynamics

CHAPTER 6

HEATING FROM CONTINUOUS NUMBER DENSITY MEASUREMENTS IN OPTICAL LATTICES

6.1 Introduction

One of the most important recent advances in cold atom experiments is single-site resolved imaging in optical lattices [6, 56, 111, 137]. Presently these techniques are destructive, and do not directly yield dynamical information. While back-action from measurement is inherent to quantum mechanics, a less destructive local probe is desirable, as it would enable whole classes of new experiments [116]. Here we explore the ultimate limits on such a program, calculating how correlations evolve during ideal continuous local density measurements. We quantify the heating in weakly and strongly interacting gases.

Quantum back action arises when the system's energy eigenstates and the measurement operator do not commute. While this back action can be a useful resource [10, 34, 43, 45, 73, 106, 135], more often it leads to unwanted heating or decoherence [33, 52, 57, 65, 102]. We consider measuring the local density of atoms in a lattice. Such a measurement localizes individual atoms to single sites, projecting their wavefunctions to superpositions of momentum states. As noted by Poletti et al., [123], in the long-time limit, this results in an infinite temperature system where all kinetically accessible many-body Fock states are equally likely.

We quantify the approach to this steady state using a master equation for the non-unitary evolution of the density matrix and observables. In the weakly-interacting limit, where atoms are highly delocalized, off-diagonal elements of the

single particle correlation function fall off exponentially with time. In the strongly-interacting limit, where number density is nearly a good quantum number, we find slower evolution: an exponential stage where quasiparticle momenta are scrambled is followed by a slow proliferation of excitations and a parallel decay in correlations.

This heating arises even if the measurement photons are never detected. Thus our formalism is nearly identical to that used by others [22, 37, 101, 118, 119, 122, 123, 134] to study spontaneous off-resonant light scattering in an optical lattice. Other works approached the subject using different formalisms [8, 55, 74, 86, 131].

Our principal results come from from applying variants of the Bogoliubov approximation and calculating the time dependence of single particle correlation functions. Such approaches work well in both the weakly and strongly interacting limits, but do not accurately describe intermediate coupling strength [68]. Previous works used one-dimensional numerical techniques or assumed slow photon scattering rates. Our approximations apply to three-dimensional systems and do not restrict the scattering rate. Our results are consistent with previous studies, and in many places extend our understanding. For example, the doublon-holon picture we present in Section 6.4 gives a clear explanation of the two timescale that have been previously observed in the Mott regime [123] and allows us to quantify the decay rates associated with each.

Our paper is organized as follows. In Section 6.2, we introduce our model and the master equations used to calculate the evolution of the system. From the form of the expressions we make some general observation about the evolution of momentum states and single-particle correlations. In Section 6.3, we use a Bogoliubov approach to integrate the master equations for weakly interacting bosons. In Section 6.4 we extend these calculations to the Mott regime through a doublon-holon

formalism. Finally, in Section 6.5 we consider the use of longer-wavelength light in measurement, exploring the trade-off between information extracted from the system and the heating caused by measurement.

6.2 Model

We model the optical lattice system with the single-band Hubbard model, rewritten slightly as

$$\begin{aligned}\hat{H} &= -J\sum_{\langle i,j\rangle}\left(\hat{a}_i^\dagger\hat{a}_j + \hat{a}_j^\dagger\hat{a}_i\right) + \sum_i \tfrac{U}{2}\hat{n}_i(\hat{n}_i-1) - (\mu - 2JD)\hat{n}_i \\ &= \sum_k (J\epsilon_k - \mu)\hat{n}_k + \tfrac{U}{2}\sum_i \hat{n}_i(\hat{n}_i-1)\end{aligned} \tag{6.1}$$

where $\hat{a}_i$ ($\hat{a}_i^\dagger$) is the annihilation (creation) operator at site i; $\langle i,j\rangle$ are nearest neighbor sites i and j; $\hat{n}_i = \hat{a}_i^\dagger\hat{a}_i$ is the occupation operator at site i; $\hat{n}_k = \hat{a}_k^\dagger\hat{a}_k$ is the occupation of the momentum mode $\boldsymbol{k}$; and $2D$ is the number of nearest neighbors per site. J, U and μ are the hopping energy, interaction energy and chemical potential, respectively. Here we define $\hat{a}_k = \frac{1}{\sqrt{N_s}}\sum_i e^{i\boldsymbol{k}\cdot\boldsymbol{r}_i}\hat{a}_i$, summing over N_s sites at positions $\boldsymbol{r}_i$. The kinetic energy is given by $J\epsilon_k = J\sum_\Delta 4\sin^2(\boldsymbol{k}\cdot\boldsymbol{\Delta}/2)$ where the sum is over all lattice basis vectors $\boldsymbol{\Delta}$.

We model the measurement process as an additional term of the form $\hat{H}_I = \lambda\sum_\alpha\left(\hat{c}_\alpha + \hat{c}_\alpha^\dagger\right)\hat{M}_\alpha$ where $\hat{c}_\alpha$ are annihilation operators for a set of independent zero-temperature photon baths. For single-site resolved position measurements, we take $\hat{M}_\alpha = \hat{n}_i$. We consider a more general operator in Section 6.5. Following Gardiner [53] we adiabatically eliminate the density matrix of the photons to derive a master equation for $\hat{\rho}$, the density matrix of the atoms,

$$\frac{d}{dt}\hat{\rho} = i\left[\hat{\rho}, \hat{H}\right] - \frac{1}{2}\gamma\sum_i [\hat{n}_i, [\hat{n}_i, \hat{\rho}]], \tag{6.2}$$

where we have used that λ is real and $\hat{n}_i$ is Hermitian. Here γ is an energy scale related to the measurement rate. It is proportional to λ and the density of photon states. A more detailed derivation is found in [118].

While the density matrix contains all information about the system, it has an exponentially large number of terms. Thus it is more convenient to work with observables such $\hat{n}_i$, $\hat{n}_i^2$ that are experimentally accessible. Using $\left\langle \hat{O} \right\rangle = \mathrm{Tr}\left[\hat{\rho}\hat{O}\right]$, the evolution of observables is governed by

$$\frac{d}{dt}\left\langle \hat{O} \right\rangle = i\left\langle \left[\hat{H}, \hat{O}\right] \right\rangle - \frac{1}{2}\gamma \sum_i \left\langle \left[\hat{n}_i, \left[\hat{n}_i, \hat{O}\right]\right] \right\rangle. \tag{6.3}$$

Most of our results concern bosonic atoms, though we briefly address the case of noninteracting, spinless fermions. Much of the intuition gained carries over to interacting fermions. Irregardless of statistics, each photon scattered localizes a particle, generically heating the system by increasing the kinetic energy.

Throughout, we assume a homogenous system.

6.2.1 Equations of motion for single-particle observables

The single particle correlations can be studied in momentum space or position space. In a homogenous system, the relevant observables evolve as

$$\frac{d}{dt}\langle \hat{n}_k \rangle = -2U\tfrac{1}{N_s} \sum_{p,q} \mathrm{Im}\left[\left\langle \hat{a}^\dagger_{p-q}\hat{a}^\dagger_{k+q}\hat{a}_p\hat{a}_k \right\rangle\right] - \gamma(\langle \hat{n}_p \rangle - \rho), \tag{6.4}$$

$$\frac{d}{dt}\left\langle \hat{a}^\dagger_i\hat{a}_j \right\rangle = iU\Big(\left\langle \hat{a}^\dagger_i\hat{n}_i\hat{a}_j \right\rangle - \left\langle \hat{a}^\dagger_i\hat{n}_j\hat{a}_j \right\rangle\Big) - \gamma\Big(\left\langle \hat{a}^\dagger_i\hat{a}_j \right\rangle - \rho\delta_{i,j}\Big). \tag{6.5}$$

where $\rho = N_p/N_s$ is the average occupation per site. These are related by $\left\langle \hat{a}_i^\dagger \hat{a}_j \right\rangle = \frac{1}{N_s} \sum_k e^{i\boldsymbol{k}(\boldsymbol{r}_i - \boldsymbol{r}_j)} \langle \hat{n}_k \rangle$. Setting $i = j$ in Eq. (6.5) produces the intuitively obvious result that the average density $\rho = \left\langle \hat{a}_i^\dagger \hat{a}_i \right\rangle$ is constant.

6.2.2 Energy gain

Applying Eq. (6.3) to the Hamiltonian, we find irrespective of interactions

$$\frac{d}{dt}\langle E \rangle = \frac{d}{dt}\left\langle \hat{H} \right\rangle = \gamma J \sum_{\boldsymbol{k}} \epsilon_k (\rho - \langle \hat{n}_k \rangle). \tag{6.6}$$

The instantaneous rate of energy gain depends only on the kinetic energy in the system. It is proportional to the difference between the kinetic energy and the "infinite-temperature" kinetic energy of a system with $\langle \hat{n}_k \rangle = \rho$.

Equation (6.6) applies to both bosons and fermions. Fermions tend to have broader equilibrium momentum distributions, hence lower rates of energy gains. For free bosons at zero temperature $\langle \hat{n}_k \rangle = \delta_{k,0} N_p$, and one finds initially $\frac{1}{N_p} \frac{d}{dt} \langle E \rangle = 2\gamma J \times D$. The equivalent result for free fermions is shown in Fig. 6.1 as a function of filling. As $\langle n_i \rangle \to 0$, the fermionic rate approaches the bosonic rate.

This result differs from Eq. (31) in [118]. There the off-resonant light scattering from the lattice can drive atoms to high bands, while we consider measurements that are engineered to keep atoms in the lowest band. For example, in [116], Raman side-band cooling rapidly returns atoms to the lowest band.

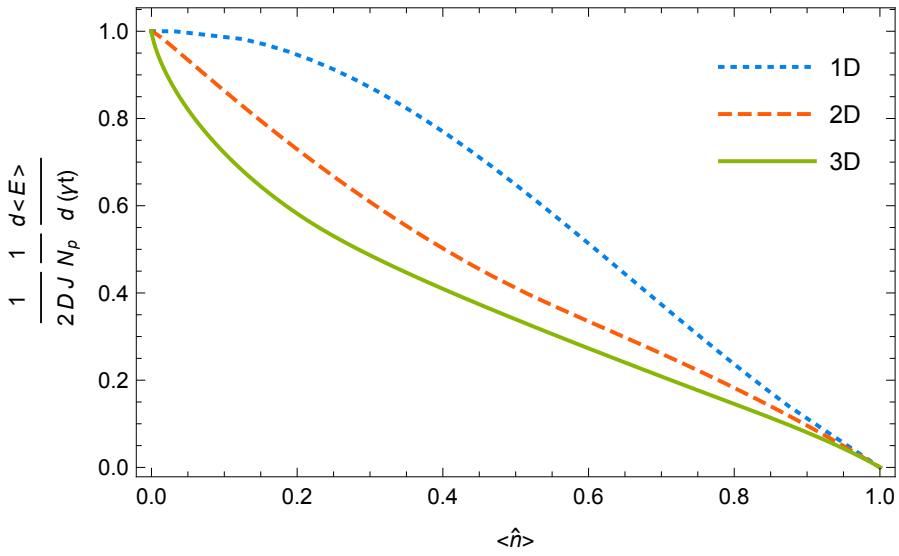

Figure 6.1: Initial rate of energy gain, $\frac{1}{2\gamma JD}\frac{1}{N_p}\frac{d}{dt}\langle E\rangle$ as function of the filling fraction $\langle\hat{n}\rangle$ for spinless fermions, in various dimensions. For noninteracting bosons, the initial rate is always $\frac{1}{N_p}\frac{d}{dt}\langle E\rangle = 2\gamma JD$. Here J is the hopping energy, γ the measurement rate and D is the dimension of the system.

Non-interacting particles

If $U = 0$, Eqs. (6.4) and (6.5) are readily integrated,

$$\langle\hat{n}_k\rangle = (\langle\hat{n}_k\rangle_{t=0} - \rho)e^{-\gamma t} + \rho \tag{6.7}$$

$$\left\langle\hat{a}_i^\dagger\hat{a}_j\right\rangle = \left(\left\langle\hat{a}_i^\dagger\hat{a}_j\right\rangle_{t=0} - \delta_{ij}\rho\right)e^{-\gamma t} + \delta_{ij}\rho. \tag{6.8}$$

These expressions hold for both noninteracting bosons and fermions, the only difference being initial conditions. The correlations decay exponentially with a time constant $\tau_m = 1/\gamma$ set by the measurement rate. The occupation of momentum states approaches a uniform distribution.

6.3 Weakly Interacting Bosons

We extend our analysis to the weakly interacting case by a variant of the Hartree-Fock-Bogoliubov-Popov (HFBP) approach [60]. This approximation is well validated for static quantities in dimensions greater than one. It is a gapless model which includes interactions between atoms and discards some of the coherences between non-condensed particles.

Within this formalism we calculate $\langle \hat{n}_k(t) \rangle$ for $k \neq 0$, then infer the condensate density via $\rho_c = \frac{\langle \hat{n}_0 \rangle}{N_s} = \rho - \frac{1}{N_s} \sum_{\boldsymbol{k} \neq 0} \langle \hat{n}_k \rangle$. The occupation numbers evolve with Eq. (6.3), where we approximate $\hat{H}$ by the HFBP Hamiltonian

$$\begin{aligned} \hat{H}_{\mathrm{HFBP}} &= -\frac{U}{2}(2\rho - \rho_c)\langle \hat{n}_0 \rangle \\ &+ \sum_{\boldsymbol{k} \neq 0} (J\epsilon_k + U\rho_c)\hat{n}_k + \frac{1}{2} U\rho_c \Big(\hat{a}_k \hat{a}_{-k} + \hat{a}_k^\dagger \hat{a}_{-k}^\dagger \Big). \end{aligned} \tag{6.9}$$

Evaluationg the commutators in Eq. (6.3) yields

$$\frac{d}{dt}\langle \hat{n}_k \rangle = -2U\rho_c \mathrm{Im}[\langle \hat{a}_k \hat{a}_{-k} \rangle] - \gamma(\langle \hat{n}_k \rangle - \rho), \tag{6.10}$$

$$\begin{aligned} \frac{d}{dt}\langle \hat{a}_k \hat{a}_{-k} \rangle &= -2i(J\epsilon_k + U\rho_c)\langle \hat{a}_k \hat{a}_{-k} \rangle - iU\rho_c(\langle \hat{n}_k \rangle + \langle \hat{n}_{-k} \rangle + 1) \\ &- \gamma \Bigg(\langle \hat{a}_k \hat{a}_{-k} \rangle + \tfrac{1}{N_s} \textstyle\sum_p \langle \hat{a}_p \hat{a}_{-p} \rangle \Bigg), \end{aligned} \tag{6.11}$$

whereby the equations of motion of $\langle \hat{n}_k \rangle$ are coupled to those of $\langle \hat{a}_k \hat{a}_{-k} \rangle$.

Consistent with the Popov approximation, we replace $\sum_p \langle \hat{a}_p \hat{a}_{-p} \rangle \to \rho_c$. This approximation only discards terms which vanish as $N_s \to \infty$.

These coupled equations can be perturbatively integrated for $U \ll J\epsilon_k$, yielding

to first order in U/J,

$$\langle \hat{n}_k \rangle \approx (\langle \hat{n}_k \rangle_{t=0} - \rho) e^{-\gamma t} + \rho \frac{U\rho^2}{J} \frac{4J^2\epsilon_k}{\gamma^2 + 4J^2{\epsilon_k}^2} e^{-\gamma t}\left(1 - e^{-\gamma t}\right) + \frac{U\rho^2}{J} \frac{2\gamma\left(\gamma \sin^2(J\epsilon_k t) + J\epsilon_k \sin(2J\epsilon_k t)\right)}{\epsilon_k(\gamma^2 + 4J^2{\epsilon_k}^2)} e^{-2\gamma t}. \tag{6.12}$$

By integrating over all momenta we find the condensate density. The leading behavior coincides with Eqs. (6.7) and (6.8). The deviation from this form is shown for a range of γ/J in Fig. 6.2. In three dimensions, this deviation is capped at $\rho_c - \rho e^{-\gamma t} \sim 0.1\frac{U\rho^2}{J}$. We expect detecting it would be very difficult.

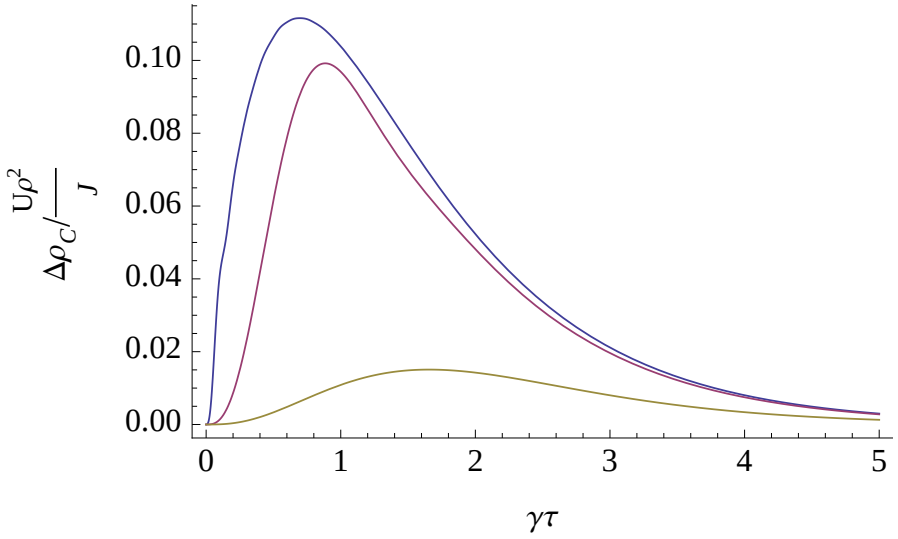

Figure 6.2: Corrections to the exponential decay of the condensate density, $\Delta\rho_c = \rho_c(t) - \rho e^{-\gamma t}$, induced by weak interactions. From top to bottom (blue, magenta, yellow) the corrections for $\gamma/J = 0.1, 1, 5$ in a three-dimensional cubic lattice.

6.4 Strongly-Interacting Bosons

The low-energy states of the $U/J \gg 1$ Bose-Hubbard model with near integer filling, $|\rho - \bar{n}| \ll 1$ for some integer $\bar{n}$, can be described by the subspace made up of states where the single site occupations are $\bar{n}, \bar{n} \pm 1$ [9]. We model this behavior by introducing "doublons" and "holons" as hard-core particles representing an

occupation of one-higher or one lower than the mean $\bar{n}$,

$$\hat{a}_i \to \sqrt{\bar{n}+1}\hat{d}_i + \sqrt{\bar{n}}\hat{h}_i^\dagger \tag{6.13}$$

with $\hat{d}_i^2 = \hat{h}_i^2 = \hat{h}_i\hat{d}_i = 0$. The names "doublons" and "holons" are motivated by the most common case, $\bar{n} = 1$. The effective Hamiltonian becomes

$$\begin{aligned}\hat{H}_{\mathrm{DH}} = \sum_k &\left[\frac{U}{2} + J\left(\sqrt{\tilde{n}^2 + \tfrac{1}{4}} + \tfrac{1}{2}\right)\varepsilon_k\right]\hat{d}_k^\dagger\hat{d}_k \\ &+ \left[\frac{U}{2} + J\left(\sqrt{\tilde{n}^2 + \tfrac{1}{4}} - \tfrac{1}{2}\right)\varepsilon_k\right]\hat{h}_k^\dagger\hat{h}_k \\ &+ J\tilde{n}\varepsilon_k\left(\hat{d}_k\hat{h}_{-k} + \hat{h}_{-k}^\dagger\hat{d}_k^\dagger\right)\end{aligned} \tag{6.14}$$

where $\hat{d}_k, \hat{h}_k$ are related to $\hat{d}_i, \hat{h}_i$ in the same way as $\hat{a}_k$ is to $\hat{a}_i$. Here the kinetic energy is $J\varepsilon_k = J(\epsilon_k - 2D) = -2J\sum_{\Delta\boldsymbol{r}}\cos(\boldsymbol{k}\cdot\Delta\boldsymbol{r})$ and $\tilde{n} = \sqrt{\bar{n}(\bar{n}+1)}$.

This structure is similar to that in Eq. (6.9) with two exceptions. First, the Hamiltonian of Eq. (6.14) allows for the creation of doublons and holons in pairs. Second, the hard-core constraints give non-bosonic commutation relations (see Eq. (6.30) in the appendix). Neglecting non-coherent summations, these relations become

$$\left[\hat{d}_k, \hat{d}_q^\dagger\right] \to \delta_{k,q}\big(1 - 2\hat{n}^d - \hat{n}^h\big), \tag{6.15}$$

where $\hat{n}^d = \frac{1}{N_s}\sum_k \hat{d}_k^\dagger\hat{d}_k$ is the density of doublons and $\hat{n}^h$ the density of holons. This approximation is equivalent to a mean field theory of the interactions.

We apply Eq. (6.3) to the Hamiltonian of Eq. (6.14), using the approximate commutation relations of Eq. (6.15). We decouple the equations for two-point functions from higher order correlations by assuming

$$\left\langle \hat{n}^d\hat{d}_k^\dagger\hat{d}_k\right\rangle \to n^d\left\langle \hat{d}_k^\dagger\hat{d}_k\right\rangle \tag{6.16}$$

and similarly for combinations of $\hat{n}^d, \hat{n}^h$ with $\hat{d}_k^\dagger\hat{d}_k, \hat{h}_k^\dagger\hat{h}_k$ or $\hat{d}_k\hat{h}_{-k}$. Here $n^d = \langle\hat{n}^d\rangle$.

Under these assumptions, we find a set of coupled equations for $\left\langle \hat{d}_k^\dagger \hat{d}_k \right\rangle$, $\left\langle \hat{h}_k^\dagger \hat{h}_k \right\rangle$, $\left\langle \hat{d}_k \hat{h}_{-k} \right\rangle$ and n^d, n^h. Working in the commensurate case, $\rho = \bar{n}$ and hence $n^d = n^h$, we solve these equations as detailed in Section 6.7.

We find that the behavior of the system is characterized by two processes with two corresponding time scales.

The first process, occurring at a rate $1/\tau_m \sim \gamma$, involves the localization of quasiparticles when they are detected. It is illustrated by the occupation number of doublons with momentum k,

$$\begin{aligned} \left\langle \hat{d}_k^\dagger \hat{d}_k \right\rangle = &\left[\left\langle \hat{d}_k^\dagger \hat{d}_k \right\rangle_{t=0} - n_k^d \right] e^{-\gamma t} + n_k^d \\ &- e^{-\gamma t} \Delta_k [\tfrac{\gamma^2}{U^2}(1 - \cos(Ut)) + \tfrac{\gamma}{U} \sin(Ut)] + O\big(\tfrac{J}{U}\big)^3. \end{aligned} \tag{6.17}$$

Apart from the structure of the transient oscillatory term, this behavior is similar to the weakly-interacting case in Eq. (6.12). The momentum distribution of the quasiparticles is driven to one which is slowly varying and nearly uniform,

$$n_k^d = n^d + \frac{J^2}{U^2} \frac{2\tilde{n}^2 \big(1 - 3n^d\big)^2 U^2}{(1 - 3n^d)^2 U^2 + \gamma^2} \big(1 - n^d\big)\big(\varepsilon_k^2 - 2D\big). \tag{6.18}$$

As is explicit in the form of the correction, this represents a competition between the coherent creation of quasiparticles and the measurement-induced destruction of coherences.

In parallel, the measurement process results in a slow increase in the total number of quasiparticles. The rate of this process is characterized by $1/\tau_p \sim \frac{4D\tilde{n}^2 J^2}{U^2+\gamma^2}\gamma$ and it is governed by the nonlinear equation of motion

$$\begin{aligned} \frac{d}{dt} n^d = &\frac{J^2}{U^2} \frac{4D\tilde{n}^2 \big(1 - 3n^d\big)^2 U^2}{(1 - 3n^d)^2 U^2 + \gamma^2} \big(1 - n^d\big)\gamma \times \\ &\left[1 - e^{-\gamma t} \big(\cos(Ut) + \tfrac{\gamma}{U} \sin(Ut) \big) + O\big(\tfrac{J}{U}\big) \right]. \end{aligned} \tag{6.19}$$

One intuition for this growth comes from picturing the Mott insulator state as filled with virtual doublon-holon pairs. Whenever a virtual doublon or holon is imaged, the pair is converted into a real doublon and holon.

For shorter times, $\gamma t \ll \left(\frac{J}{U}\right)^{-2}$, the number of excitations remains small, $n^d \ll 1$. Then the right hand side of Eq. (6.19) may be integrated,

$$n^d = n^d_{t=0} + \frac{4D\tilde{n}J^2}{U^2+\gamma^2}\Big[\gamma t - \tfrac{2\gamma^2}{U^2+\gamma^2}\big(1 - e^{-\gamma t}\Xi(t)\big) + O\big(\tfrac{J}{U}, n^d\big)\Big], \tag{6.20}$$

where the transient oscillations

$$\Xi(t) = \cos(Ut) - \frac{1}{2}\Big(\frac{U}{\gamma} - \frac{\gamma}{U}\Big)\sin(Ut) \tag{6.21}$$

are followed by linear growth in the excitation density.

The complete time evolution of $\langle n^d \rangle$ is plotted in Fig. 6.3 for typical parameters.

Within our approximations, $n^d \to \frac{1}{3}$ as long times. This is the infinite temperature limit of the model in Eq. (6.14): each site is equally likely to be empty, have a doublon or have a holon. However, once n^d is of order unity, the model no longer fully describes the physics, and one must include larger fluctuation in the site occupation to fully capture the physics.

The atom correlation functions can be calculated from those of the doublons and holons. They will be short ranged, dominated by nearest neighbor correlations, such as

$$\begin{aligned}\left\langle \hat{a}_i^\dagger \hat{a}_{i+1} \right\rangle = \frac{J}{U}\frac{2\tilde{n}^2\big(1-3n^d\big)^2U^2}{(1-3n^d)^2U^2+\gamma^2}\big(1-n^d\big)\times \\ \Big[1 + e^{-\gamma t}\big(\tfrac{\gamma^2}{U^2}\cos(Ut) - \tfrac{\gamma}{U}\sin(Ut)\big) + O\big(\tfrac{J}{U}\big)\Big]\end{aligned} \tag{6.22}$$

These are plotted in Fig. 6.4 for typical parameters. As discussed above, two time scale are apparent in the graph.

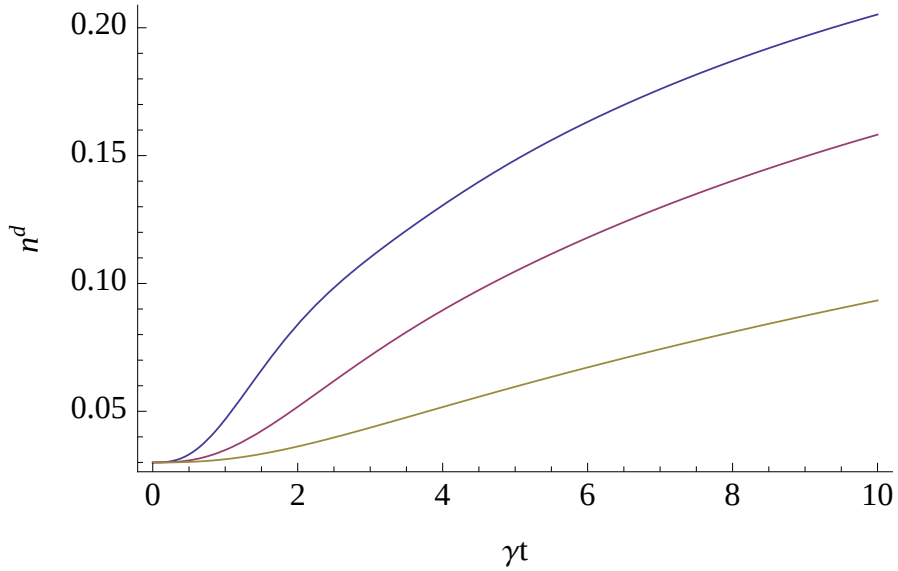

Figure 6.3: Growth in doublon density with measurement in a Mott system. At short times, the measurement process primarily scatters doublons into a uniform momentum occupation. This is followed by a growth in doublon density that is initially linear and levels off as a result of the hard-core constraints on doublon occupation. From top to bottom (blue, magenta, yellow) $\gamma/U = 0.5, 1, 2$, in a three-dimensional cubic lattice with $J/U = 0.05$, $\bar{n} = 1$.

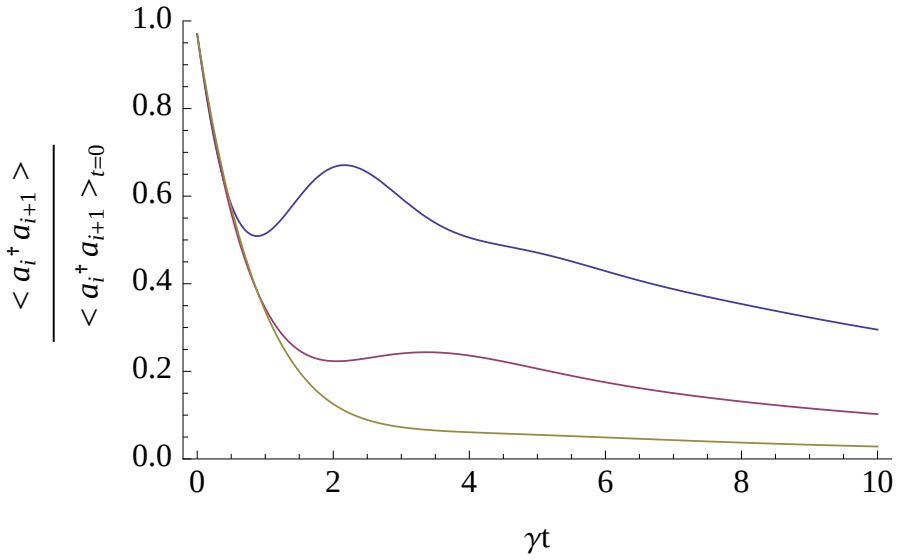

Figure 6.4: The evolution of the nearest-neighbor single-particle correlation function $\left\langle \hat{a}_i^\dagger \hat{a}_{i+1} \right\rangle$ in a Mott system. From top to bottom (blue, magenta, yellow) $\gamma = 0.5, 1, 2$, in a three-dimensional cubic lattice with $J = 0.05U$, $\bar{n} = 1$.

6.5 Long wavelength measurements

We have explored so far the destruction of non-local correlations from the spontaneous localization of atoms to single lattice sites. As previously noted [69, 118], the length scale of the localization is determined by the wavelength of the emitted light. Here we extend our argument to the case where the wavelength of light measuring the system is larger than the lattice spacing.

A simple model of such a measurement is

$$\hat{M}_i = \hat{n}_i^{\xi} = \frac{1}{\mathcal{N}_\xi} \sum_j e^{-\frac{1}{2}\left(\frac{r_j - r_i}{\xi}\right)^2} \hat{n}_j, \tag{6.23}$$

where the normalization is $\mathcal{N}_\xi = \sum_i e^{-\frac{1}{2}(r_i/\xi)^2}$ is proportional to the width of the measurement.

Measurement with such long wavelength light does not localize the atoms to single lattice sites. One learns less about the system, but perturbs it proportionally less.

For free particles, the evolution of momentum states is replaced by the equation

$$\frac{d}{dt}\langle \hat{n}_k \rangle = -\frac{\mathcal{N}_{\xi/\sqrt{2}}}{(\mathcal{N}_\xi)^2} \gamma \Big(\langle \hat{n}_k \rangle - \tfrac{1}{N_s} \sum G_\xi(p) \langle \hat{n}_{k+p} \rangle \Big) \tag{6.24}$$

where $G_\xi(p) = \sum_i e^{-\frac{1}{4}\left(\frac{r_i}{\xi}\right)^2} e^{ipr_i}$. For the two-point correlation we find the closed form

$$\begin{aligned} \left\langle \hat{a}_i^\dagger \hat{a}_j \right\rangle &= \left\langle \hat{a}_i^\dagger \hat{a}_j \right\rangle_{t=0} e^{-\bar{\gamma}_{|i-j|} t} \\ \bar{\gamma}_{|i-j|} &= g_\xi \sqrt{\tfrac{1}{\pi}} \tfrac{\Delta r}{2D\xi} \left(1 - \exp\left[-\tfrac{1}{4} \left(\tfrac{r_i - r_j}{\xi} \right)^2 \right] \right), \end{aligned} \tag{6.25}$$

where Δr is the spacing between sites and the function $g_\xi = \frac{\mathcal{N}_{\xi/\sqrt{2}}}{(\mathcal{N}_\xi)^2} \left[\sqrt{\frac{1}{\pi}} \frac{\Delta r}{2D\xi} \right]^{-1}$ has $g_\xi \approx 1$ for $|\xi| \gtrsim |\Delta r|$. Thus the rate at which correlations are lost is suppressed

linearly in ξ and correlations on scales smaller than ξ decay at a much reduced rate.

6.6 Summary

We would like to have non-destructive site-resolved measurements. Unfortunately, no measurement is entirely non-destructive. Here we have quantified the effect of an ideal density measurement on a lattice system. In the superfluid regime, we use Bogoliubov theory to show that all spatial correlations decay exponentially with γt, the number of photons scattered. In the Mott regime, we find that the momenta of the quasiparticles are quickly scrambled, leading to a slowly evolving quasi-steady state. In this slow-proliferation stage, fluctuations in the on-site density gradually grow. Similar physics was seen in numerical studies [122, 123].

We predict how momentum occupation and single-particle correlations evolve with time. The former can be studied through time of flight experiments [35]. Protocols exist for the direct measurement of the single particle correlation function [63, 64, 130, 146]. Finally, though our focus is on measurement, the formalism and all of our results apply to spontaneous emission (in the absence of excitations to higher bands). As such they provide a quantitative estimate of the effects of spontaneous emission on coherence.

It is useful to put the loss of correlations into the context of the information gained as light is emitted. Assuming no dynamics, the continual measurement reduces the uncertainty in the number of atoms on a given site with time, $\delta n_i^2 \sim e^{-\gamma t}$ [58]. Thus, in the superfluid regime, the uncertainty falls at the same rate as do the correlations. In the Mott regime the uncertainty falls faster.

In this regard, long-wavelength measurements may be advantageous. If one wishes to measure the total number of particles in the cloud, the reduced uncertainty is set by the number of scattered photons, not their wavelength. As seen above, however, the backaction is reduced for long-wavelength probes. In general, one would wish to tailor the process of measurement so that all information carried by the probe is experimentally accessible.

6.7 Full Derivation of the Strongly Interacting Model

We present here the full derivation of our results for strongly interacting bosons.

Our starting point is the Hamiltonian

$$\begin{aligned}\hat{H}_{\mathrm{DH}} = \sum_k \Bigg[&\tfrac{U}{2} + J\left(\sqrt{\tilde{n}^2 + \tfrac{1}{4}} + \frac{1}{2}\right)\varepsilon_k \Bigg] \hat{d}_k^\dagger \hat{d}_k \\ &+ \left[\tfrac{U}{2} + J\left(\sqrt{\tilde{n}^2 + \tfrac{1}{4}} - \frac{1}{2}\right)\varepsilon_k\right] \hat{h}_k^\dagger \hat{h}_k \\ &+ J\tilde{n}\varepsilon_k \left(\hat{d}_k \hat{h}_{-k} + \hat{h}_{-k}^\dagger \hat{d}_k^\dagger\right)\end{aligned} \tag{6.26}$$

where as before, $\varepsilon_k = -2\sum_{\Delta \boldsymbol{r}} \cos(\boldsymbol{k} \cdot \Delta \boldsymbol{r})$ and $\tilde{n} = \sqrt{\bar{n}(\bar{n}+1)}$. With this Hamiltonian the difference between the total number of doublons and holons is constant. We work in the commensurate case, where the particle density is given by the integer $\bar{n}$ and the total number of doublons equals the total number of holons.

The operators $\hat{d}_i$ and $\hat{h}_i$ have a hard core constraint $\hat{d}_i^2 = \hat{h}_i^2 = \hat{d}_i \hat{h}_i = 0$. In equilibrium, at small J/U and T/U, this constraint has little effect as the densities of doublons and holons is small. During the measurement process, however, the number of quasiparticles grows, and we will need to include these constraints.

6.7.1 Initial State

The initial equilibrium properties of Eq. (6.26) can be calculated by performing a Bogoliubov transformation, as in Section 2.6.2,

$$\begin{aligned} \hat{d}_k &= \cosh\theta_k \tilde{d}_k + \sinh\theta_k \tilde{h}^\dagger_{-k}, \\ \hat{h}_k &= \cosh\theta_k \tilde{h}_k + \sinh\theta_k \tilde{d}^\dagger_{-k}, \end{aligned} \qquad \tanh(2\theta_k) = -\frac{2J\tilde{n}\varepsilon_k}{U + 2J\sqrt{\bar{n}^2 + \frac{1}{4}\varepsilon_k}}. \tag{6.27}$$

Neglecting the hard-core constraints, which can be ignored for low-defect densities, $\tilde{d}_k$, $\tilde{h}_k$ are bosonic operators and the Hamiltonian takes the diagonal form

$$\begin{aligned} \hat{H}_{\mathrm{DHB}} &= \sum_k \left(\tilde{E}_k + \frac{1}{2}J\varepsilon_k\right)\tilde{d}^\dagger_k \tilde{d}_k + \left(\tilde{E}_k - \frac{1}{2}J\varepsilon_k\right)\tilde{h}^\dagger_k \tilde{h}_k, \\ \tilde{E}_k &= \frac{1}{2}\sqrt{\left(U + 2J\sqrt{\tilde{n}^2 + \tfrac{1}{4}\varepsilon_k}\right)^2 - (2J\tilde{n}\varepsilon_k)^2}. \end{aligned} \tag{6.28}$$

We take our initial conditions to correspond to the ground state, where $\left\langle \tilde{d}^\dagger_k \tilde{d}_k \right\rangle = \left\langle \tilde{h}^\dagger_k \tilde{h}_k \right\rangle = 0$, and hence

$$\begin{aligned} \left\langle \hat{d}^\dagger_k \hat{d}_k \right\rangle_{t=0} = \left\langle \hat{h}^\dagger_k \hat{h}_{-k} \right\rangle_{t=0} &= \left(\tfrac{J}{U}\right)^2 \tilde{n}^2 \varepsilon_k^2 + O\left(\tfrac{J}{U}\right)^3, \\ \left\langle \hat{d}_k \hat{h}_{-k} \right\rangle_{t=0} &= -\tfrac{J}{U}\tilde{n}\varepsilon_k + O\left(\tfrac{J}{U}\right)^2. \end{aligned} \tag{6.29}$$

The calculation may be easily extended to low finite temperatures as long as the initial particle densities remain of the order $\left(\frac{J}{U}\right)^2$.

6.7.2 Evolution Equations

To obtain the full evolution equations we must now include the hard core constraints. In momentum space, these constraints lead to the commutation relations

$$\begin{aligned}\left[\hat{d}_k, \hat{d}_q^\dagger\right] &= \delta_{k,q} - \tfrac{1}{N_s}\sum_p 2\hat{d}_{q+p}^\dagger \hat{d}_{k+p} + \hat{h}_{q+p}^\dagger \hat{h}_{k+p} \\ \left[\hat{h}_k, \hat{h}_q^\dagger\right] &= \delta_{k,q} - \tfrac{1}{N_s}\sum_p \hat{d}_{q+p}^\dagger \hat{d}_{k+p} + 2\hat{h}_{q+p}^\dagger \hat{h}_{k+p} \\ \left[\hat{d}_k, \hat{h}_q^\dagger\right] &= -\tfrac{1}{N_s}\sum_p \hat{h}_{q+p}^\dagger \hat{d}_{k+p}.\end{aligned} \tag{6.30}$$

In these sums, the terms where operators have different momentum indices will add incoherently, suggesting the approximation

$$\begin{aligned}\left[\hat{d}_k, \hat{d}_q^\dagger\right] &\approx \delta_{k,q}\big(1 - 2\hat{n}^d - \hat{n}^h\big), \\ \left[\hat{h}_k, \hat{h}_q^\dagger\right] &\approx \delta_{k,q}\big(1 - 2\hat{n}^h - \hat{n}^d\big), \qquad \left[\hat{d}_k, \hat{h}_q^\dagger\right] \approx 0,\end{aligned} \tag{6.31}$$

where $\hat{n}^d = \frac{1}{N_s}\sum_k \hat{d}_k^\dagger \hat{d}_k$ and similarly for $\hat{n}^h$.

We substitute Eq. (6.26) into Eq. (6.3), using the commutators in Eq. (6.31), for $\hat{O} = \hat{d}_k^\dagger \hat{d}_k$ and $\hat{O} = \hat{d}_k \hat{h}_{-k}$. We assume that the total number of quasiparticles is uncorrelated with their momentum distribution,

$$\begin{aligned}\left\langle \hat{n}^d \hat{d}_k^\dagger \hat{d}_k \right\rangle &\approx n^d \left\langle \hat{d}_k^\dagger \hat{d}_k \right\rangle, \qquad \left\langle \hat{n}^d \hat{h}_k^\dagger \hat{h}_k \right\rangle \approx n^d \left\langle \hat{h}_k^\dagger \hat{h}_k \right\rangle, \\ \left\langle \hat{n}^d \hat{d}_k \hat{h}_{-k} \right\rangle &\approx n^d \left\langle \hat{d}_k \hat{h}_{-k} \right\rangle, \qquad \left\langle \hat{n}^h \hat{d}_k^\dagger \hat{d}_k \right\rangle \approx n^h \left\langle \hat{d}_k^\dagger \hat{d}_k \right\rangle, \\ \left\langle \hat{n}^h \hat{h}_k^\dagger \hat{h}_k \right\rangle &\approx n^h \left\langle \hat{h}_k^\dagger \hat{h}_k \right\rangle, \qquad \left\langle \hat{n}^h \hat{d}_k \hat{h}_{-k} \right\rangle \approx n^h \left\langle \hat{d}_k \hat{h}_{-k} \right\rangle,\end{aligned} \tag{6.32}$$

where $n^{d,h} = \langle \hat{n}^{d,h} \rangle$. One can formally derive these relations through perturbation theory in J/U, although their validity is wider.

The evolution is then governed by two coupled nonlinear differential equations,

$$\frac{d}{dt}\left\langle \hat{d}_k^\dagger \hat{d}_k \right\rangle = -2\tilde{n}\bar{J}_t \varepsilon_k \mathrm{Im}\left[\left\langle \hat{d}_k \hat{h}_{-k} \right\rangle\right] - \gamma\left(\left\langle \hat{d}_k^\dagger \hat{d}_k \right\rangle - n^d\right) \tag{6.33}$$

$$\frac{d}{dt}\left\langle \hat{d}_k \hat{h}_{-k} \right\rangle = -i\tilde{n}\bar{J}_t \varepsilon_k P_t - i\left(\bar{U}_t + 2\sqrt{\tilde{n}^2 + \tfrac{1}{4}}\bar{J}_t \varepsilon_k\right)\left\langle \hat{d}_k \hat{h}_{-k} \right\rangle - \gamma\left\langle \hat{d}_k \hat{h}_{-k} \right\rangle. \tag{6.34}$$

where all k dependence is through $\varepsilon_k = -2\sum_{\Delta \boldsymbol{r}} \cos(\boldsymbol{k}\cdot\Delta\boldsymbol{r})$. Here

$$\bar{J}_t = J\big(1-3n^d\big), \qquad \bar{U}_t = U\big(1-3n^d\big), \qquad P_t = \Big(1+2\Big\langle \hat{d}_k^\dagger \hat{d}_k\Big\rangle - 3n^d\Big) \tag{6.35}$$

are time dependent, but, as we will see, vary at a rate much slower than γ.

In the commensurate case, $n^d = n^h$, and one finds identical initial values and evolution equations for the momentum occupation of holons and doublons, hence $\Big\langle \hat{d}_k^\dagger \hat{d}_k\Big\rangle = \Big\langle \hat{h}_k^\dagger \hat{h}_k\Big\rangle$ at all times.

6.7.3 Ansatz Solution

All of the k-dependence in Eqs. (6.33) and (6.34) arises from terms of the form $J\varepsilon_k$. Since $J \ll U$, we can expand in this product, finding

$$\begin{aligned} \Big\langle \hat{d}_k^\dagger \hat{d}_k\Big\rangle = \Big\langle \hat{h}_{-k}^\dagger \hat{h}_{-k}\Big\rangle &= dd^{(0)} + dd^{(2)}\big(\tfrac{J}{U}\big)^2\varepsilon_k^2 + O\big(\tfrac{J}{U}\big)^3 \\ \Big\langle \hat{d}_k \hat{h}_{-k}\Big\rangle &= dh^{(1)}\big(\tfrac{J}{U}\big)\varepsilon_k + O\big(\tfrac{J}{U}\big)^2. \end{aligned} \tag{6.36}$$

where $dd^{(0)}, dd^{(2)}, dh^{(1)}$ are functions of time but not k. By Fourier transforming these expressions we can relate them to the more familiar

$$n^d = dd^{(0)} + 2D\big(\tfrac{J}{U}\big)^2 dd^{(2)} + O\big(\tfrac{J}{U}\big)^3, \qquad \Big\langle \hat{d}_i \hat{h}_{i+1}\Big\rangle = -\tfrac{J}{U} dh^{(1)} + O\big(\tfrac{J}{U}\big)^2. \tag{6.37}$$

Equations (6.33) and (6.34) then reduce to

$$\frac{d}{dt} n^d = \big(\tfrac{J}{U}\big) 4D\tilde{n}\bar{J}_t \mathrm{Im}\Big[\Big\langle \hat{d}_i \hat{h}_{i+1}\Big\rangle / \tfrac{J}{U}\Big] + O\Big(\tfrac{J^3}{U^2}\Big) \tag{6.38}$$

$$\frac{d}{dt}\Big\langle \hat{d}_i \hat{h}_{i+1}\Big\rangle = i\tilde{n}\bar{J}_t\big(1-n^d\big) - i\bar{U}_t\Big\langle \hat{d}_i \hat{h}_{i+1}\Big\rangle - \gamma\Big\langle \hat{d}_i \hat{h}_{i+1}\Big\rangle + O\Big(\tfrac{J^2}{U}\Big) \tag{6.39}$$

$$\frac{d}{dt}dd^{(2)} = 2\tilde{n}\bar{U}_t \mathrm{Im}\Big[\Big\langle \hat{d}_i\hat{h}_{i+1}\Big\rangle / \tfrac{J}{U}\Big] - \gamma dd^{(2)} + O(J) \tag{6.40}$$

while the initial conditions are

$$n^d_{t=0} = \left(\tfrac{J}{U}\right)^2 2D\tilde{n}^2, \qquad dd^{(2)}_{t=0} = \tilde{n}^2, \qquad \Big\langle \hat{d}_i\hat{h}_{i+1}\Big\rangle_{t=0} = \tfrac{J}{U}\tilde{n}. \tag{6.41}$$

We note that Eqs. (6.38) and (6.39) are coupled to each other but independent of Eq. (6.40). At this point, the equations may be numerically integrated for any given values of γ, J, U. Typical values are plotted in in Figs. 6.3 and 6.4.

6.7.4 Short Time Behavior

The initial and short-time behavior of Eqs. (6.38) and (6.39) can be analyzed using $n^d_{t=0} \sim \left(\tfrac{J}{U}\right)^2$. Thus, we can neglect the non-linear terms, $\bar{J}_t \approx J, \bar{U}_t \approx U$ finding

$$\frac{d}{dt}n^d = \tfrac{J}{U} 4D\tilde{n}J\,\mathrm{Im}\Big[\Big\langle \hat{d}_i\hat{h}_{i+1}\Big\rangle / \tfrac{J}{U}\Big] + O\Big(\tfrac{J^3}{U^2}, n^d\Big) \tag{6.42}$$

$$\frac{d}{dt}\Big\langle \hat{d}_i\hat{h}_{i+1}\Big\rangle = i\tilde{n}J - iU\Big\langle \hat{d}_i\hat{h}_{i+1}\Big\rangle - \gamma\Big\langle \hat{d}_i\hat{h}_{i+1}\Big\rangle + O\Big(\tfrac{J^2}{U}, n^d\Big). \tag{6.43}$$

Equation (6.43) produces a function which oscillates with frequency U while decaying at a rate γ to a steady state value,

$$\Big\langle \hat{d}_i\hat{h}_{i+1}\Big\rangle = \Big[\Big\langle \hat{d}_i\hat{h}_{i+1}\Big\rangle_{t=0} - \tfrac{iJ\tilde{n}}{iU+\gamma}\Big] e^{-\gamma t}e^{-iUt} + \tfrac{iJ\tilde{n}}{iU+\gamma}. \tag{6.44}$$

Using this result to calculate the number of doublons, we find

$$\begin{aligned} n^d = {} & n^d_{t=0} \\ & + \frac{4D\tilde{n}^2J^2}{U^2+\gamma^2}\Big[\gamma t - \tfrac{2\gamma^2}{U^2+\gamma^2}\Big(1 - e^{-\gamma t}\Big[\cos(Ut) - \tfrac{1}{2}\Big(\tfrac{U}{\gamma} - \tfrac{\gamma}{U}\Big)\sin(Ut)\Big]\Big)\Big]. \end{aligned} \tag{6.45}$$

Aside from small transients, we see a linear increase in n^d with characteristic rate $1/\tau_p = \frac{4D\tilde{n}^2J^2}{U^2+\gamma^2}\gamma$. Physically, this is the rate at which virtual doublon-holon pairs are imaged. This linearized theory breaks down when $n^d \sim 1$. Thus it is valid until $t \sim \tau_p \gg 1/\gamma$.

6.7.5 General Behavior

Given the separation of timescales between the rate of change in n^d and $\left\langle \hat{d}_i\hat{h}_{i+1}\right\rangle$, we can adiabatically eliminate the nonlinear terms in Eq. (6.38), rather than simply neglecting them. This yields

$$\begin{aligned}\left\langle \hat{d}_i\hat{h}_{i+1}\right\rangle = \left\langle \hat{d}_i\hat{h}_{i+1}\right\rangle_{t=0} e^{-\gamma t}e^{-iUt} + \left\langle \hat{d}_i\hat{h}_{i+1}\right\rangle^{long} \\ + \big(1-e^{-\gamma t}e^{-iUt}\big)\frac{i\tilde{n}J\big(1-3n^d\big)}{iU(1-3n^d)+\gamma}\big(1-n^d\big) + O\big(\tfrac{J}{U}\big)^2\end{aligned} \tag{6.46}$$

at all times. When $n^d \ll 1$, this reduces to Eq. (6.44).

Substituting this expression into Eq. (6.38) yields

$$\frac{d}{dt}n^d = \frac{J^2}{U^2}\frac{4D\tilde{n}^2\big(1-3n^d\big)^2U^2}{(1-3n^d)^2U^2+\gamma^2}\big(1-n^d\big)\gamma\big[1-e^{-\gamma t}\big(\cos(Ut)+\tfrac{\gamma}{U}\sin(Ut)\big)\big] \tag{6.47}$$

which simplifies to Eqs. (6.44) and (6.45) for $n^d \ll 1$. Likewise, we adiabatically eliminate Eq. (6.40) to obtain Eq. (6.20) in the main text.

CHAPTER 7

THE DYNAMICS OF LATTICE INTERACTION RAMPS ACROSS THE PHASE BOUNDARY

7.1 Introduction

The dynamics of systems driven through a phase transition are a source of rich physics [136]. The phenomenology is particularly interesting in zero-temperature systems driven through a quantum phase transition [5,144]. In recent years, breakthrough experimental techniques in atomic physics have given us a direct probe of such transitions [27, 59, 71, 114, 147]. In this paper, we model a bosonic lattice system driven from a Mott insulator state to into the superfluid regime. We introduce a novel mean-field theory, building on commonly used doublon-holon models [9]. We calculate how correlations develop during a lattice ramp through the phase transition.

The phase diagram of bosonic lattice systems has been explored thoroughly [44, 61, 75, 138, 149]. In the strongly interacting regime, at commensurate filling, lattice bosons form an incompressible Mott insulator. Conversely, for weak interactions the ground state is a superfluid Bose-Einstein condensate with long range order. When the system begins in a Mott insulator state and interactions are turned off, correlations grow as quasiparticles propagate across the system [29, 108].

The Mott and superfluid phases can be approximated by distinct mean-field quasiparticle models. The excitations in the superfluid phase are well described by Bogoliubov quasiparticles made up of superpositions of particles and holes in the condensate [60]. In the Mott insulator regime, on-site number fluctuations

are small and the occupation of each site can be truncated to a small number of possibilities [9]. This approximate Hamiltonian is referred to as the "doublon-holon" model. These two descriptions are incompatible, making it challenge to model the dynamics across the phase boundary.

Previous work has produced partial understanding of this transition [38, 126]. Product state methods such as the Gutzwiller ansatz can be used to look for the the phase transition point but typically cannot calculate correlations [164, 167]. Other approaches have included calculations on small lattices [31], field theory calculations for large particle density [2,110,124,153] and various numerical techniques, which work well in one dimension but are otherwise more limited [79, 89, 133]. There has also been significant work on sudden quenches [125, 152] Here, we provide an analytical model that is particularly suitable for the small mean occupation numbers common in atomic experiments, provides access to coherence data, and is applicable at dimensionality.

7.2 Model

We perform our calculation within an approximate "doublon-holon" model. The model restricts the state of each site i to the subspace

$$|i\rangle \in \{|\bar{n}+1\rangle, |\bar{n}\rangle, |\bar{n}-1\rangle\} \tag{7.1}$$

where $\bar{n}$ is the median number of particles per site. The system can then be thought of in terms of a mean-occupation background and hard-core quasiparticle excitations of "holons" (an $\bar{n}-1$ occupation) and "doublons" ($\bar{n}+1$ occupation). The annihilation operators at site i for these quasiparticles are, as defined by their

operation on the vector $\Big(|\bar{n}+1\rangle_i, \quad |\bar{n}\rangle_i, \quad |\bar{n}-1\rangle_i\Big)^T$,

$$\hat{d}_i \equiv \begin{pmatrix} 0 & 1 & 0 \\ 0 & 0 & 0 \\ 0 & 0 & 0 \end{pmatrix} \quad \hat{h}_i \equiv \begin{pmatrix} 0 & 0 & 0 \\ 0 & 0 & 0 \\ 0 & 1 & 0 \end{pmatrix}. \tag{7.2}$$

Under this approximation, the Hamiltonian is

$$\begin{aligned} \hat{H} = \sum_k \Bigg[& \frac{U}{2} + J\Bigg(\sqrt{\tilde{n}^2 + \tfrac{1}{4}} + \tfrac{1}{2}\Bigg)\varepsilon_k \Bigg] \hat{d}_k^\dagger \hat{d}_k \\ & + \Bigg[\frac{U}{2} + J\Bigg(\sqrt{\tilde{n}^2 + \tfrac{1}{4}} - \tfrac{1}{2}\Bigg)\varepsilon_k \Bigg] \hat{h}_k^\dagger \hat{h}_k \\ & + J\tilde{n}\varepsilon_k \Big(\hat{d}_k \hat{h}_{-k} + \hat{h}_{-k}^\dagger \hat{d}_k^\dagger \Big). \end{aligned} \tag{7.3}$$

Here, $\hat{d}_k = \frac{1}{\sqrt{N_s}} \sum_i e^{i\boldsymbol{k}\cdot\boldsymbol{r}_i} \hat{d}_i$, summing over all sites i, and similar for $\hat{h}_k$, while $\varepsilon_k = -2\sum_\Delta \cos(\boldsymbol{k}\cdot\boldsymbol{\Delta})$, summing over lattice basis vectors, $\boldsymbol{\Delta} = \Delta\hat{x}, \Delta\hat{y}, \Delta\hat{z}$ in three dimensions, or a subset of those in lower dimensions. These represent a cubic lattice with lattice constant Δ. U and J are the interaction and hopping strength, respectively, and $\tilde{n} = \sqrt{\bar{n}(\bar{n}+1)}$. N_s is the number of sites in the lattice.

The doublon-holon model is an approximation for the single-band Bose-Hubbard model [44, 70]. It is most accurate in the low-temperature, strongly-interacting limit, as the energy of a state increases quadratically with the deviation from the mean particle number. However, for low occupation numbers $\bar{n}$, it can be a good approximation in the weakly-interacting limit as well. In a noninteracting superfluid gas with $\bar{n} = 1$, the probability of finding more than two particles on a given site is less than 10%.

We do all our calculations in this regime, $\langle \hat{n}_i \rangle = \bar{n} + \left\langle \hat{d}_i^\dagger \hat{d}_i \right\rangle - \left\langle \hat{h}_i^\dagger \hat{h}_i \right\rangle = \bar{n} = 1$.

Though the Hamiltonian of Eq. (7.3) is quadratic, the hard-core constraints on

$\hat{d}$ and $\hat{h}$ translate into non-trivial commutation relations,

$$\begin{gathered}\left[\hat{d}_k, \hat{d}_q^\dagger\right] = \delta_{k,q} - 2\hat{n}_{q-k}^d - \hat{n}_{q-k}^h, \quad \left[\hat{d}_k^\dagger, \hat{h}_q\right] = \hat{\nu}_{q-k} \\ \left[\hat{h}_k, \hat{h}_q^\dagger\right] = \delta_{k,q} - \hat{n}_{q-k}^d - 2\hat{n}_{q-k}^h, \quad \left[\hat{h}_k^\dagger, \hat{d}_q\right] = \hat{\nu}_{k-q}^\dagger \\ \left[\hat{d}_k, \hat{d}_q\right] = \left[\hat{h}_k, \hat{h}_q\right] = \left[\hat{d}_k, \hat{h}_q\right] = 0,\end{gathered} \tag{7.4}$$

where we define the quasiparticle density operators

$$\hat{n}_k^d = \tfrac{1}{N_s}\sum_i e^{-i\boldsymbol{k}\cdot r_i}\hat{d}_i^\dagger\hat{d}_i, \quad \hat{n}_k^h = \tfrac{1}{N_s}\sum_i e^{-i\boldsymbol{k}\cdot r_i}\hat{h}_i^\dagger\hat{h}_i, \quad \hat{\nu}_k^\dagger = \tfrac{1}{N_s}\sum_i e^{-i\boldsymbol{k}\cdot r_i}\hat{h}_i^\dagger\hat{d}_i. \tag{7.5}$$

We mark $\hat{n}_{d,h} \equiv \hat{n}_0^{d,h}$, the density of doublons and holons, respectively. In the Mott equilibrium limit, these density operators can be neglected and the quasiparticles can be treated as noninteracting bosons to a good degree. This is not true in other regimes, such as after the interaction strength has been reduced.

Equations of motion can be derived from Eq. (7.3). Equations of motion can be derived from the Hamiltonian, Eq. (2.40), via the Heisenberg equation,

$$\frac{d}{dt}\left\langle \hat{X} \right\rangle = i\left\langle \left[\hat{X}, \hat{H}\right] \right\rangle. \tag{7.6}$$

We focus on the two-point observables,

$$\begin{aligned}\frac{d}{dt}\left\langle \hat{d}_k^\dagger\hat{d}_k \right\rangle &= iJ\tilde{n}\varepsilon_k\left(\left\langle \hat{d}_k\hat{h}_{-k} \right\rangle - \left\langle \hat{d}_k^\dagger\hat{h}_{-k}^\dagger \right\rangle\right) \\ &\quad - iJ\tilde{n}\sum_q \varepsilon_q \begin{bmatrix} \left(\sqrt{1+\frac{1}{4\tilde{n}^2}} + \frac{1}{2\tilde{n}}\right)\left\langle \hat{d}_q^\dagger(2\hat{n}_{k-q}^d + \hat{n}_{k-q}^h)\hat{d}_k \right\rangle \\ +\left(\sqrt{1+\frac{1}{4\tilde{n}^2}} - \frac{1}{2\tilde{n}}\right)\left\langle \hat{h}_{-q}^\dagger\hat{\nu}_{-k-q}\hat{d}_k \right\rangle \\ +\left\langle (2\hat{n}_{k-q}^d + \hat{n}_{k-q}^h)\hat{h}_{-q}\hat{d}_k \right\rangle + \left\langle \hat{\nu}_{-q-k}\hat{d}_q\hat{d}_k \right\rangle \end{bmatrix} - \text{h. c.}\end{aligned} \tag{7.7}$$

$$\begin{aligned}\frac{d}{dt}\left\langle \hat{h}_{-k}^\dagger\hat{h}_{-k} \right\rangle &= iJ\tilde{n}\varepsilon_k\left(\left\langle \hat{d}_k\hat{h}_{-k} \right\rangle - \left\langle \hat{d}_k^\dagger\hat{h}_{-k}^\dagger \right\rangle\right) \\ &\quad - iJ\tilde{n}\sum_q \varepsilon_q \begin{bmatrix} \left(\sqrt{1+\frac{1}{4\tilde{n}^2}} - \frac{1}{2\tilde{n}}\right)\left\langle \hat{h}_{-q}^\dagger(2\hat{n}_{q-k}^h + \hat{n}_{q-k}^d)\hat{h}_{-k} \right\rangle \\ +\left(\sqrt{1+\frac{1}{4\tilde{n}^2}} + \frac{1}{2\tilde{n}}\right)\left\langle \hat{d}_q^\dagger\hat{\nu}_{-q-k}^\dagger\hat{h}_{-k} \right\rangle \\ +\left\langle (2\hat{n}_{q-k}^h + \hat{n}_{q-k}^d)\hat{d}_q\hat{h}_{-k} \right\rangle + \left\langle \hat{\nu}_{-q-k}^\dagger\hat{h}_{-q}\hat{h}_{-k} \right\rangle \end{bmatrix} - \text{h. c.}\end{aligned} \tag{7.8}$$

$$
\begin{aligned}
&\frac{d}{dt}\Big\langle \hat{d}_k \hat{h}_{-k} \Big\rangle = \\
&-iU\Big\langle \hat{d}_k \hat{h}_{-k} \Big\rangle - iJ\tilde{n}\varepsilon_k(1-3n_d-3n_h+2n_{d,d}+2n_{h,h}+5n_{d,h}+n_{\nu,\nu}) \\
&-iJ\tilde{n}\sum_q \varepsilon_q\Big(\delta_{k,q}-\tfrac{1}{N_s}\Big)\Big[2\sqrt{1+\tfrac{1}{4\tilde{n}^2}}\Big\langle \hat{d}_q \hat{h}_{-q}\Big\rangle + \Big\langle \hat{d}_q^\dagger \hat{d}_q\Big\rangle + \Big\langle \hat{h}_{-q}^\dagger \hat{h}_{-q}\Big\rangle\Big] \\
&+iJ\tilde{n}\sum_q \varepsilon_q \begin{bmatrix}
\Big(\sqrt{1+\frac{1}{4\tilde{n}^2}}+\frac{1}{2\tilde{n}}\Big)\begin{pmatrix}\Big\langle \hat{h}_{-q}\big(2\hat{n}^d_{k-q}+\hat{n}^h_{k-q}\big)\hat{d}_k\Big\rangle \\ +\Big\langle \hat{d}_q\hat{\nu}_{-q-k}\hat{d}_k\Big\rangle\end{pmatrix} \\
+\Big(\sqrt{1+\frac{1}{4\tilde{n}^2}}-\frac{1}{2\tilde{n}}\Big)\begin{pmatrix}\Big\langle \hat{d}_q\big(\hat{n}^d_{q-k}+2\hat{n}^h_{q-k}\big)\hat{h}_{-k}\Big\rangle \\ +\Big\langle \hat{h}_{-q}\hat{\nu}^\dagger_{-q-k}\hat{h}_{-k}\Big\rangle\end{pmatrix} \\
+\Big\langle \hat{h}_{-q}^\dagger\big(2\hat{n}^d_{q-k}+\hat{n}^h_{q-k}\big)\hat{h}_{-k}\Big\rangle + \Big\langle \hat{d}_q^\dagger\hat{\nu}^\dagger_{-q-k}\hat{h}_{-k}\Big\rangle \\
+\Big\langle \hat{d}_q^\dagger\big(\hat{n}^d_{k-q}+2\hat{n}^h_{k-q}\big)\hat{d}_k\Big\rangle + \Big\langle \hat{h}_{-q}^\dagger\hat{\nu}_{-q-k}\hat{d}_k\Big\rangle
\end{bmatrix},
\end{aligned}
\tag{7.9}
$$

$$
\begin{aligned}
n_{d,d} &= \big\langle \hat{n}_i^d \hat{n}^d_{i+\boldsymbol{\Delta}}\big\rangle, \qquad & n_{h,h} &= \big\langle \hat{n}_i^h \hat{n}^h_{i+\boldsymbol{\Delta}}\big\rangle \\
n_{d,h} &= \big\langle \hat{n}_i^d \hat{n}^h_{i+\boldsymbol{\Delta}}\big\rangle, \qquad & n_{\nu,\nu} &= \Big\langle \hat{h}_i^\dagger \hat{d}^\dagger_{i+\boldsymbol{\Delta}}\hat{h}_{i+\boldsymbol{\Delta}}\hat{d}_i\Big\rangle,
\end{aligned}
\tag{7.10}
$$

Here h. c. stands for the Hermitian conjugate, while the functions of Eq. (7.10) are all independent of $i, \boldsymbol{\Delta}$ in a cubic lattice.

To perform the time evolution, we must make approximations for the quartic terms, such as

$$
\mathcal{C}_k^1 = \sum_q \varepsilon_q \Big\langle \hat{d}_q^\dagger \hat{n}^h_{k-q}\hat{d}_k\Big\rangle = \tfrac{1}{N_s}\sum_{p,q}\varepsilon_q\Big\langle \hat{d}_q^\dagger \hat{h}^\dagger_{-p-q}\hat{h}_{-p-k}\hat{d}_k\Big\rangle \equiv \tfrac{1}{N_s}\sum_{p,q}\varepsilon_q C_{k,q,p}. \tag{7.11}
$$

These can be written out as

$$
\begin{aligned}
\mathcal{C}_k^1 = {}& \tfrac{1}{N_s}\sum_p \varepsilon_k\Big\langle \hat{d}_k^\dagger \hat{h}^\dagger_{-k-p}\hat{h}_{-k-p}\hat{d}_k\Big\rangle + \tfrac{1}{N_s}\sum_q \varepsilon_q\Big\langle \hat{d}_q^\dagger \hat{h}^\dagger_{-q}\hat{h}_{-k}\hat{d}_k\Big\rangle \\
&- \tfrac{1}{N_s}\varepsilon_k\Big\langle \hat{d}_k^\dagger \hat{h}^\dagger_{-k}\hat{h}_{-k}\hat{d}_k\Big\rangle + \tfrac{1}{N_s}\sum_{\substack{p,q \\ q\neq k, p\neq 0}} \varepsilon_q\Big\langle \hat{d}_q^\dagger \hat{h}^\dagger_{-p-q}\hat{h}_{-k-q}\hat{d}_k\Big\rangle.
\end{aligned}
\tag{7.12}
$$

The first two sums on the right hand side add up coherently, and we expect them to dominate. The third term is inversely proportional to the system size and

so negligible. For bosonic operators, one may expect the final sum to add up incoherently, as in the Hartree-Fock-Bogoliubov approximation [60], suggesting the form

$$\begin{aligned}\mathcal{C}_k^1 \approx \tilde{\mathcal{C}}_k^1 = &\left(\tfrac{1}{N_s}\sum_p \left\langle \hat{h}^\dagger_{-k-p}\hat{h}_{-k-p}\right\rangle\right)\varepsilon_k\left\langle \hat{d}_k^\dagger \hat{d}_k\right\rangle \\ &+\left(\tfrac{1}{N_s}\sum_q \varepsilon_q\left\langle \hat{d}_q^\dagger \hat{h}^\dagger_{-q}\right\rangle\right)\left\langle \hat{h}_{-k}\hat{d}_k\right\rangle.\end{aligned} \tag{7.13}$$

This intuition fails in the hard-core case. This can be seen by summing over k,

$$\begin{aligned}\sum_k \mathcal{C}_k^1 = \tfrac{1}{N_s}\sum_{p,q,k}\varepsilon_q\left\langle \hat{d}_q^\dagger \hat{h}^\dagger_{-p-q}\hat{h}_{-p-k}\hat{d}_k\right\rangle = \tfrac{1}{N_s}\sum_{p,q,i} e^{ipr_i}\varepsilon_q\left\langle \hat{d}_q^\dagger \hat{h}^\dagger_{-p-q}\hat{h}_i\hat{d}_i\right\rangle = 0 \\ \sum_k \tilde{\mathcal{C}}_k^1 = \left(\tfrac{1}{N_s}\sum_p \left\langle \hat{h}^\dagger_{-k-p}\hat{h}_{-k-p}\right\rangle\right)\left(\sum_k \varepsilon_k\left\langle \hat{d}_k^\dagger \hat{d}_k\right\rangle\right).\end{aligned} \tag{7.14}$$

To account for the hard core constraints, we expand the term in the summand

$$\begin{aligned}C^1_{k,p,q} = \left\langle \hat{d}_q^\dagger \hat{h}^\dagger_{-p-q}\hat{h}_{-p-k}\hat{d}_k\right\rangle = \\ \delta_{k,q}\left\langle \hat{h}^\dagger_{-p-q}\hat{h}_{-p-k}\right\rangle \hat{d}_k^\dagger\hat{d}_k + \delta_{p,0}\left\langle \hat{d}_q^\dagger\hat{h}^\dagger_{-q}\right\rangle\left\langle \hat{h}_{-k}\hat{d}_k\right\rangle - \tfrac{\alpha_{k,p,q}}{N_s}\left\langle \hat{d}_k^\dagger\hat{d}_k\right\rangle,\end{aligned} \tag{7.15}$$

where this equation defines $\alpha_{k,p,q}$. We approximate this function with the hard core constraint in mind,

$$\alpha_{k,p,q} \approx \frac{1}{\langle \hat{n}^d\rangle}\left\langle \hat{h}^\dagger_{-p-q}\hat{h}_{-p-q}\right\rangle\left\langle \hat{d}_q^\dagger\hat{d}_q\right\rangle, \tag{7.16}$$

so that $\sum_k C^1_{k,p,q} = 0$. We then find

$$\mathcal{C}_k^1 = \tfrac{1}{N_s}\sum_{p,q} C^1_{k,p,q} \approx \langle \hat{n}^h\rangle\left(\varepsilon_k - \varepsilon_0\tfrac{\xi_d}{n_d}\right)\left\langle \hat{d}_k^\dagger\hat{d}_k\right\rangle + \varepsilon_0\eta^*\left\langle \hat{d}_k\hat{h}_{-k}\right\rangle \tag{7.17}$$

where

$$n_d = \langle \hat{n}^d\rangle \qquad \xi_d = \tfrac{1}{N_s}\sum_k \tfrac{\varepsilon_k}{\varepsilon_0}\left\langle \hat{d}_k^\dagger\hat{d}_k\right\rangle \qquad \eta = \tfrac{1}{N_s}\sum_k \tfrac{\varepsilon_k}{\varepsilon_0}\left\langle \hat{d}_k\hat{h}_{-k}\right\rangle. \tag{7.18}$$

We make similar approximations for the other terms,

$$\begin{aligned}
\Big\langle \hat{d}_q^\dagger \hat{d}_{p-q}^\dagger \hat{d}_{p-k} \hat{d}_k \Big\rangle &\approx \delta_{q,k} \Big\langle \hat{d}_{p-k}^\dagger \hat{d}_{p-k} \Big\rangle \Big\langle \hat{d}_k^\dagger \hat{d}_k \Big\rangle + \delta_{p-q,k} \Big\langle \hat{d}_q^\dagger \hat{d}_q \Big\rangle \Big\langle \hat{d}_k^\dagger \hat{d}_k \Big\rangle \\
&\quad - \tfrac{2}{N_s} \tfrac{1}{n_d} \Big\langle \hat{d}_q^\dagger \hat{d}_q \Big\rangle \Big\langle \hat{d}_{p-q}^\dagger \hat{d}_{p-q} \Big\rangle \Big\langle \hat{d}_k^\dagger \hat{d}_k \Big\rangle \\
\Big\langle \hat{h}_{-q}^\dagger \hat{d}_{p+q}^\dagger \hat{h}_{p-k} \hat{d}_k \Big\rangle &\approx \delta_{p,0} \Big\langle \hat{h}_{-q}^\dagger \hat{d}_q^\dagger \Big\rangle \Big\langle \hat{d}_k \hat{h}_{-k} \Big\rangle + \delta_{p+q,k} \Big\langle \hat{h}_{-q}^\dagger \hat{h}_{-q} \Big\rangle \Big\langle \hat{d}_k^\dagger \hat{d}_k \Big\rangle \\
&\quad - \tfrac{1}{N_s} \tfrac{1}{n_d} \Big\langle \hat{h}_{-q}^\dagger \hat{h}_q \Big\rangle \Big\langle \hat{d}_{p+q}^\dagger \hat{d}_{p+q} \Big\rangle \Big\langle \hat{d}_k^\dagger \hat{d}_k \Big\rangle
\end{aligned} \tag{7.19}$$

$$\begin{aligned}
\Big\langle \hat{h}_{-q} \hat{h}_{-p-q}^\dagger \hat{h}_{-p-k} \hat{d}_k \Big\rangle &\approx \delta_{q,k} \Big\langle \hat{h}_{-p-k}^\dagger \hat{h}_{-p-k} \Big\rangle \Big\langle \hat{d}_k \hat{h}_{-k} \Big\rangle + \delta_{p,0} \Big\langle \hat{h}_{-q} \hat{h}_{-q}^\dagger \Big\rangle \Big\langle \hat{d}_k \hat{h}_{-k} \Big\rangle \\
&\quad - \tfrac{1}{N_s} \tfrac{1}{n_d} \Big\langle \hat{h}_{-p-q}^\dagger \hat{h}_{-p-q} \Big\rangle \Big\langle \hat{d}_q \hat{h}_{-q} \Big\rangle \Big\langle \hat{d}_k^\dagger \hat{d}_k \Big\rangle \\
\Big\langle \hat{h}_{-q} \hat{d}_{p-q}^\dagger \hat{d}_{p-k} \hat{d}_k \Big\rangle &\approx \delta_{q,k} \Big\langle \hat{d}_{p-k}^\dagger \hat{d}_{p-k} \Big\rangle \Big\langle \hat{d}_k \hat{h}_{-k} \Big\rangle + \delta_{p-q,k} \Big\langle \hat{d}_q \hat{h}_{-q} \Big\rangle \Big\langle \hat{d}_k^\dagger \hat{d}_k \Big\rangle \\
&\quad - \tfrac{2}{N_s} \tfrac{1}{n_d} \Big\langle \hat{d}_q \hat{h}_{-q} \Big\rangle \Big\langle \hat{d}_{p-q}^\dagger \hat{d}_{p-q} \Big\rangle \Big\langle \hat{d}_k^\dagger \hat{d}_k \Big\rangle \\
\Big\langle \hat{d}_q \hat{d}_{p+q}^\dagger \hat{h}_{p-k} \hat{d}_k \Big\rangle &\approx \delta_{p,0} \Big\langle \hat{d}_q \hat{d}_q^\dagger \Big\rangle \Big\langle \hat{d}_k \hat{h}_{-k} \Big\rangle + \delta_{p+q,k} \Big\langle \hat{d}_q \hat{h}_{-q} \Big\rangle \Big\langle \hat{d}_k^\dagger \hat{d}_k \Big\rangle \\
&\quad - \tfrac{1}{N_s} \tfrac{1}{n_d} \Big\langle \hat{d}_q \hat{h}_{-q} \Big\rangle \Big\langle \hat{d}_{p+q}^\dagger \hat{d}_{p+q} \Big\rangle \Big\langle \hat{d}_k^\dagger \hat{d}_k \Big\rangle .
\end{aligned} \tag{7.20}$$

Applying these approximations to Eqs. (7.7) to (7.9), we find a closed set of non-linear, coupled differential equations,

$$\begin{aligned}
\frac{d}{dt} \Big\langle \hat{d}_k^\dagger \hat{d}_k \Big\rangle &= iJ\tilde{n}\varepsilon_k \Big(\Big\langle \hat{d}_k \hat{h}_{-k} \Big\rangle - \Big\langle \hat{d}_k^\dagger \hat{h}_{-k}^\dagger \Big\rangle \Big) \\
&\quad - iJ\tilde{n} \begin{bmatrix} 3\Big(\varepsilon_k n_d \Big\langle \hat{d}_k \hat{h}_{-k} \Big\rangle - \varepsilon_0 \eta \Big\langle \hat{d}_k^\dagger \hat{d}_k \Big\rangle \Big) \\ +2\varepsilon_0 \Big(\sqrt{1 + \frac{1}{4\tilde{n}^2}}\, \eta^* \Big\langle \hat{d}_k \hat{h}_{-k} \Big\rangle + \xi_d \Big\langle \hat{d}_k \hat{h}_{-k} \Big\rangle \Big) \end{bmatrix} - \text{h. c.}
\end{aligned} \tag{7.21}$$

$$\begin{aligned}
&\frac{d}{dt} \Big\langle \hat{d}_k \hat{h}_{-k} \Big\rangle = -iU \Big\langle \hat{d}_k \hat{h}_{-k} \Big\rangle - iJ\tilde{n}\varepsilon_k \big(1 - 6n_d + 9\big(n_d^2 - \xi_d^2 \big) + 6|\eta|^2 \big) \\
&- 2iJ\tilde{n} \Big[\sqrt{1 + \tfrac{1}{4\tilde{n}^2}} \Big(\Big\langle \hat{d}_q \hat{h}_{-q} \Big\rangle - \eta \Big) + \Big\langle \hat{d}_k^\dagger \hat{d}_k \Big\rangle - \xi_d \Big] \\
&+ 2iJ\tilde{n} \begin{bmatrix} \sqrt{1 + \frac{1}{4\tilde{n}^2}} \Big(3\Big(\varepsilon_k n_d \Big\langle \hat{d}_k \hat{h}_{-k} \Big\rangle - \varepsilon_0 \eta \Big\langle \hat{d}_k^\dagger \hat{d}_k \Big\rangle \Big) + 2\varepsilon_0 \xi_d \Big\langle \hat{d}_k \hat{h}_{-k} \Big\rangle \Big) \\ +3(\varepsilon_k n_d - \varepsilon_0 \xi_d) \Big\langle \hat{d}_k^\dagger \hat{d}_k \Big\rangle + 3\varepsilon_0 \eta^* \Big\langle \hat{d}_k \hat{h}_{-k} \Big\rangle \end{bmatrix},
\end{aligned} \tag{7.22}$$

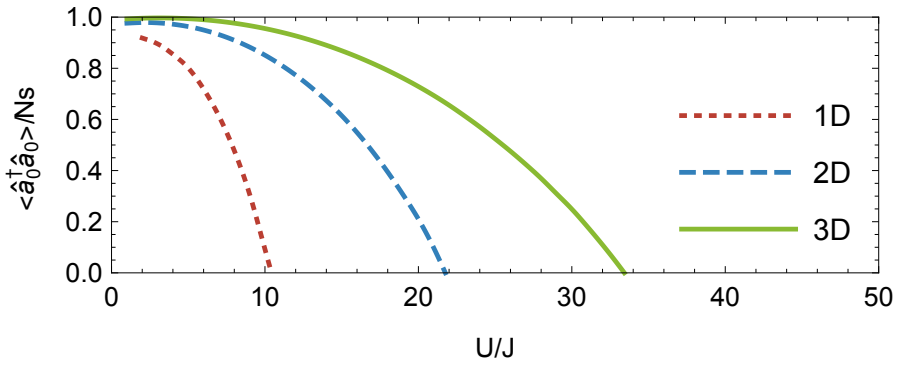

(a) Condensate Fraction

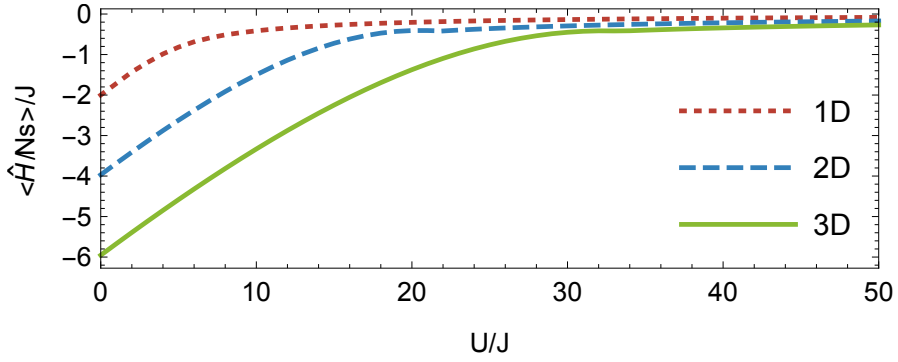

(b) Energy density

Figure 7.1: Equilibrium properties of the hard-core doublon-holon model as approximated in Eqs. (7.21) and (7.22),for a cubic lattice with mean filling $\bar{n} = 1$. Shown as a function of the interaction strength U/J, (a) the equilibrium condensate fraction, (b) energy density.

with $\left\langle \hat{h}^\dagger_{-k} \hat{h}_{-k} \right\rangle = \left\langle \hat{d}^\dagger_k \hat{d}_k \right\rangle$.

We numerically integrate these equations to find all quasiparticle two-point correlation functions at any time. From these we can easily extract the correlation functions for real particles, $\left\langle \hat{a}^\dagger_i \hat{a}_j \right\rangle$ and $\left\langle \hat{a}^\dagger_k \hat{a}_k \right\rangle$.

7.3 Equilibrium State

We find the equilibrium state under this model by minimizing the expectation value $\left\langle \hat{H} \right\rangle$ of the Hamiltonian of Eq. (2.40) while requiring $\frac{d}{dt}\left\langle \hat{d}_k^\dagger \hat{d}_k \right\rangle = \frac{d}{dt}\left\langle \hat{d}_k \hat{h}_{-k} \right\rangle = 0$. As seen in Fig. 7.1, we find a phase transition at a critical value of $U_c/J = 10.4, 21.8, 33.4$ in one-, two- and three-dimensions. These are similar to the standard mean-field values of $U_c/J = 11.6, 23.2, 34.8$ [17, 138] and somewhat higher than numerically calculated values $U_c/J = 3.6, 16.9, 29.3$ [23, 24, 39, 46, 104, 150].

7.4 Interaction Ramps

We use the model above to explore the behavior of a gas subject to a non-adiabatic ramp of the interaction through the phase transition. We perform an interaction ramp of the form

$$U = U_i (U_f/U_i)^{t/\tau_r}, \tag{7.23}$$

where the ground state of the system is a Mott insulator for $U = U_i$ and superfluid for $U = U_f$. The time scale τ_r sets the speed of the ramp. This form approximates the relation U/J obtained in an optical lattice if the inter-particle interaction strength remains fixed while the lattice depth is reduced [75].

We initialize the system in the ground state at the initial lattice depth, in the Mott regime, and perform a finite-element time integration of the evolution equations as the interaction strength is reduced. We calculate the momentum space density throughout this evolution for various values of τ_r. Figure 7.2 shows the behavior for a typical ramp, with $J\tau_r = 2$. We have full access to all two-point observables at any time along the ramp.

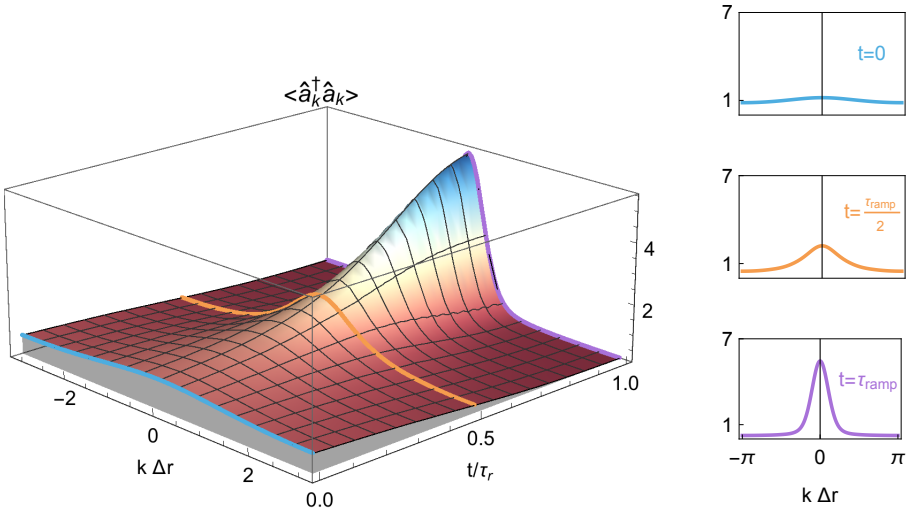

(a) Momentum density distribution (b)

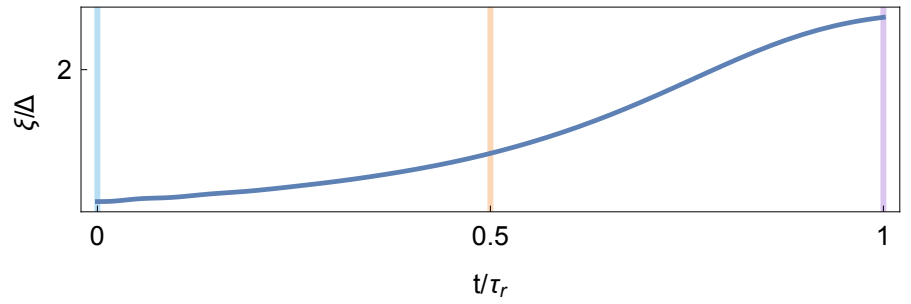

(c) Correlation length

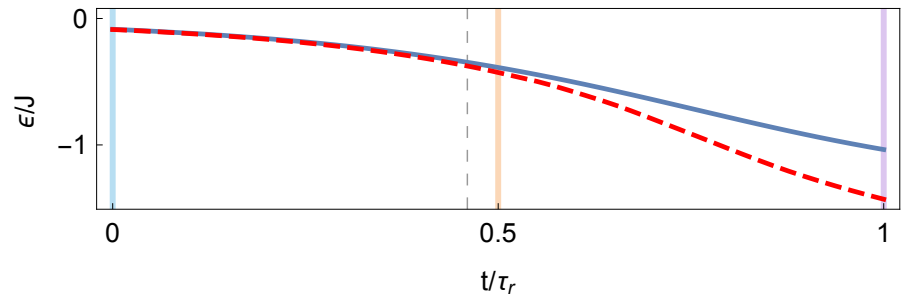

(d) Energy density evolution

Figure 7.2: Evolution of the momentum density distribution function $\left\langle \hat{a}_k^\dagger \hat{a}_k \right\rangle$ as the interaction strength is slowly ramped down, $U = U_i(U_f/U_i)^{t/\tau_r}$ in a one-dimensional lattice. Here $U_i = 47J, U_f = 2J, J\tau_r = 2$. (a) Shows the complete evolution of the momentum density function while (b) shows snapshots of the momentum density at the beginning, middle and end of the ramp. (c) Shows the evolution of the effective coherence length ξ (see Eq. (7.24)). (d) Shows the energy per particle, $\varepsilon = \frac{1}{N_s}\left\langle \hat{H} \right\rangle$, as a solid blue line, compared with the ground state energy (red dashed line). The dashed grey grid line at $t/\tau_r \approx 0.52$ corresponds to $U(t)/J = (U/J)_c$.

We first characterize the behavior of the system at the end of the ramp. We define an effective correlation length, ξ, by comparing correlations in the system to the form $\left\langle \hat{a}_i^\dagger \hat{a}_j \right\rangle = \bar{n} e^{-|\boldsymbol{r}_j - \boldsymbol{r}_i|/\xi}$. We calculate ξ by fitting to the width of the momentum distribution, as defined by the first moment, yielding

$$\frac{\xi}{\Delta} = -1/\log\left[\frac{1}{N_s}\sum_k \frac{\varepsilon_k}{\varepsilon_0}\left\langle \hat{a}_k^\dagger \hat{a}_k \right\rangle\right]. \tag{7.24}$$

Though it is infinite for a superfluid system, ξ remains finite at any finite time for a system that is not initially superfluid [29].

Figure 7.3 shows the effective correlation length at the end of the ramp for varying ramp times. In one dimension, our calculation agrees well with the result of an exact diagonalization of a small lattice. Our results also agree with the experimental results of [21], up to $J\tau_r \sim 2$. For longer ramp times, finite size effects become significant.

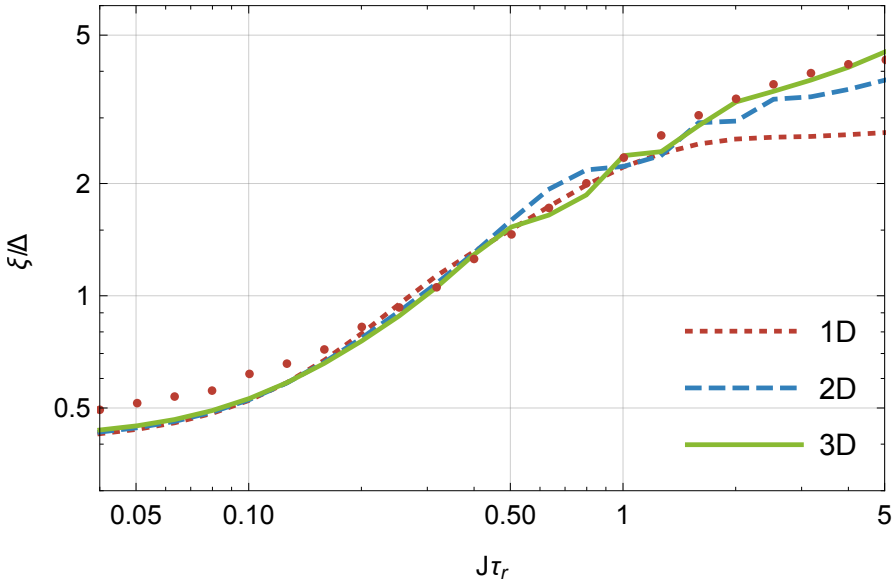

Figure 7.3: Effective correlation length ξ normalized by the lattice constance Δ, at the end of a ramp of the interaction strength of the form $U = U_i(U_f/U_u)^{t/\tau_r}$. Here $U_f = 47J, U_i = 2J$. The correlation length ξ is defined by the width of the momentum peak (see Eq. (7.24)). The red dots are the result of an exact diagonalization calculation for an 11-site one-dimensional lattice.

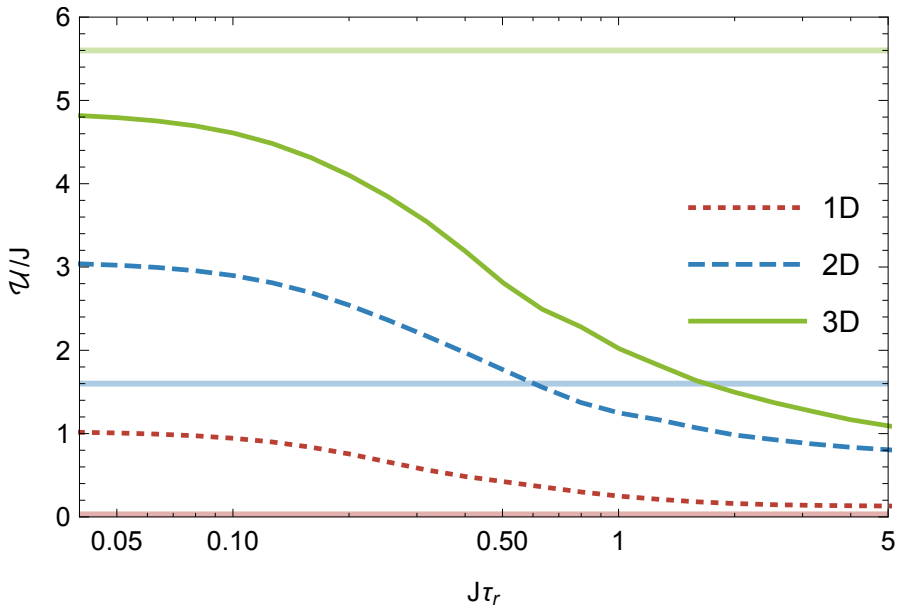

Figure 7.4: The energy density $\mathcal{U} = \frac{1}{N_s}\left[\left\langle \hat{H} \right\rangle - \left\langle \hat{H} \right\rangle_{gs}\right]$ following an interaction ramp of length τ_r. Horizontal lines show the energy density at the superfluid critical temperature, $\mathcal{U}_c/J = 0, 2.1, 5.1$ at $T_c/J = 0, 1.7, 5.9$ in one, two and three dimensions [23, 24].

7.5 Final Energy Density

After the ramp has ended, the system continues to evolve, and the correlation length continues to grow. However, the energy of the system is now conserved. At long times, we expect the state of the system to resemble a thermal state at a temperature determined by the energy density $\mathcal{U} = \frac{1}{N_s}\left\langle \hat{H} \right\rangle - \left\langle \hat{H} \right\rangle_{gs}$, where $\left\langle \hat{H} \right\rangle_{gs}$ is the energy of the new ground state of the system. We plot $\mathcal{U}$ in Fig. 7.4.

For ramp times much shorter than the hopping time scale, $J\tau_r \lesssim 0.2$, the final energy density varies slowly with τ_r. As seen in Fig. 7.3, the correlation length ξ at the end of the ramp does grow. However, we find that the correlation length measured at $Jt = 0.2$ is similar for any τ_r in this range, as seen in Fig. 7.5. Thus, ramps in this regime are indistinguishable from instantaneous quenches, and the

final state of the system, if allowed to equilibrate, would be similar for any τ_r in this regime.

A similar observation can be made for ramp times of $J\tau \gtrsim 2$. Here, the process is nearly adiabatic, and the system would be expected to equilibrate at a low-temperature state if allowed.

For ramps on the order of the hopping time, $J\tau \sim 1$, the final state of the system is strongly affected by the length of the ramp. As we switch from an near-instantaneous to near-adiabatic ramp, the energy density falls quickly with the length of the ramp.

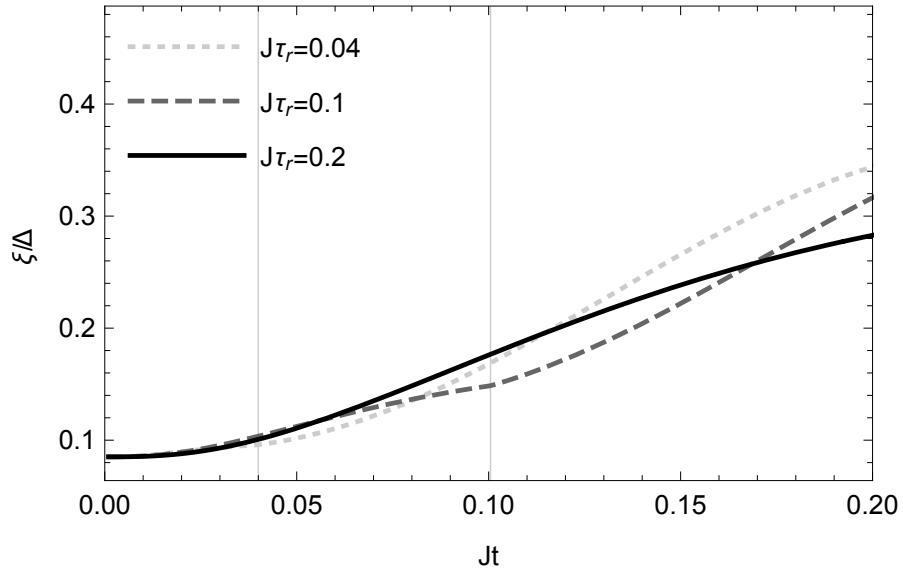

Figure 7.5: Evolution of the effective correlation length ξ, for an interaction strength ramp of the form $U = \begin{cases} U_i(U_f/U_i)^{t/\tau_r} & t \leq \tau_r \\ U_f & t > \tau_r \end{cases}$, with $J\tau_r = 0.04, 0.1, 0.2$ The grid lines denote the end of the ramp shorter ramps. The correlation length continues to grow in a similar way in all cases as the system relaxes. Shown here for a one-dimensional system with $\bar{n} = 1$.

7.6 Decoherence

In an ideal, closed, quantum system, all evolution is unitary. The final energy of the system rises monotonously with the rate of the ramp in such systems. Conversely, any real system faces decoherence caused by interaction with its environment. As a result, experimental dynamic systems always face a competition between the system's reaction time and external processes.

The physics of decoherence has been explored in detail [22, 118, 119, 122, 123, 134]. Here, we return to a mechanism we have previously used to described the effect of density measurement by light scattering [161]. The same formalism describes inelastic light scattering, where an external photon scatters off of a trapped atom. This is one of the major sources of decoherence in atomic experiments.

As in Chapter 6, we neglect out of band effects, which cause particle loss. We focus on in-band scattering, which would directly decrease the coherence of the remaining gas and reduce the correlation length measured above. In an ensemble description, this leads to a nonunitary evolution term of the form

$$\frac{d}{dt}\left\langle \hat{d}_k^\dagger \hat{d}_k \right\rangle = -i\left\langle \left[\hat{d}_k^\dagger \hat{d}_k, \hat{H}\right]\right\rangle - \gamma\left(\left\langle \hat{d}_k^\dagger \hat{d}_k \right\rangle - n_d\right) \tag{7.25}$$

$$\frac{d}{dt}\left\langle \hat{d}_k \hat{h}_{-k} \right\rangle = -i\left\langle \left[\hat{d}_k \hat{h}_{-k}, \hat{H}\right]\right\rangle - \gamma\left\langle \hat{d}_k \hat{h}_k \right\rangle \tag{7.26}$$

where γ is proportional to the frequency of light scattering per site.

We calculate the effect of this decoherence on the behavior of the correlation length ξ, as show in Fig. 7.6. As expected, no effect is seen at time scales shorter than $1/\gamma$, but at longer time scales, the decoherence dominates over the increase

in adiabaticity. The overall effect is similar to experimental observations for long ramp times [21].

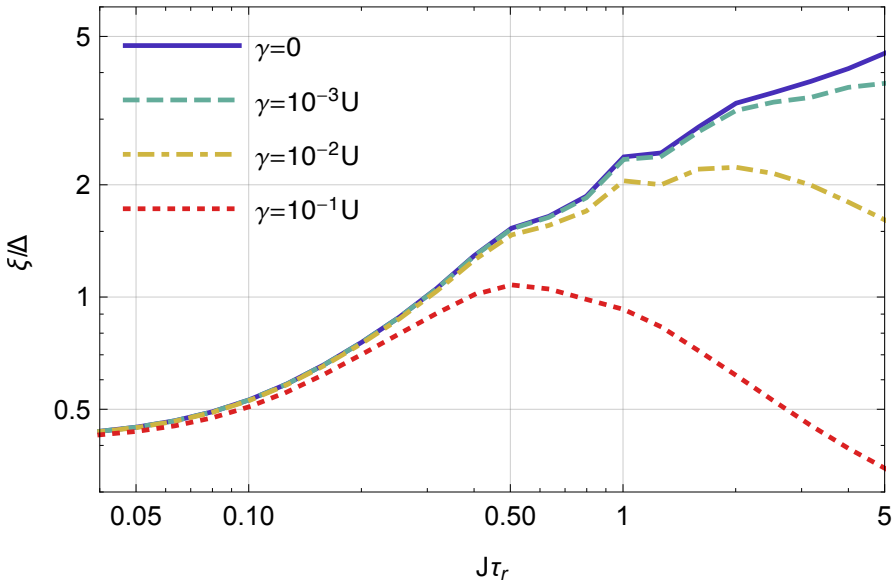

Figure 7.6: Effective correlation length ξ, normalized by the lattice constance Δ, at the end of a ramp of the interaction strength of the form $U = U_i(U_f/U_u)^{t/\tau_r}$, in a system coupled to the environment in the form shown in Eqs. (7.25) and (7.26). Here $U_f = 47J, U_i = 2J$, in a three-dimensional cubic lattice. In an optical lattice setup, the rate of inelastic light scattering events changes with lattice depth similarly to the interaction strength [75, 118].

7.7 Outlook

The physics of ultracold atomic systems is driven by multiple energy scales. In driven experimental systems, the relaxation time of the system, the driving time scale and the rate of decoherence imposed by interaction with the environment. Here, we have quantified the effect of the quench time in Bose-Hubbard systems crossing the phase boundary. We find that an effectively-adiabatic transition can be achieved by performing quenches at the hopping rate. For transitions at a slower rate, the behavior of the system is dictated by its relaxation dynamics. We

have also demonstrated that inelastic light scattering can be quite destructive on longer time scale, underscoring the usefulness of shorter experimental runs.

APPENDIX A

GLOSSARY

The following variables are commonly used across this work. Some terms, defined and used in specific sections, do not appear here.

a_0	The lattice constant for the periodic potential
$\hat{a}_0, \hat{a}_0^\dagger$	The annihilation and creation operator, respectively, for a particle with momentum $k = 0$
$\hat{a}_i, \hat{a}_i^\dagger$	The annihilation and creation operator for a particle at site i (also j, etc.)
$\hat{a}_k, \hat{a}_k^\dagger$	The annihilation and creation operator for a particle with momentum k (also p, etc.)
$\hat{d}_i, \hat{d}_i^\dagger$	The annihilation and creation operator for a doublone at site i (also j, etc.); see Section 2.6.2
$\hat{d}_k, \hat{d}_k^\dagger$	The annihilation and creation operator for a particle with momentum k (also p, etc.); see Section 2.6.2
$\boldsymbol{\Delta}, \Delta$	A basis vector for the periodic potential, and its length, $\Delta = \lvert\boldsymbol{\Delta}\rvert$
ε_k	The single-particle kinetic energy on the lattice, $\varepsilon_k = -2\sum_\Delta \cos(\boldsymbol{\Delta}\cdot\boldsymbol{k})$
ϵ_k	The relative kinetic energy, $\epsilon_k = \varepsilon_k - \varepsilon_0 = 4\sum_\Delta \sin^2(\boldsymbol{\Delta}\cdot\boldsymbol{k}/2)$
γ	The rate constant for inelastic light scattering off the bosons, induced for measurement or by an imperfect environment.
$\hat{h}_i, \hat{h}_i^\dagger$	The annihilation and creation operator for a particle at site i (also j, etc.); see Section 2.6.2
$\hat{h}_k, \hat{h}_k^\dagger$	The annihilation and creation operator for a particle with momentum k (also p, etc.); see Section 2.6.2
J	The hopping parameter for the Bose-Hubbard model; see Eq. (2.8)
μ	The chemical potential
$\bar{n}$	The mean number of particles per site on the lattice
$\hat{n}_i$	The real-space number density operator, $\hat{n}_i = \hat{a}_i^\dagger \hat{a}_i$ (also j, etc.)
$\hat{n}_k$	The momentum space number density operator, $\hat{n}_k = \hat{a}_k^\dagger \hat{a}_k$ (also p, etc.)
N_s	The number of sites in the lattice, generally going to infinity $N_s \gg 1$
$\boldsymbol{R}_i$	The position of the i-th lattice site (also j, etc.)
U	The interaction strength for the Bose-Hubbard model; see Eq. (2.8)

APPENDIX B

NOBODY REALLY GETS QUANTUM

On Yom Kippur eve Quantum walked over to Einstein's house to seek forgiveness. "I'm not here," yelled Einstein through a closed door. On the way home everybody taunted him and somebody even hit him with an empty can of coke. Quantum pretended not to care, but deep inside he was really hurt. Nobody really gets Quantum, everybody hates him. "Parasite!" people cry out when he's walking down the street, "draft dodger!" - "I wanted to enlist," Quantum tries to say, "but they wouldn't take me, because I'm so small." Not that anybody listens to Quantum. Nobody listens to Quantum when he tries to speak up for himself, but when he says something that can be misconstrued, oh, then suddenly everybody's paying attention. Quantum can say something innocuous like "wow, what a cat!" and right away some reporter calls it a provocation and runs off to talk to Schrödinger. And anyway, the media hates Quantum most, because once, in an interview in Scientific American, Quantum said that the observer affects the observed event, and all the journalists thought he was talking about the coverage of the war and said he was deliberately inciting violence. And Quantum can keep talking all day about how he didn't mean it and he has no political agenda, nobody believes him anyway. Everybody knows he's friends with Yuval Ne'eman[1].

A lot of people think Quantum is cold, that he has no feelings, but that's not true at all. On Friday, after a documentary about Hiroshima, he was one of the experts on the discussion panel. And he couldn't even speak. Just sat in front of the open mic and cried, and all of the viewers at home, that don't really know Quantum, couldn't understand that Quantum was crying, they just thought he

[1]Physicists know Ne'eman through his work with Gell-Mann on particle physics, but in Israel he was also known as an opponent of reconciliation with the Palestinians in the 80's and 90's

was avoiding the question. And the sad thing about it is, even if Quantum writes dozens of letters to the editors of all the scientific journals in the world and proves beyond any doubt that for the whole atomic bomb thing he was just being used and he never thought it would end this way, it wouldn't help him, because nobody really gets quantum. Least of all the physicists.

Etgar Keret [81]; translated by YY

BIBLIOGRAPHY

[1] A. Altland and B. Simons. *Condensed Matter Field Theory.* (Cambridge University Press, Cambridge, UK, second edition, 2010.

[2] L. Amico and V. Penna. Dynamical Mean Field Theory of the Bose-Hubbard Model. *Physical Review Letters*, 80(10):2189–2192, 1998.

[3] M. H. Anderson, J. R. Ensher, M. R. Matthews, C. E. Wieman, and E. A. Cornell. Observation of Bose-Einstein Condensation in a Dilute Atomic Vapor. *Science*, 269(5221):198–201, 1995.

[4] A. F. Andreev. Structure of vacancies in solid He3. *Soviet Journal of Experimental Theory Letters*, 24(11):564–565, 1976.

[5] H. Aoki, N. Tsuji, M. Eckstein, M. Kollar, T. Oka, and P. Werner. Nonequilibrium dynamical mean-field theory and its applications. *Reviews of Modern Physics*, 86(2):779–837, 2014.

[6] W. S. Bakr, J. I. Gillen, A. Peng, S. Fölling, and M. Greiner. A quantum gas microscope for detecting single atoms in a Hubbard-regime optical lattice. *Nature*, 462(7269):74–77, Nov. 2009.

[7] M. Baranger, M. A. M. de Aguiar, F. Keck, H. J. Korsch, and B. Schellhaaß. Semiclassical approximations in phase space with coherent states. *Journal of Physics A: Mathematical and General*, 34(36):7227–7286, 2001.

[8] P. Barmettler and C. Kollath. Controllable manipulation and detection of local densities and bipartite entanglement in a quantum gas by a dissipative defect. *Physical Review A*, 84(4):041606, Oct. 2011.

[9] P. Barmettler, D. Poletti, M. Cheneau, and C. Kollath. Propagation front of correlations in an interacting Bose gas. *Physical Review A*, 85(5):053625, May 2012.

[10] G. Barontini, R. Labouvie, F. Stubenrauch, A. Vogler, V. Guarrera, and H. Ott. Controlling the Dynamics of an Open Many-Body Quantum System with Localized Dissipation. *Physical Review Letters*, 110(3):035302, Jan. 2013.

[11] D. M. Basko, I. L. Aleiner, and B. L. Altshuler. On the problem of many-body localization. *arXiv preprint*, pages cond–mat/0602510v1, 2006.

[12] G. Baym. The Microscopic Description of Superfluidity. In R. C. Clark and G. H. Derrick, editors, *Mathematical Methods in Solid State and Superfluid Theory*. Oliver and Boyd, Edinburgh, 1969.

[13] V. Belinicher, C. Providencia, and J. da Providencia. Instanton picture of the spin tunnelling in the Lipkin-Meshkov-Glick model. *Journal of Physics A: Mathematical and General*, 30:5633, 1999.

[14] J. Billy, V. Josse, Z. Zuo, A. Bernard, B. Hambrecht, P. Lugan, D. Clément, L. Sanchez-Palencia, P. Bouyer, and A. Aspect. Direct observation of Anderson localization of matter waves in a controlled disorder. *Nature*, 453(7197):891–894, 2008.

[15] I. Bloch. Ultracold quantum gases in optical lattices. *Nature Physics*, 1(1):23–30, 2005.

[16] I. Bloch, J. Dalibard, and S. Nascimbène. Quantum simulations with ultracold quantum gases. *Nature Physics*, 8(4):267–276, 2012.

[17] I. Bloch and W. Zwerger. Many-body physics with ultracold gases. *Reviews of Modern Physics*, 80(3):885–964, July 2008.

[18] C. C. Bradley, C. A. Sacket, and R. G. Hulet. Bose-Einstein Condensation of Lithium: Observation of Limited Condensate Number Hysical R Eview Letters. *Physical Review Letters*, 78(6):985–989, 1997.

[19] C. Braun and A. Garg. Semiclassical coherent-state propagator for many particles. *Journal of Mathematical Physics*, 48(3):032104, 2007.

[20] C. Braun and A. Garg. Semiclassical coherent-state propagator for many spins. *Journal of Mathematical Physics*, 48(10):102104, 2007.

[21] S. Braun and M. Friesdorf. Emergence of coherence and the dynamics of quantum phase transitions. *Proceedings of the National Academy of Sciences of the United States of America*, 112(12):3641–3646, 2014.

[22] Z. Cai and T. Barthel. Algebraic versus Exponential Decoherence in Dissipative Many-Particle Systems. *Physical Review Letters*, 111(15):150403, Oct. 2013.

[23] B. Capogrosso-Sansone, N. V. Prokofev, and B. V. Svistunov. Phase diagram

and thermodynamics of the three-dimensional Bose-Hubbard model. *Physical Review B*, 75(13):134302, Apr. 2007.

[24] B. Capogrosso-Sansone, . G. Söyler, N. V. Prokof'ev, and B. Svistunov. Monte Carlo study of two-dimensional Bose-Hubbard model. *Physical Review A*, 77:015602, 2007.

[25] I. Carusotto and Y. Castin. Nonequilibrium and local detection of the normal fraction of a trapped two-dimensional Bose gas. *Physical Review A*, 84(5):053637, Nov. 2011.

[26] J. Catani, L. De Sarlo, G. Barontini, F. Minardi, and M. Inguscio. Degenerate Bose-Bose mixture in a three-dimensional optical lattice. *Physical Review A*, 77(1):011603, Jan. 2008.

[27] D. Chen, M. White, C. Borries, and B. Demarco. Quantum quench of an atomic mott insulator. *Physical Review Letters*, 106(23):23530, 2011.

[28] Y. P. Chen, J. Hitchcock, D. Dries, M. Junker, C. Welford, and R. G. Hulet. Phase coherence and superfluid-insulator transition in a disordered Bose-Einstein condensate. *Physical Review A*, 77(3):033632, 2008.

[29] M. Cheneau, P. Barmettler, D. Poletti, M. Endres, P. Schauss, T. Fukuhara, C. Gross, I. Bloch, C. Kollath, S. Kuhr, P. Schauß, T. Fukuhara, C. Gross, I. Bloch, C. Kollath, and S. Kuhr. Light-cone-like spreading of correlations in a quantum many-body system. *Nature*, 481(7382):484–487, Jan. 2012.

[30] C.-M. Chung, S. Fang, and P. Chen. Quantum and thermal transitions out of the pair-supersolid phase of two-species bosons on a square lattice. *Physical Review B*, 85(21):214513, June 2012.

[31] F. M. Cucchietti, B. Damski, J. Dziarmaga, and W. H. Zurek. Dynamics of the Bose-Hubbard model: Transition from a Mott insulator to a superfluid. *Physical Review A*, 75(2):023603, 2007.

[32] F. Dalfovo, S. Giorgini, L. P. Pitaevskii, and S. Stringari. Theory of Bose-Einstein condensation in trapped gases. *Reviews of Modern Physics*, 71(3):463–512, 1999.

[33] D. A. R. Dalvit, J. Dziarmaga, and R. Onofrio. Continuous quantum measurement of a Bose-Einstein condensate: A stochastic Gross-Pitaevskii equation. *Physical Review A*, 65(5):053604, Apr. 2002.

[34] D. A. R. Dalvit, J. Dziarmaga, and R. Onofrio. Measurement-induced squeezing of a Bose-Einstein condensate. *Physical Review A*, 65(3):033620, Feb. 2002.

[35] K. B. Davis, M. O. Mewes, M. R. Andrews, N. J. Van Druten, D. S. Durfee, D. M. Kurn, and W. Ketterle. Bose-Einstein condensation in a gas of sodium atoms. *Physical Review Letters*, 75(22):3969–3973, 1995.

[36] B. Deissler, M. Zaccanti, G. Roati, C. D'Errico, M. Fattori, M. Modugno, G. Modugno, and M. Inguscio. Delocalization of a disordered bosonic system by repulsive interactions. *Nature Physics*, 6(5):8, 2009.

[37] S. Diehl, A. Micheli, A. Kantian, B. Kraus, H. P. Büchler, and P. Zoller. Quantum states and phases in driven open quantum systems with cold atoms. *Nature Physics*, 4(11):878–883, Sept. 2008.

[38] J. Dziarmaga. Dynamics of a quantum phase transition and relaxation to a steady state. *Advances in Physics*, 59(6):1063–1189, 2010.

[39] N. Elstner and H. Monien. Dynamics and thermodynamics of the Bose-Hubbard model. *Physical Review B*, 59(19):12184–12187, 1999.

[40] M. Enz and R. Schilling. Spin tunnelling in the semiclassical limit. *Journal of Physics C: Solid State Physics*, 19(11):1765, 1986.

[41] L. Fallani, J. Lye, V. Guarrera, C. Fort, and M. Inguscio. Ultracold Atoms in a Disordered Crystal of Light: Towards a Bose Glass. *Physical Review Letters*, 98(13):130404, Mar. 2007.

[42] D. V. Fil and S. I. Shevchenko. Drag of superfluid current in bilayer Bose systems. *Low temperature physics*, 30(10):770, 2004.

[43] M. C. Fischer, B. Gutiérrez-Medina, and M. G. Raizen. Observation of the Quantum Zeno and Anti-Zeno Effects in an Unstable System. *Physical Review Letters*, 87(4):040402, July 2001.

[44] M. P. A. Fisher, P. B. Weichman, G. Grinstein, and D. S. Fisher. Boson localization and the superfluid-insulator transition. *Physical Review B*, 40(1):546–570, Nov. 1989.

[45] A. G. Fowler, M. Mariantoni, J. M. Martinis, and A. N. Cleland. Surface

codes: Towards practical large-scale quantum computation. *Physical Review A*, 86:032324, 2012.

[46] J. K. Freericks and H. Monien. Phase diagram of the Bose-Hubbard Model. *Europhysics Letters*, 26(7):545–550, 1994.

[47] T. Fukuhara, A. Kantian, M. Endres, M. Cheneau, P. Schauß, S. Hild, D. Bellem, U. Schollwock, T. Giamarchi, C. Gross, I. Bloch, and S. Kuhr. Quantum dynamics of a single, mobile spin impurity. *Nature Physics*, 9:235–241, 2013.

[48] K. Funahashi, T. Kashiwa, S. Nima, and S. Sakoda. More about path integrals for spin. *Nuclear Physics B*, 453(1-2):508–528, Oct. 1995.

[49] K. Funahashi, T. Kashiwa, S. Sakoda, and K. Fujii. Coherent states, path integral, and semiclassical approximation. *Journal of Mathematical Physics*, 36(7):3232, 1995.

[50] B. Gadway, D. Pertot, J. Reeves, M. Vogt, and D. Schneble. Glassy Behavior in a Binary Atomic Mixture. *Physical Review Letters*, 107(14):145306, Sept. 2011.

[51] B. Gadway, D. Pertot, R. Reimann, and D. Schneble. Superfluidity of Interacting Bosonic Mixtures in Optical Lattices. *Physical Review Letters*, 105(4):045303, July 2010.

[52] J. Gambetta, A. Blais, M. Boissonneault, A. A. Houck, D. I. Schuster, and S. M. Girvin. Quantum trajectory approach to circuit QED: Quantum jumps and the Zeno effect. *Physical Review A*, 77(1):012112, Jan. 2008.

[53] C. W. Gardiner. *Handbook of Stochastic Methods*. Springer-Verlag Berlin Heidelberg, 2nd edition, 1985.

[54] A. Garg, E. Kochetov, K.-S. Park, and M. Stone. Spin coherent-state path integrals and the instanton calculus. *Journal of Mathematical Physics*, 44(1):48, 2003.

[55] F. Gerbier and Y. Castin. Heating rates for an atom in a far-detuned optical lattice. *Physical Review A*, 82(1):013615, July 2010.

[56] T. Gericke, P. Würtz, D. Reitz, T. Langen, and H. Ott. High-resolution

scanning electron microscopy of an ultracold quantum gas. *Nature Physics*, 4(12):949–953, Oct. 2008.

[57] V. Giovannetti, S. Lloyd, and L. Maccone. Quantum-enhanced measurements: beating the standard quantum limit. *Science*, 306(5700):1330–6, Nov. 2004.

[58] P. Gregory. Bayesian inference with Poisson sampling. In *Bayesian Logical Data Analysis for the Physical Sciences : A Comparative Approach with Mathematica Support*, chapter 14, pages 376–388. Cambridge University Press, Cambridge, UK, 2005.

[59] M. Greiner, O. Mandel, and T. Esslinger. Quantum phase transition from a superfluid to a Mott insulator in a gas of ultracold atoms. *Nature*, 415:39–44, 2002.

[60] A. Griffin. Conserving and gapless approximations for an inhomogeneous Bose gas at finite temperatures. *Physical Review B*, 53(14):9341–9347, Apr. 1996.

[61] V. Gurarie, L. Pollet, N. V. Prokofev, B. V. Svistunov, and M. Troyer. Phase diagram of the disordered Bose-Hubbard model. *Physical Review B*, 80(21):214519, Dec. 2009.

[62] M. C. Gutzwiller. Effect of Correlation on the Ferromagnetism of Transition Metals. *Physical Review*, 134(4A):3–6, 1964.

[63] Z. Hadzibabic, P. Krüger, M. Cheneau, B. Battelier, and J. Dalibard. Berezinskii-Kosterlitz-Thouless crossover in a trapped atomic gas. *Nature*, 441(7097):1118–21, June 2006.

[64] E. Hagley, L. Deng, M. Kozuma, M. Trippenbach, Y. Band, M. Edwards, M. Doery, P. Julienne, K. Helmerson, S. Rolston, and W. Phillips. Measurement of the Coherence of a Bose-Einstein Condensate. *Physical Review Letters*, 83(16):3112–3115, Oct. 1999.

[65] M. Hatridge, S. Shankar, M. Mirrahimi, F. Schackert, K. Geerlings, T. Brecht, K. M. Sliwa, B. Abdo, L. Frunzio, S. M. Girvin, R. J. Schoelkopf, and M. H. Devoret. Quantum back-action of an individual variable-strength measurement. *Science*, 339(6116):178–181, Jan. 2013.

[66] M. Héritier and P. Lederer. Spin polarons in narrow, almost half-filled s band : A valid concept in b.c.c. 3He? *J. Physique Lett.*, 38(10):209, 1977.

[67] T.-L. Ho and Q. Zhou. Obtaining the phase diagram and thermodynamic quantities of bulk systems from the densities of trapped gases. *Nature Physics*, 6(2):131–134, Dec. 2009.

[68] P. Hohenberg and P. Martin. Microscopic theory of superfluid helium. *Annals of Physics*, 34(2):291–359, Sept. 1965.

[69] M. Holland, S. Marksteiner, P. Marte, and P. Zoller. Measurement induced localization from spontaneous decay. *Physical Review Letters*, 76(20):3683–3686, May 1996.

[70] J. Hubbard. Electron Correlations in Narrow Energy Bands. *Proceedings of the Royal Society A: Mathematical, Physical and Engineering Sciences*, 276(1365):238–257, 1963.

[71] C. L. Hung, X. Zhang, N. Gemelke, and C. Chin. Slow mass transport and statistical evolution of an atomic gas across the superfluid-mott-insulator transition. *Physical Review Letters*, 104(16):160403, 2010.

[72] A. Itah, H. Veksler, O. Lahav, and A. Blumkin. Direct observation of number squeezing in an optical lattice. *Physical Review Letters*, 104:113001, 2010.

[73] W. M. Itano, D. J. Heinzen, J. J. Bollinger, and D. J. Wineland. Quantum Zeno effect. *Physical Review A*, 41(5):2295–2300, 1990.

[74] Ivana Vidanovic, D. Cocks, and W. Hofstetter. Dissipation through localized loss in bosonic systems with long-range interactions. *Physical Review A*, 89(5):053614, 2014.

[75] D. Jaksch, C. Bruder, J. I. Cirac, C. W. Gardiner, and P. Zoller. Cold bosonic atoms in optical lattices. *Physical Review Letters*, 81(15):3108–3111, Oct. 1998.

[76] S. T. John, Z. Hadzibabic, and N. R. Cooper. Spectroscopic method to measure the superfluid fraction of an ultracold atomic gas. *Physical Review A*, 83(2):023610, Feb. 2011.

[77] J. E. Jones. On the Determination of Molecular Fields - II From the Equation

of a States of a Gas. *Proceedings of the Royal Society A: Mathematical, Physical and Engineering Sciences*, 106(738):463, 1924.

[78] M. Karski, L. Förster, J. M. Choi, W. Alt, A. Widera, and D. Meschede. Nearest-Neighbor Detection of Atoms in a 1D Optical Lattice by Fluorescence Imaging. *Physical Review Letters*, 102(5):053001, Feb. 2009.

[79] V. A. Kashurnikov, N. V. Prokof'ev, and B. V. Svistunov. Revealing Superfluid–Mott-Insulator Transition in an Optical Lattice. *Physical Review A*, 66(3):031601, 2002.

[80] V. M. Kaurov, A. B. Kuklov, and A. E. Meyerovich. Drag effect and topological complexes in strongly interacting two-component lattice superfluids. *Physical Review Letters*, 95(9):90403, 2005.

[81] E. Keret. *Tzinorot*. Zmora Beitan, Tel Aviv, 1992.

[82] J. R. Klauder. The Feynman Path Integral : An Historical Slice The Feynman Path Integral , 1948. *arXiv preprint*, arXiv:quant–ph/0303034, 2003.

[83] J. R. Klauder and B.-S. Skagerstam. *Coherent states: Applications in physics and mathematical physics*. World Scientific, Singapore, 1985.

[84] H. Kleinert. *Path integrals in quantum mechanics, statistics, polymer physics, and financial markets*. World Scientific, Singapore, 2009.

[85] H. Kleinert, Z. Narzikulov, and A. Rakhimov. Phase Transitions in Three-Dimensional Bosonic Optical Lattices. *Journal of Statistical Mechanics: Theory and Experiment*, 2014(1):01003, 2014.

[86] M. Knap, D. A. Abanin, and E. Demler. Dissipative Dynamics of a Driven Quantum Spin Coupled to a Bath of Ultracold Fermions. *Physical Review Letters*, 111:265302, 2013.

[87] E. Kochetov and V. Yarunin. Representation of the t-J model via spin-charge variables. *Physical Review B*, 56(5):2703–2711, Aug. 1997.

[88] E. a. Kochetov. SU(2) coherent-state path integral. *Journal of Mathematical Physics*, 36(9):4667, 1995.

[89] C. Kollath, A. M. Läuchli, and E. Altman. Quench dynamics and nonequi-

librium phase diagram of the Bose-Hubbard model. *Physical Review Letters*, 98(18):180601, 2007.

[90] W. Krauth, M. Caffarel, and J. P. Bouchaud. Gutzwiller wave function for a model of strongly interacting bosons. *Physical Review B*, 45(6):3137, 1992.

[91] W. Krauth, N. Trivedi, and D. M. Ceperley. Superfluid-Insulator Transition in Disordered Boson Systems. *Physical review letters*, 67(17):2307, 1991.

[92] A. B. Kuklov, N. V. Prokofev, and B. V. Svistunov. Superfluid-Superfluid Phase Transitions in a Two-Component Bose-Einstein Condensate. *Physical Review Letters*, 92(3):030403, Jan. 2004.

[93] A. B. Kuklov and B. V. Svistunov. Counterflow superfluidity of two-species ultracold atoms in a commensurate optical lattice. *Physical Review Letters*, 90(10):100401, 2003.

[94] L. D. Landau. The theory of superfluidity of helium II. *J. Phys. USSR*, 5(71), 1941.

[95] J. S. Langer. Coherent States in the Theory of Superfluidity. *Physical Review*, 167(1):183, 1968.

[96] P. A. Lee, N. Nagaosa, and X.-G. Wen. Doping a Mott Insulator: Physics of High Temperature Superconductivity. *Reviews of Modern Physics*, 78(1):17, 2006.

[97] A. J. Leggett. On the Superfluid Fraction of an Arbitrary Many-Body System at T=0. *Journal of Statistical Physics*, 93(3/4):927–941, Nov. 1998.

[98] A. J. Leggett. Superfluidity. *Reviews of Modern Physics*, 71(2):S318–S323, 1999.

[99] A. J. Leggett. Bose-Einstein condensation in the alkali gases: Some fundamental concepts. *Reviews of Modern Physics*, 73(April):307–356, 2001.

[100] C. Lobo, A. Recati, S. Giorgini, and S. Stringari. Normal State of a Polarized Fermi Gas at Unitarity. *Physical Review Letters*, 97(20):200403, Nov. 2006.

[101] I. B. Mekhov and H. Ritsch. Quantum optics with ultracold quantum gases: towards the full quantum regime of the lightmatter interaction. *Journal of Physics B: Atomic, Molecular and Optical Physics*, 45(10):102001, May 2012.

[102] J. J. Mendoza-Arenas, T. Grujic, D. Jaksch, and S. R. Clark. Dephasing enhanced transport in nonequilibrium strongly correlated quantum systems. *Physical Review B*, 87(23):235130, June 2013.

[103] D. N. Mermin and N. W. Ashcroft. *Solid State Physics*. Saunders, Philadelphia, 1976.

[104] H. Monien and T. D. Kühner. Phases of the one-dimensional Bose-Hubbard model. *Physical Review B*, 58(22):741–744, 1998.

[105] Y. Nagaoka. Ferromagnetism in a narrow, almost half-filled s band. *Physical Review*, 147(1):392–405, 1966.

[106] A. Naik, O. Buu, M. D. LaHaye, A. D. Armour, A. Clerk, M. P. Blencowe, and K. C. Schwab. Cooling a nanomechanical resonator with quantum back-action. *Nature*, 443(7108):193–196, Sept. 2006.

[107] R. Nandkishore and D. a. Huse. Many-Body Localization and Thermalization in Quantum Statistical Mechanics. *Annual Review of Condensed Matter Physics*, 6(1):15–38, 2015.

[108] S. S. Natu, D. C. McKay, B. DeMarco, and E. J. Mueller. Evolution of condensate fraction during rapid lattice ramps. *Physical Review A*, 85(6):061601, June 2012.

[109] S. S. Natu and E. J. Mueller. Pairing, ferromagnetism, and condensation of a normal spin-1 Bose gas. *Physical Review A*, 84:053625, 2011.

[110] P. Navez and R. Schützhold. Emergence of coherence in the Mott-insulator-superfluid quench of the Bose-Hubbard model. *Physical Review A*, 82(6):063603, 2010.

[111] K. D. Nelson, X. Li, and D. S. Weiss. Imaging single atoms in a three-dimensional array. *Nature Physics*, 3(8):556–560, June 2007.

[112] P. Nozières and D. Saint James. Particle vs. pair condensation in attractive Bose liquids. *J. Physique*, 43:1133, 1982.

[113] M. Okumura, S. Yamada, M. Machida, and H. Aoki. Phase-separated ferromagnetism in a spin-imbalanced system of Fermi atoms loaded in an optical ladder: A density-matrix renormalization-group study. *Physical Review A*, 83(3):031606, Mar. 2011.

[114] C. Orzel, A. K. Tuchman, M. L. Fenselau, M. Yasuda, and M. A. Kasevich. Squeezed States in a Bose-Einstein Condensate. *Science*, 291:2386–2390, 2001.

[115] T. Ozaki and T. Nikuni. Phase Separation in BoseBose Mixtures in an Optical Lattice. *Journal of the Physical Society of Japan*, 81(2):024001, Jan. 2012.

[116] Y. S. Patil, L. M. Aycock, C. S, and M. Vengalattore. Nondestructive imaging of an ultracold lattice gas. *Physical Review A*, 90:033422, 2014.

[117] C. J. Pethick and H. Smith. *Bose-Einstein Condensation in Dilute Gases*. Cambridge University Press, Cambridge, UK, 2002.

[118] H. Pichler, A. J. Daley, and P. Zoller. Nonequilibrium dynamics of bosonic atoms in optical lattices: Decoherence of many-body states due to spontaneous emission. *Physical Review A*, 82(6):063605, Dec. 2010.

[119] H. Pichler, J. Schachenmayer, A. J. Daley, and P. Zoller. Heating dynamics of bosonic atoms in a noisy optical lattice. *Physical Review A*, 87(3):033606, Mar. 2013.

[120] S. Pilati, G. Bertaina, S. Giorgini, and M. Troyer. Itinerant ferromagnetism of a repulsive atomic Fermi gas: A quantum Monte Carlo study. *Physical Review Letters*, 105(3):030405, 2010.

[121] M. Pletyukhov, C. Amann, M. Mehta, and M. Brack. Semiclassical Theory of Spin-Orbit Interactions using Spin Coherent States. *Physical Review Letters*, 89(11):116601, Aug. 2002.

[122] D. Poletti, P. Barmettler, A. Georges, and C. Kollath. Emergence of glass-like dynamics for dissipative and strongly interacting bosons. *Physical Review Letters*, 111(19):195301, 2013.

[123] D. Poletti, J.-S. Bernier, A. Georges, and C. Kollath. Interaction-Induced Impeding of Decoherence and Anomalous Diffusion. *Physical Review Letters*, 109(4):045302, July 2012.

[124] A. Polkovnikov. Universal adiabatic dynamics in the vicinity of a quantum critical point. *Physical Review B*, 72(16):161201, 2005.

[125] A. Polkovnikov, S. Sachdev, and S. M. Girvin. Non-equilibrium Gross-Pitaevskii dynamics of boson lattice models. *Physical Review A*, 66(5):053607, 2002.

[126] A. Polkovnikov, K. Sengupta, A. Silva, and M. Vengalattore. Colloquium: Nonequilibrium dynamics of closed interacting quantum systems. *Reviews of Modern Physics*, 83(3):863–883, 2011.

[127] E. L. Pollock and D. M. Ceperley. Path-integral computation of superfluid densities. *Physical Review B*, 36(16):8343–8352, Dec. 1987.

[128] N. V. Prokofev and B. V. Svistunov. Fermi-polaron problem: Diagrammatic Monte Carlo method for divergent sign-alternating series. *Physical Review B*, 77(2):020408, Jan. 2008.

[129] R. Raghavan and V. Elser. Thermal evolution of spin-polarons. *Physical Review Letters*, 75(22):4083–4085, 1995.

[130] S. Richard, F. Gerbier, J. H. Thywissen, M. Hugbart, P. Bouyer, and A. Aspect. Momentum Spectroscopy of 1D Phase Fluctuations in Bose-Einstein Condensates. *Physical Review Letters*, 91(1):010405, July 2003.

[131] J.-F. Riou, L. A. Zundel, A. Reinhard, and D. S. Weiss. The effect of optical lattice heating on the momentum distribution of a 1D Bose gas. *Physical Review A*, 90(3):033401, 2014.

[132] G. Roati, C. D'Errico, L. Fallani, M. Fattori, C. Fort, M. Zaccanti, G. Modugno, M. Modugno, and M. Inguscio. Anderson localization of a non-interacting Bose-Einstein condensate. *Nature*, 453(7197):895–898, 2008.

[133] J. D. Sau, B. Wang, and S. Das Sarma. Quench-induced Mott-insulator-to-superfluid quantum phase transition. *Physical Review A*, 85(1):013644, 2012.

[134] J. Schachenmayer, L. Pollet, M. Troyer, and A. J. Daley. Spontaneous emission and thermalization of cold bosons in optical lattices. *Physical Review A*, 89(1):011601, Jan. 2014.

[135] F. Schäfer, I. Herrera, S. Cherukattil, C. Lovecchio, F. S. Cataliotti, F. Caruso, and A. Smerzi. Experimental realization of quantum zeno dynamics. *Nature Communications*, 5:3194, 2014.

[136] J. P. Sethna. *Statistical mechanics : entropy, order parameters, and complexity*. Oxford University Press, Oxford ; New York, 2006.

[137] J. F. Sherson, C. Weitenberg, M. Endres, M. Cheneau, I. Bloch, and S. Kuhr. Single-atom-resolved fluorescence imaging of an atomic Mott insulator. *Nature*, 467(7311):68–72, Sept. 2010.

[138] K. Sheshadri, H. R. Krishnamurthy, R. Pandit, and T. V. Ramaktishnan. Superfluid and insulating phases in an interacting-boson model: mean-field theory and the RPA. *Europhysics Letters*, 257(22):257–263, 1993.

[139] J. Shibata and S. Takagi. Method of collective degrees of freedom in spin-coherent-state path integral. *Physics of Atomic Nuclei*, 64(12):2206–2211, Dec. 2001.

[140] V. V. Smirnov. On the estimation of a path integral by means of the saddle point method. *Journal of Physics A: Mathematical and Theoretical*, 43(46):465303, Nov. 2010.

[141] H. G. Solari. Semiclassical treatment of spin system by means of coherent states. *Journal of Mathematical Physics*, 28(5):1097, 1987.

[142] P. Soltan-Panahi, J. Struck, P. Hauke, A. Bick, W. Plenkers, G. Meineke, C. Becker, P. Windpassinger, M. Lewenstein, and K. Sengstock. Multi-component quantum gases in spin-dependent hexagonal lattices. *Nature Physics*, 7(5):434–440, Feb. 2011.

[143] A. Sommer, M. Ku, and M. W. Zwierlein. Spin transport in polaronic and superfluid Fermi gases. *New Journal of Physics*, 13(5):055009, May 2011.

[144] S. L. Sondhi, S. M. Girvin, J. P. Carini, and D. Shahar. Continuous quantum phase transitions. *Reviews Of Modern Physics*, 69(1):315–333, 1997.

[145] I. B. Spielman, W. D. Phillips, and J. V. Porto. Mott-Insulator Transition in a Two-Dimensional Atomic Bose Gas. *Physical Review Letters*, 98(8):080404, Feb. 2007.

[146] J. Stenger, S. Inouye, A. P. Chikkatur, D. M. Stamper-Kurn, D. E. Pritchard, and W. Ketterle. Bragg spectroscopy of a Bose-Einstein condensate. *Physical Review Letters*, 82(23):4569–4573, 1999.

[147] T. Stöferle, H. Moritz, C. Schori, M. Köhl, and T. Esslinger. Transition from

a strongly interacting 1D superfluid to a Mott insulator. *Physical Review Letters*, 92(13):130403, 2004.

[148] M. Stone, K.-S. Park, and A. Garg. The semiclassical propagator for spin coherent states. *Journal of Mathematical Physics*, 41(12):8025, 2000.

[149] H. Tasaki. The Hubbard Model: Introduction and Selected Rigorous Results. *Journal of Physics: Condensed Matter*, 10:4353, 1998.

[150] N. Teichmann, D. Hinrichs, M. Holthaus, and A. Eckardt. Bose-Hubbard phase diagram with arbitrary integer filling. *Physical Review B*, 79(10):100503, 2009.

[151] D. Thouless. Exchange in solid 3He and the Heisenberg Hamiltonian. *Proceedings of the Physical Society*, 86(5):893, 1965.

[152] A. K. Tuchman, C. Orzel, A. Polkovnikov, and M. A. Kasevich. Nonequilibrium coherence dynamics of a soft boson lattice. *Physical Review A*, 74(5):051601, 2006.

[153] M. Tylutki, J. Dziarmaga, and W. H. Zurek. Dynamics of the Mott Insulator to Superfluid quantum phase transition in the truncated Wigner approximation. *Journal of Physics: Conference Series*, 414:012029, 2013.

[154] D. van Oosten, P. van der Straten, and H. T. C. Stoof. Quantum phases in an optical lattice. *Physical Review A*, 63(5):053601, Apr. 2001.

[155] T. F. Viscondi and M. A. M. de Aguiar. Semiclassical propagator for SU(n) coherent states. *Journal of Mathematical Physics*, 52(5):052104, 2011.

[156] J. von Stecher, E. Demler, M. D. Lukin, and a. M. Rey. Probing interaction-induced ferromagnetism in optical superlattices. *New Journal of Physics*, 12(5):055009, May 2010.

[157] M. Wallin, E. S. Sorensen, S. M. Girvin, and A. P. Young. Superconductor-insulator transition in two-dimensional dirty boson systems. *Physical Review B*, 49(17):12115, 1994.

[158] M. White, M. Pasienski, D. McKay, S. Q. Zhou, D. Ceperley, and B. DeMarco. Strongly Interacting Bosons in a Disordered Optical Lattice. *Physical Review Letters*, 102(5):055301, Feb. 2009.

[159] J. H. Wilson and V. Galitski. Breakdown of the Coherent State Path Integral: Two Simple Examples. *Physical Review Letters*, 106(11):110401, Mar. 2011.

[160] Y. Yanay and E. J. Mueller. Superfluid Density of Weakly Interacting Bosons on a Lattice. *arXiv preprint*, arXiv:1209.2446, 2012.

[161] Y. Yanay and E. J. Mueller. Heating from continuous number density measurements in optical lattices. *Physical Review A*, 90(2):023611, Aug. 2014.

[162] Y. Yanay and E. J. Mueller. Corrections to the continuous time semiclassical coherent state path integral. *The European Physical Journal Special Topics*, 224(3):591–596, 2015.

[163] Y. Yanay, E. J. Mueller, and V. Elser. Magnetic polarons in two-component hard-core bosons. *Physical Review A*, 87(4):043622, 2013.

[164] J. Zakrzewski. Mean-field dynamics of the superfluid-insulator phase transition in a gas of ultracold atoms. *Physical Review A*, 71(4):043601, 2005.

[165] W.-M. Zhang. Coherent states in field theory. *arXiv preprint*, arXiv:hep–th/9908117, 1999.

[166] W.-M. Zhang, R. Gilmore, and D. H. Feng. Coherent states: theory and some applications. *Reviews of Modern Physics*, 62(4):867, 1990.

[167] W. Zwerger. MottHubbard transition of cold atoms in optical lattices. *Journal of Optics B: Quantum and Semiclassical Optics*, 5(2):S9–S16, 2003.